GENERAL RESPONSE OF KNEADING-COMPACTED UNSATURATED SILTY SAND UNDER DRAINED AND UNDRAINED TRUE TRIAXIAL TESTING

by

SANG CHUL PYO

Presented to the Faculty of the Graduate School of

The University of Texas at Arlington in Partial Fulfillment

of the Requirements

for the Degree of

MASTER OF SCIENCE IN CIVIL ENGINEERING

THE UNIVERSITY OF TEXAS AT ARLINGTON

AUGUST 2006

ACKNOWLEDGEMENTS

The author would like to thank his supervising professor, Dr. Laureano R. Hoyos, for his guidance and support throughout the course of this research effort.

Thanks are also extended to the other members of his thesis committee, Drs. Anand J. Puppala and Mohamed S. Hossain, for their valuable advice and review of this manuscript. In addition, the author would like to thank the faculty and staff of the Department of Civil and Environmental Engineering at The University of Texas at Arlington for their valuable assistance during his academic studies.

The author also would like to thank all Geotechnical Engineering graduate students in this institution for their help and support. Special thanks are extended to Arthit Laikram.

Finally, and most of all, the author would like to thank his family for their love, encouragement, and great support. It is the best thing in his life to be a part of this family.

July 24, 2006

ABSTRACT

GENERAL RESPONSE OF KNEADING-COMPACTED UNSATURATED SILTY SAND UNDER DRAINED AND UNDRAINED TRUE TRIAXIAL TESTING

Publication No. _____

Sang Chul Pyo, M.S.

The University of Texas at Arlington, 2006

Supervising Professor: Laureano R. Hoyos

A comprehensive series of 36 drained and 36 undrained true triaxial tests was accomplished to investigate the stress-strain-strength behaviour of kneading-compacted unsaturated silty sand (SP-SM) under multi-axial stress states. Test specimens were prepared at three different initial moist contents (6, 8, 10%) to achieve different compaction-induced suction conditions prior to testing. All samples were then subjected to either a drained or undrained multi-axial stress paths, including conventional triaxial compression (CTC), triaxial compression (TC), triaxial extension (TE), or simple shear (SS) stress path. Initial compaction-induced matric suction was assessed via the SWCC of test soil. The experimental program focuses on soil response at high values of suction, that is, within the uppermost vadose zone regime.

Test results were plotted in terms of octahedral stress versus principal stress response. Results show that the shear strength of kneading-compacted unsaturated silty sand, regardless of initial compaction-induced suction, increase with an increase in confining pressure. However, as the initial degree of saturation increases from 27 to 61% and the initial dry density increases from 16.4 to 18.1 kN/m^3, the ultimate strength of kneading-compacted unsaturated silty sand increases. The undrained soil strength, in most multi-axial stress cases, proved to be slightly higher than that for drained conditions.

TABLE OF CONTENTS

LIST OF ILLUSTRATIONS

Figure Page

LIST OF TABLES

Table Page

CHAPTER 1

INTRODUCTION

1.1 General Background

In general, conventional laboratory soil testing is conveniently performed on soils prepared as two-phase systems, which are either fully dried or fully saturated. However, more recently, increasing attention has been devoted to the investigation of unsaturated soil behavior and its implications in engineering practice. Unsaturated soils consist mainly of three-phase comprising solid particles, air, and water. The principles of unsaturated soil mechanics have increasingly proved more effective in explaining soil behavioral patterns in geotechnical practices, where predictions of soil behaviour using saturated soil mechanics principles have resulted in overly-conservative designs.

Geographically, unsaturated soils are widely distributed in semi-arid areas of the world (Fredlund and Rahardjo 1993). Negative pore-water pressures (suction state) play a key role in unsaturated soil behavior. These negative pore-water pressures in the soil fluctuate with changes in the environmental conditions near the ground surface. Negative pore-water pressures decrease (suction increase) in the drying season, while increasing during wetting season. The changes in these pore-water pressures greatly affect the effective stress states of unsaturated soils above groundwater table.

The major problems, induced by change in negative pore-water pressure, in unsaturated soil are similar to those in saturated soil (Fredlund and Rahardjo 1993). In

natural slopes, these are undergoing continuously environmental change (e.g., heavy rainfall). The potential slip surface may be formed at which unsaturated soil with negative pore-water pressures exist above groundwater table. A prolonged period of rainfall may lead to the change in pore-water pressures and then may result in not only the change in the location of a potential slip surface, but also the local or global instability of natural slopes. In earth retaining structures, lateral pressures against them increase with wetting of the compacted backfill and this increment give rise to the dangerous lateral movements or imminent failure of the overall retaining structure system. In shallow footings, the footings often are constructed in case that the bottom of the footings is above water table. The soils below the footing, therefore, have a negative pore-water pressure affected considerably by the environmental change with time. Unconfined compressive strength, based on the assumption of constant negative pore-water pressure with time, may be much inaccurate and the bearing capacity from the unconfined compressive strength also may no longer valid.

Conventional triaxial testing has commonly been used to predict the stress-strain behavior of soils in the laboratory. In this type of testing, only axisymmetric stress states ($\sigma_2 = \sigma_3$) are attainable since the testing cannot control intermediate principal stress (σ_2) and minor principal stress (σ_3) independently. However, most problems in the geotechnical field are subjected to three-dimensional states ($\sigma_1 \neq \sigma_2 \neq \sigma_3$). To approach these actual problems, true triaxial testing devices possessing the capability of controlling the three principal stresses independently have been developed over the last half century. These devices have been successfully used to investigate the

mechanical behavior of dry or saturated soils along simple-to-complex stress paths. However, very limited attempts have dealt with investigating the stress-strain-strength behaviour of unsaturated soil along multiaxial stress states under both undrained and drained condition using a true triaxial device. The present thesis work was motivated by the lack of this type of experimental endeavors.

1.2 Objective and Scope

The main objective of this research work was to investigate the stress-strain-strength behaviour of kneading-compacted unsaturated silty sand subjected to three dimensional stress states under both drained and undrained conditions in a true triaxial apparatus.

A comprehensive series of 36 drained and 36 undrained true triaxial tests was accomplished to investigate the stress-strain-strength behaviour of kneading-compacted unsaturated silty sand (SP-SM) under multi-axial stress states. Test specimens were prepared at three different initial moist contents (6, 8, 10%) to achieve different compaction-induced suction conditions prior to testing. All samples were then subjected to either a drained or undrained multi-axial stress paths, including conventional triaxial compression (CTC), triaxial compression (TC), triaxial extension (TE), or simple shear (SS) stress path. Initial compaction-induced matric suction was assessed via the SWCC of test soil. The experimental program focuses on soil response at high values of suction, that is, within the uppermost vadose zone regime, as shown in Figure 1.

Test results were plotted in terms of octahedral stress versus principal stress response. In summary, results show that the shear strength of kneading-compacted unsaturated silty sand, regardless of initial compaction-induced suction, increase with an increase in confining pressure. However, as the initial degree of saturation increases from 27% to 61% and the initial dry density increases from 16.4 to 18.1 kN/m^3, the ultimate strength of kneading-compacted unsaturated silty sand increases. The undrained soil strength, in most multi-axial stress cases, proved to be slightly higher than that for drained conditions.

Findings from this research effort are expected to improve our understanding of the mechanical behaviour of unsaturated soils under both undrained and drained conditions along simple-to-complex multiaxial stress paths, as well as to promote further research on unsaturated soil behavior with the aim of fostering increased applications of its principles in real geotechnical engineering practice.

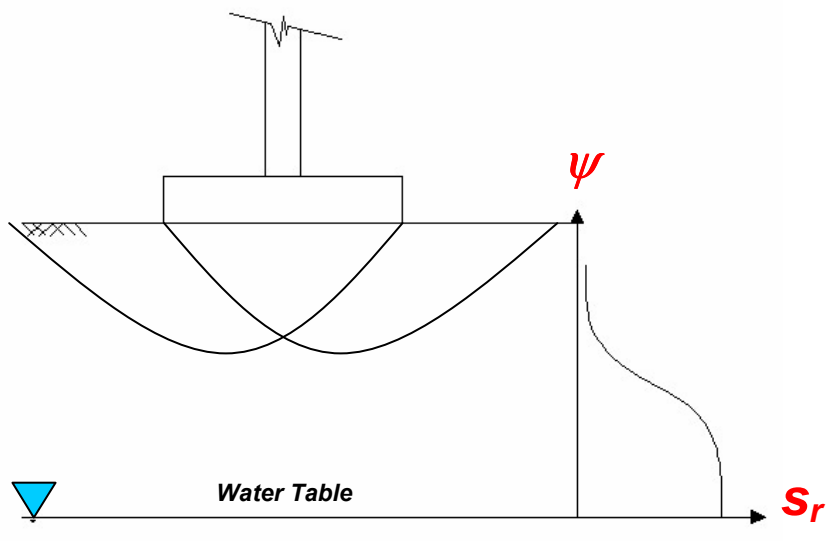

Figure 1.1 A Shallow Footing above Water Table

1.3 Outline of Thesis

A brief summary of each chapter included in this thesis is presented in the following paragraphs.

Chapter 2 presents a review of literature on fundamental concepts employed for the understanding of mechanical behavior of unsaturated soil. It also presents a literature review of previous work.

Chapter 3 describes details of main apparatus components and step by step assembling procedure of a true triaxial testing device for this research.

Chapter 4 presents the basic engineering properties of the testing soil, specimen preparation method, and test procedures.

Chapter 5 presents the results of a series of drained and undrained true triaxial tests on unsaturated silty sand. It reports the influence of octahedral stress and initial compaction-induced soil state on the stress-strain-strength behaviour of unsaturated silty sand. It also report failure envelops on octahedral plane and critical state response on p-q diagram. It finally compares the results of drained testings with those of undrained testings.

Chapter 6 presents this research's conclusion and recommendations for future research.

CHAPTER 2

LITERATURE REVIEW

2.1 Introduction

This chapter includes a brief review of the fundamental principles on unsaturated soil mechanics. The phenomenon of surface tension, matric suction, and capillarity is described. The text goes on to describe the history of shear strength of unsaturated soils from classical Terzaghi' theory using the effective stress concept to Fredlund et al.' theory employing two independent stress state variables. Previous studies on effect of initial soil conditions such as degree of saturation (or water content) and density on the strength of unsaturated soil are presented. In addition, previous various true triaxial testing devices to investigate the stress-stain-strength behaviour of soils along multiaxial stress states are described.

2.2 Fundamental Principles on Unsaturated Soil Mechanics

2.2.1 Surface Tension

Surface tension has been recently considered as one of three components needed for mechanical equilibrium in an unsaturated soil. Fredlund and Rahardjo (1993) described the physical mechanism of surface tension. Intermolecular forces acting on molecules in the contractile skin cause this surface tension. These forces, as shown in

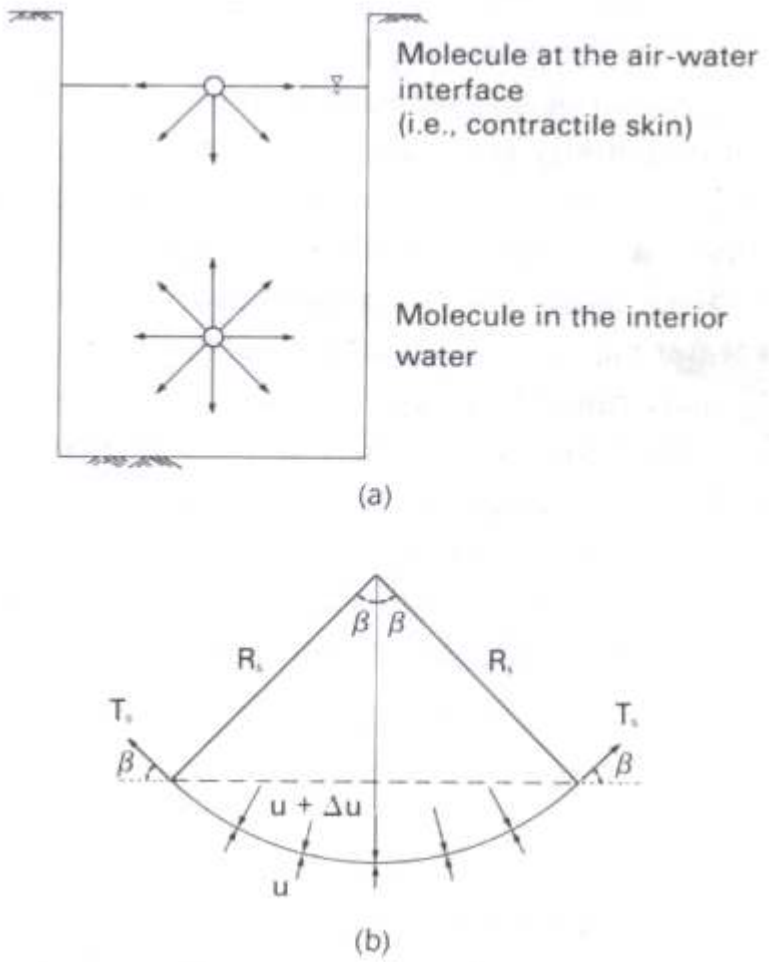

Figure 2.1 Surface Tension Phenomenon at the Air-Water Interface: (a) Intermolecular Forces on Contractile Skin and Water, (b) Pressures and Surface Tension Acting on a Curved Two-Dimensional Surface (Fredlund and Rahardjo, 1993)

Figure 2.1(a), are inconsistent with those that operating on molecules in the interior of the water.

The force which a molecule in the internal of the water undergoes is identical in all direction. It means that there is no unbalanced force. A water molecule inside the contractile skin, however, undergoes an unbalanced force towards the interior of the water. Consequently, tensile pull occur along the contractile skin to be in equilibrium.

This tensile pull, called surface tension, is generated from the characteristic of the contractile skin. The value of surface tension is calculated as the amount of tensile force applied to a given length of the contractile skin surface (i.e., units of N/m). The acting direction of surface tension is tangential to the surface of contractile skin. Its magnitude is inclined to decrease with the increase of temperature. In the case of water, its surface tension at 20°C, calculated by Kaye and Laby (1973), has a value of 72.75 mN/m.

The contractile skin is forced to act like an elastic membrane due to surface tension. If a flexible two-dimensional membrane is subordinate to different pressure on each side, the membrane must present a concave curvature toward the larger pressure and generate tension pull in the membrane to be in equilibrium. The pressure difference across the curved surface can be related to the surface tension and the radius of curvature of the surface by considering equilibrium across the membrane, as shown in Figure 2.1(b).

When the pressure difference along membrane is Δu and the membrane has a radius of membrane curvature, R_s and a surface tension, T_s, the force equilibrium in the vertical direction requires that

$$2\ T_s \sin\beta = 2\ \Delta u\ R_s \sin\beta \tag{2.1}$$

Where

$2\ R_s \sin\beta$ = length of the membrane projected onto the horizontal plane.

Solving for Δu in the equation gives,

$$\Delta u = \frac{T_s}{R_s} \tag{2.2}$$

The formula (2.2) gives the pressure difference across a two-dimensional curved surface with a radius, R_s, and a surface tension, T_s. For a warped or saddle-shaped surface (i.e., three-dimensional membrane), the formula (2) can be extended using the Laplace equation (Figure 2.2),

$$\Delta u = T_s\left(\frac{1}{R_1}+\frac{1}{R_2}\right) \tag{2.3}$$

where

R_1 and R_2 = radii of curvature of a warped membrane in two orthogonal principal planes.

If the radius of curvature, R_s, in the same in all directions, equation (2.3) becomes,

$$\Delta u = \frac{2T_s}{R_s} \tag{2.4}$$

2.2.2 Matric Suction

The theory of soil suction, which was established in the field of soil physics in the early 1900's, was principally developed with respect to the soil-water-plant system (Fredlund and Rahadjo 1993). Soil suction is ordinarily referred to as the free energy that the soil water possesses (Edlefsen and Anderson 1943). The free energy of the soil water can be obtained from using the terms of partial vapor pressure of the soil water (Richards 1965).

Soil suction is generally expressed as "total suction" can be quantified in terms of relative humidity. This total suction is comprised of two components: matric suction and osmotic suction. This can be written in the form of equation as following:

$$\psi = (u_a - u_w) + \pi \tag{2.5}$$

where

(u_a-u_w) = matric suction

u_a = pore-air pressure

u_w = pore-water pressure

π = osmotic suction

As shown in the above equation, matric suction is the pressure difference between air pressure and water pressure acting on the contractile skin. In addition, osmotic suction, π, is subjected to the existing chemicals (salt content) in the pore water and is generally neglected in most of geotechnical problems. Therefore, the change in the amount of total suction is equally considered as the change in the amount of matric suction, (u_a-u_w) (Fredlund, 1989; Fredlund, 1991).

Matric suction is dominated by two mechanisms which is adsorption and capillarity (Richards 1974, Yong and Warkentin 1975, Fredlund and Rahardjo 1993). Both adsorption and capillarity are main factors to change matric suction in highly plastic clays (Richards 1974). For inert soils like sands and silts, the capillarity just significantly influences the matric suction.

2.2.3 Capillarity

The phenomenon of capillarity is related to the pressure difference, (u_a-u_w), acting on the air-water interface. Fredlund and Rahardjo (1993) described the capillarity phenomenon. Consider a small glass tube that is placed inside water under atmospheric conditions. The water ascends in the tube since the surface tension in the air-water phase and the inclination of water to wet the surface of the glass tube. The surface tension, Ts, acts at a contact angle, α, with respect to the vertical. The magnitude of a contact angle is affected by the adhesion between the molecules in the contractile skin and the type of material comprising tube.

For the vertical force equilibrium of the capillary water in the tube shown in Figure 2.3, the vertical resultant of the surface tension (i.e., $2\pi\ r\ T_s\ \cos\alpha$) has responsibility of sustaining the weight of water column, which has a height of h_c (i.e., $\pi r^2\ h_c\ \rho_w\ g$). This can be expressed as following:

$$2\pi\ r\ T_s\ \cos\alpha = \pi r^2\ h_c\ \rho_w\ g \qquad (2.6)$$

where

r = radius of the capillary tube

T_s = surface tension of water

α = contact angle

h_c = capillary height

g = gravitational acceleration.

Rearranging the above equation provides the maximum height of water in the capillary tube, h_c:

$$h_c = \frac{2T_s}{\rho_w g R_s} \tag{2.7}$$

Where

R_s = radius of curvature of the meniscus (i.e., r/cosα).

If the contact angle, α, is zero in the case of pure water and clean glass), the radius of curvature, R_s, is identical to the radius of the tube, r (Figure 2.3). Therefore, the capillary height of pure water in a clean glass is

$$h_c = \frac{2T_s}{\rho_w g r} \tag{2.8}$$

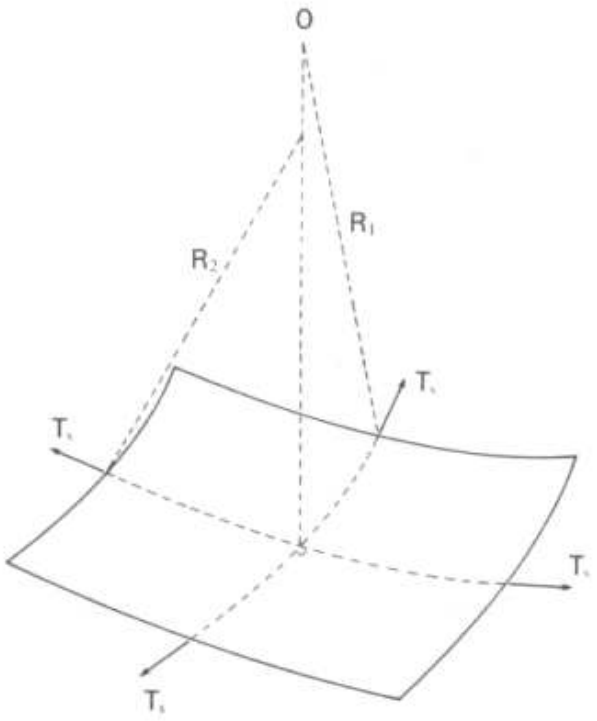

Figure 2.2 Surface Tension on a Warped Membrane (Fredlund and Rahardjo, 1993)

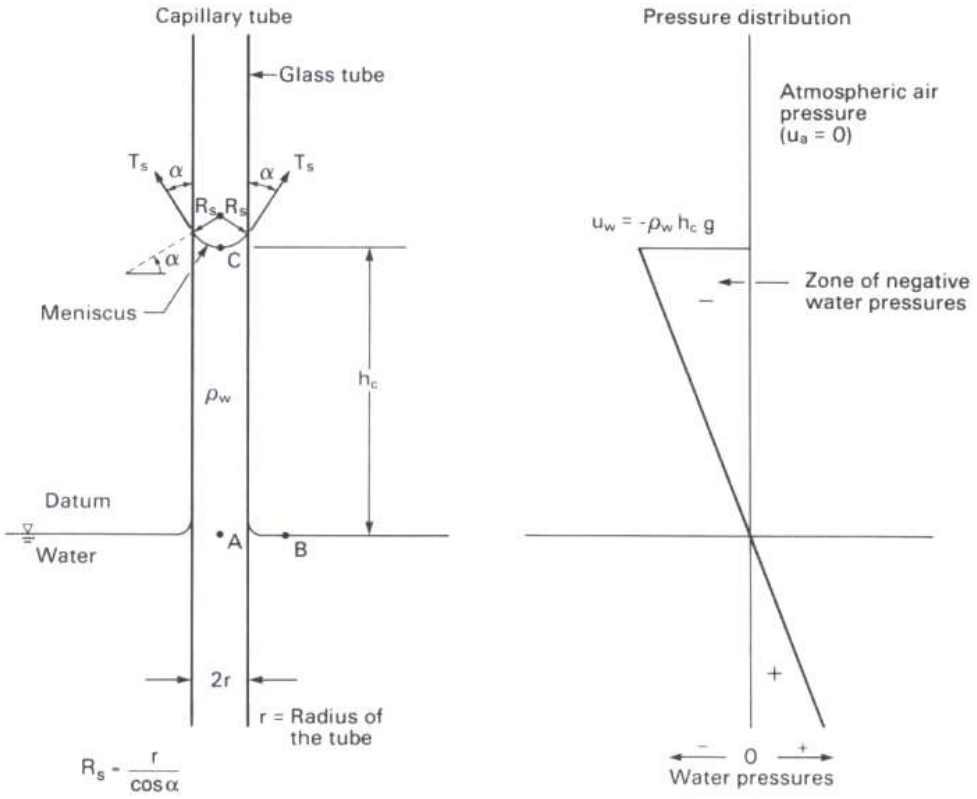

Figure 2.3 Physical Model and Phenomenon Related to Capillarity (Fredlund and Rahardjo, 1993)

2.3 History of Shear Strength Theory for Unsaturated Soils

The accurate understanding shear strength on soil necessarily is required for analyzing and solving geotechnical problems at which a certain load is applied on the soil. Terzaghi (1936) initially developed the concept of effective stress to interpret soil's strength. However, Bishop (1959) had found that the effective stress equation suggested by Terzaghi hasn't effectively reflected the strength of unsaturated soil since unsaturated soil generally showed higher strength than saturated soil. Bishop introduced new terms which are the pore air pressure, u_a and the pore water pressure, u_w, and

effective stress parameter, χ to modify Terzaghi' effective stress equation for unsaturated soil as following:

$$\sigma_n = (\sigma - u_a) + \chi(u_a - u_w) \quad (2.9)$$

This equation was used to determine effective stress in an unsaturated soil and the shear strength of unsaturated soils can be obtained from using the Mohr-Coulomb' shear strength formulation. The χ-parameter, significantly affected by degree of pore water saturation, is a material property that changes between zero and unity. However, experimental programs which found χ greater than unity indicated that χ parameter was inconsistent in predicting the effective stress of unsaturated soils. This is attributed to χ parameter is essentially material variable and therefore should not be employed in the definition of stress state. The effective stress equation including this material variable becomes the form of constitutive model rather than the definition of a stress state.

Jennings and Burland (1962) and Coleman (1962) proposed that separating the stress state variables for unsaturated soil was more adequate than incorporating them into new effective stress equation and therefore, the stress variables had to be treated independently. A null experiment performed by Fredlund and Morgenstern (1977) showed that the independent stress state variables (σ-u_a) and (u_a-u_w) could be valuably employed for describing the shear strength and volume change of unsaturated soils. Fredlund et al. (1978) developed new equation in terms of independent stress variables for the shear strength of unsaturated soil as following:

$$\tau_f = c' + (\sigma_f - u_a)_f \tan\phi' + (u_a - u_w)_f \tan\phi^b \quad (2.10)$$

Where:

c' = intercept of the "extended" Mohr-Coulomb failure envelope on the shear stress axis where the net normal stress and the matric suction at failure are equal to zero; it is also referred to as "effective cohesion"

$(\sigma_f-u_a)_f$ = net normal stress state on the failure plane at failure

u_{af} = pore-air pressure on the failure plane at failure

ø'= angle of internal friction associated with the net normal stress state variable, $(\sigma_f-u_a)_f$

$(u_a-u_w)_f$ = matric suction on the failure plane at failure

$ø^b$ = angle indicating the rate of increase in shear strength relative to the matric suction, $(u_a-u_w)_f$

2.4 Previous Work

2.4.1 Effect of Initial Soil Conditions on Unsaturated Soil Strength

Several attempts have been made in the last two decades to investigate the variation of soil strength with changing initial soil conditions such as water content (or degree of saturation) and density. Murthy et al. (1987) performed drained triaxial compression tests on two compacted unsaturated clayed soils to examine variation of soil strength due to change in degree of saturation. During the tests, all the other factors such as soil fabric and void ratio were kept constant. The results showed that at any consolidation pressure, starting from low degree of saturation, the compression strength at failure increased with an increase in degree of saturation upto a certain optimum

value beyond which the strength drops due to further increase in degree of saturation (Figure 2.4 and 2.5).

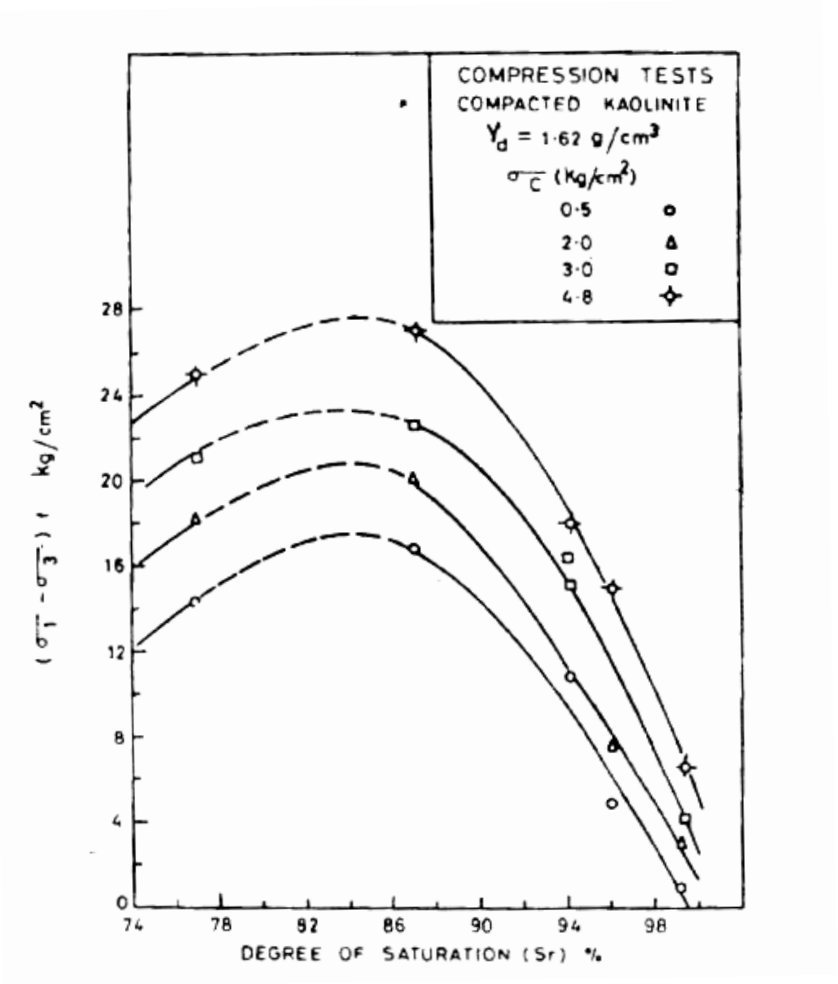

Figure 2.4 Maximum Deviator Stress vs. Degree of Saturation for Kaolinite (Murthy et al., 1987)

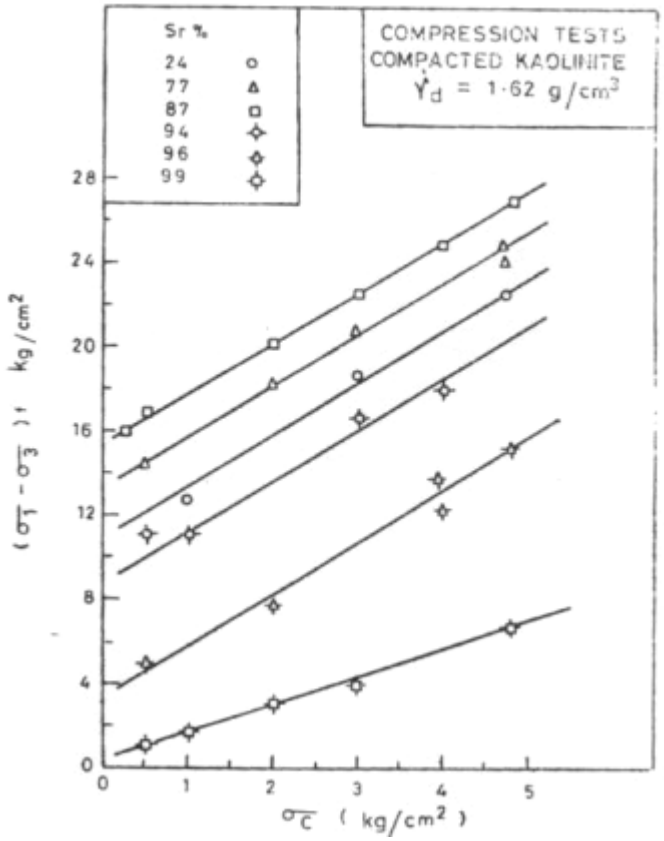

Figure 2.5 Maximum Deviator Stress vs. Consolidation Pressure for Kaolinite (Murthy et al., 1987)

Wiebe et al. (1998) carried out triaxial compression tests on unsaturated sand-bentonite buffer at elevated temperatures and pressure to investigate the effect of degree of saturation on unsaturated soil strength. Specimens were statically compacted to a constant dry density of 1.67 Mg/m^3 and to degrees of saturation between 35 and 98%. During the tests, air and water drainage line were kept closed. Figure 2.6 shows typical curves of deviator q versus axial strain ε_1. As the saturation increase, the shear strengths and stiffness increase in both Figure 2.6(a) and Figure 2.6(b). Failure modes are

predominantly ductile except the brittle failure in Figure 2.6(a) for degree of saturation $S_r = 50\%$.

Maaitah and Mahadin (2004) performed direct shear testing on unsaturated silty clay to investigate the behaviour of unsaturated soil as the degree of saturation changes. Specimens were prepared with initially different saturation to simulate different conditions. Figure 2.7 and 2.8 present the relationship between the degree of saturation and shear strength. As the initial degree of saturation increases up to 50%, the shear strength increases and then decreases as the initial saturation increases beyond 50%. Figure 2.9 and 2.10 show the results of the consolidated drained tests (CD) on fully saturated samples and the tests on the unsaturated samples. It is clear that the values of deviator stress from unsaturated sample are greater than those from the CD tests. The slope M has been found as the saturation changes from as the saturation changes from 2 to 90% when the void ratio is of 68% equals 2.21 ± 0.04 and 2.17 ± 0.04. Figure 2.11 shows the effect of initial void ratio on unsaturated strength. The shear strength increases as the void ratio decreases. It can be concluded that the density and the number of contact between the soil particles affect the shear strength of unsaturated soil. In other word, the better shear strength can be attainable through the better compaction below the roads.

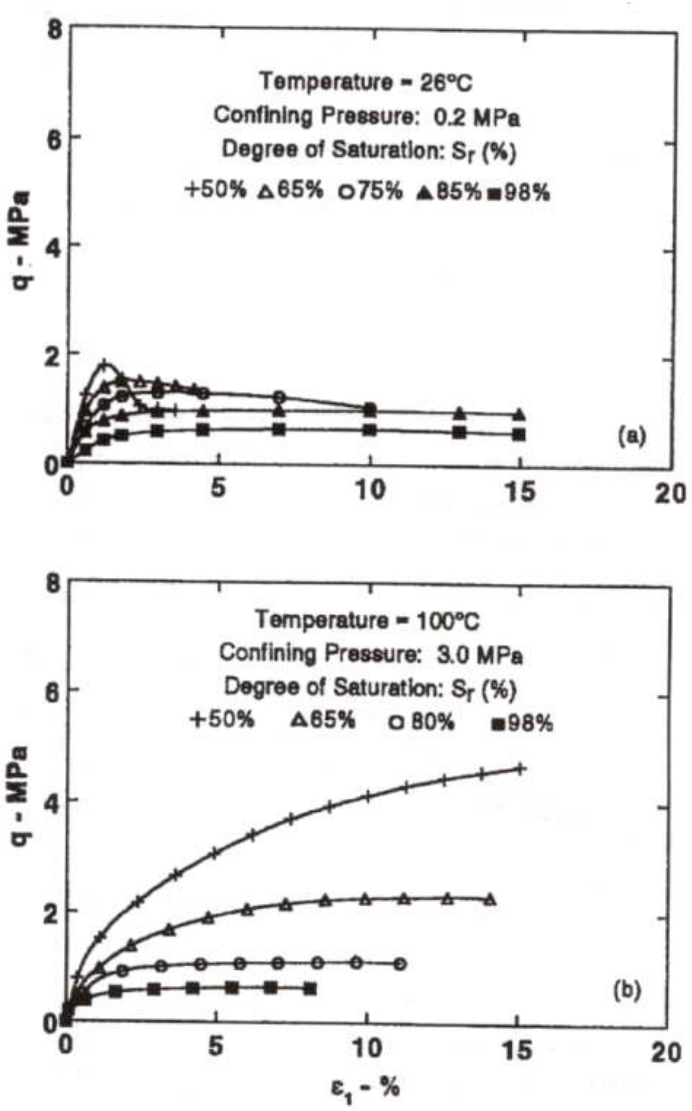

Figure 2.6 Typical Deviator Stress vs. Axial Strain Curves: (a) Low Temperatures and Pressures (26˚C and 0.2 MPa confining pressure), (b) High Temperatures and Pressures (100˚C and 3.0 MPa) (Wiebe et al., 1998)

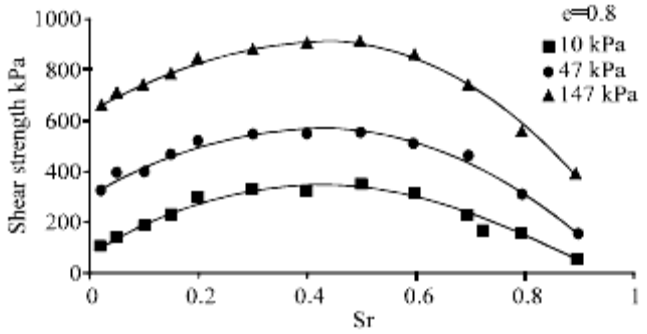

Figure 2.7 Shear Strength versus Degree of Saturation for Initial Void Ratio of 0.8 (Maaitah and Mahadin, 2004)

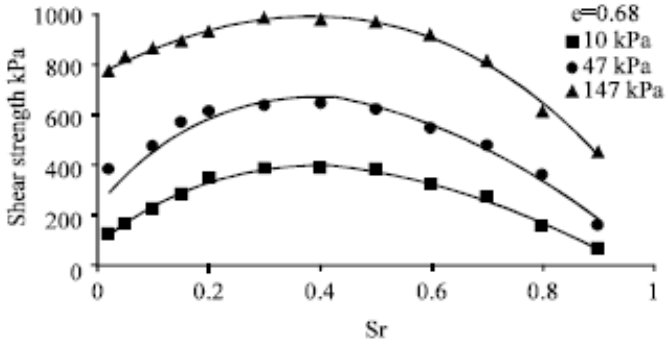

Figure 2.8 Shear Strength versus Degree of Saturation for Initial Void Ratio of 0.68 (Maaitah and Mahadin, 2004)

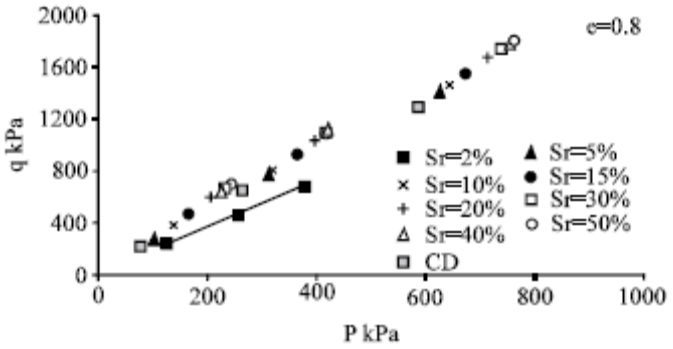

Figure 2.9 Effect of Saturation on the Strength in P-q Diagram when $S_r \leq 50\%$ (Maaitah and Mahadin, 2004)

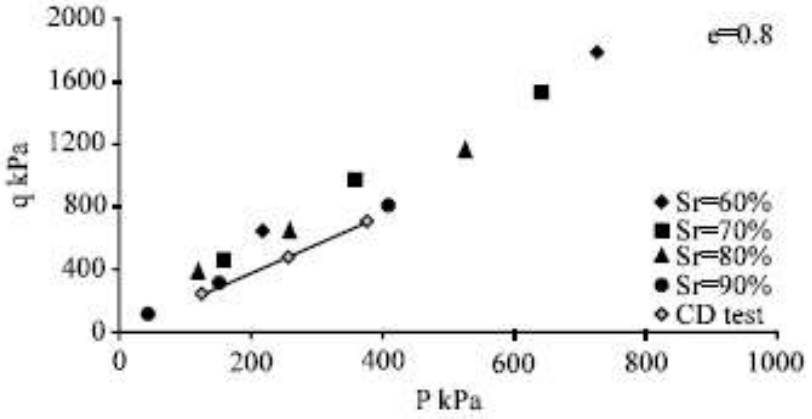

Figure 2.10 Effect of Saturation on the Strength in P-q Diagram when $S_r \geq 50\%$ (Maaitah and Mahadin, 2004)

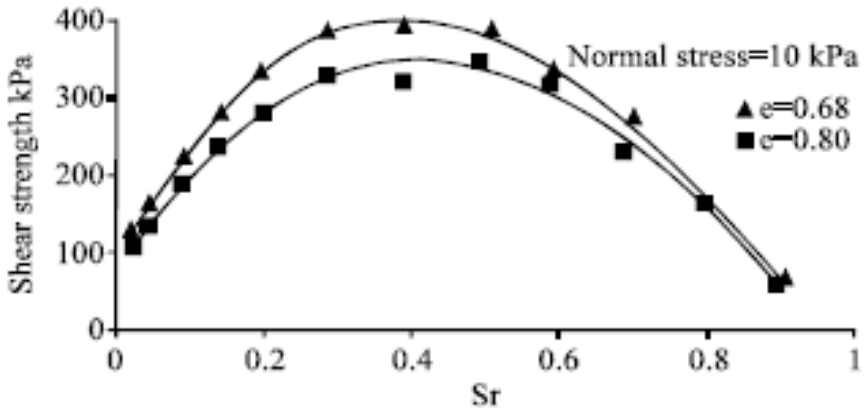

Figure 2.11 Effect of Initial Void Ratio on Unsaturated Strength (Maaitah and Mahadin, 2004)

Chen et al. (2005) carried out a series of triaxial tests to investigate the effect of initial dry density on the strength of unsaturated expansive soils. Samples were prepared with three initially different dry densities (1.42, 1.48, and 1.54)g/cm^3 for each test. Each test was repeated for three different suctions 50, 120, and 200 kPa. Figure 2.12 and 2.13 shows shearing characteristics of soils and variation of cohesive strength with different

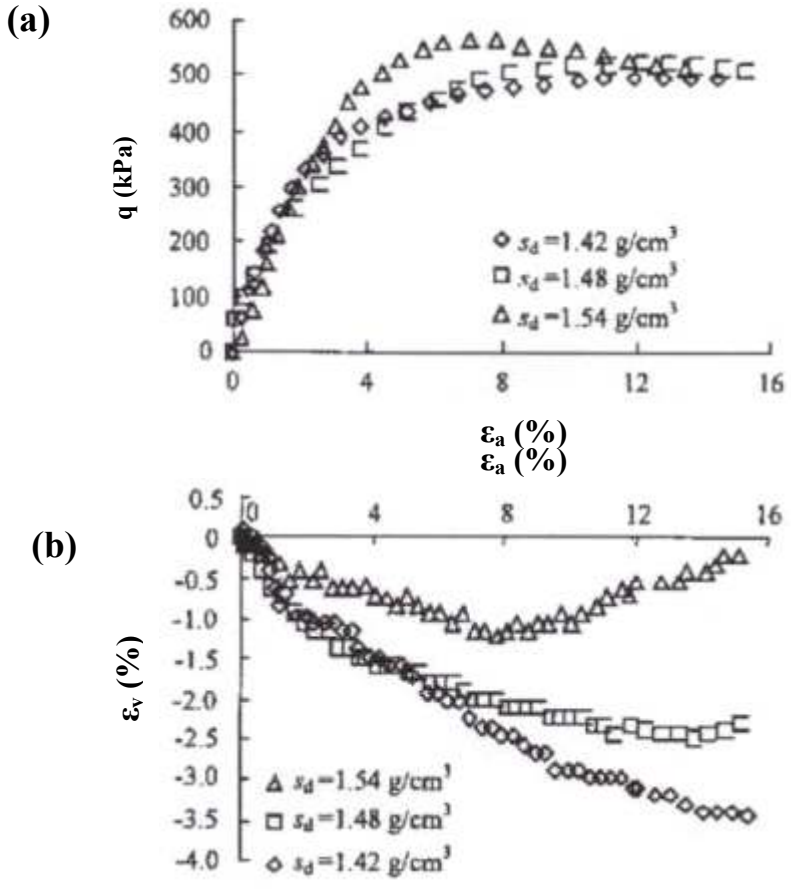

Figure 2.12 Shearing Characteristics of Soils with Different Initial Dry Densities (s = 120 kPa, (σ-u_a) = 200 kPa): (a) Deviator Stress vs. Axial Strain, (b) Volumetric Strain vs. Axial Strain (Chen et al., 2005)

initial dry densities. Soils with higher initial dry densities exhibit higher strength and more tendency to dilate when shearing.

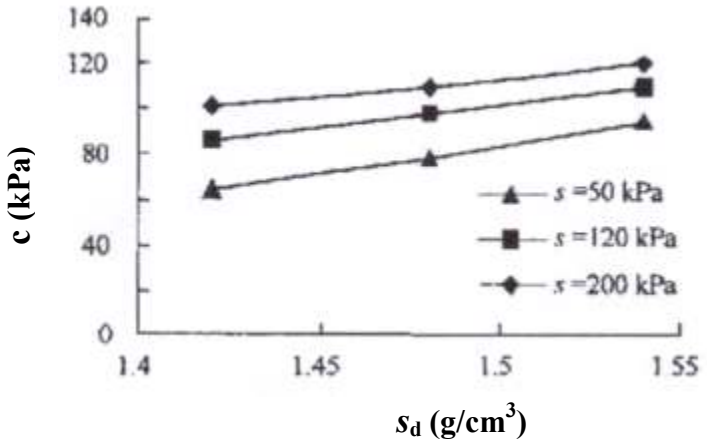

Figure 2.13 Variation of Cohesive Strength with Initial Dry Densities (Chen et al. 2005)

Maaitah (2005) investigated the behaviour of unsaturated soil at low degree of saturation. Thirty-six tests were carried out with initial degree of saturation (2, 5, 10, 15, 20, 25, 30, 40, 50, 60, and 80) % for each test. Each test was repeated for three different cell pressures 10, 50, and 100 kPa. During the testing, void ratio was 0.68 and the effective particle radius was 0.001 mm. Figure 2.14 presents relationship between degree of saturation and shear strength. As the degree of saturation increase from about 2% up to about 40% the shear strength increases and then it decreased as the saturation level increases. Figure 2.15 and 2.16 show critical state lines on the (q:p) plane and slopes of the unsaturated critical state line are parallel to those of the saturated lines.

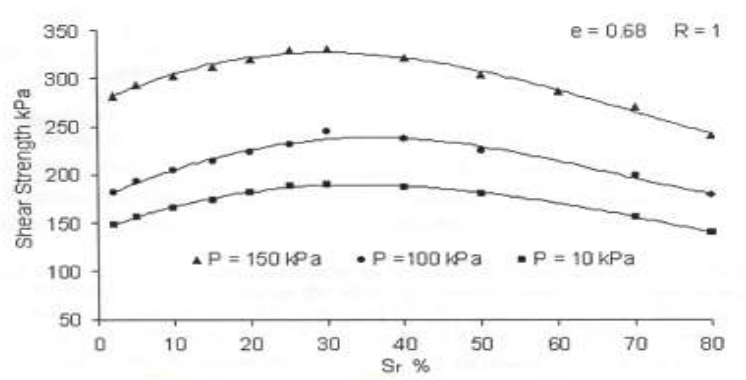

Figure 2.14 Relationship between Degree of Saturation and Shear Strength (Maaitah, 2005)

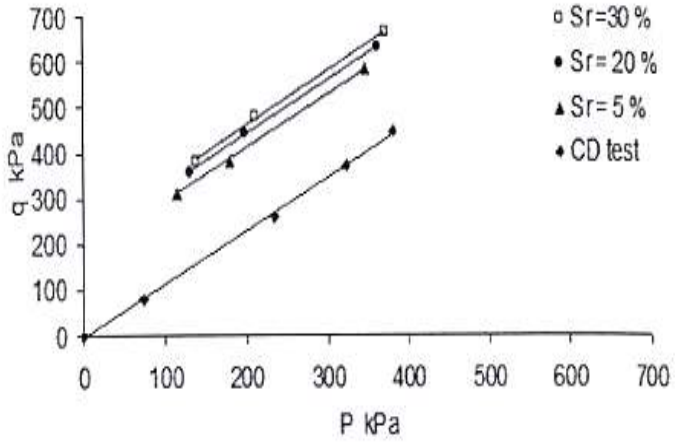

Figure 2.15 P-q Diagram for Unsaturated Sample (R = 0.001 mm, e = 0.68) (Maaitah, 2005)

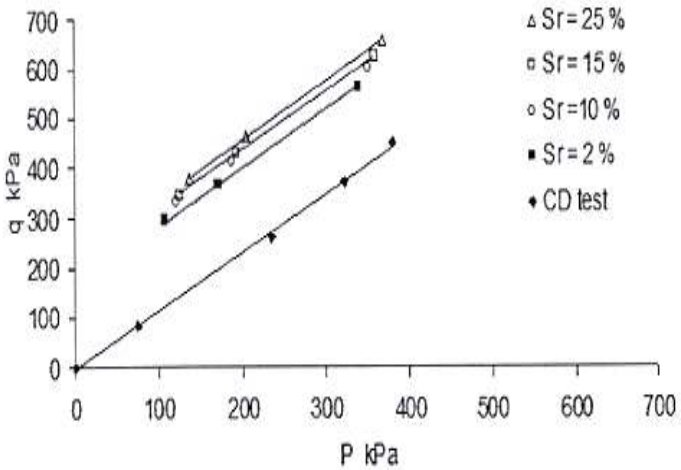

Figure 2.16 P-q Diagram for Unsaturated Sample (R = 0.001 mm, e = 0.68) (Maaitah, 2005)

2.4.2 True Triaxial Testing

In the last half century, various true triaxial testing devices have been developed for measuring stress-strain behavior of materials along multiaxial stress states. Kjellman (1936) developed the first loading device that applies a multiaxial stress state to a cubical soil specimen. Approximately 2.5 inch (62 mm) cubical specimens were used for testing and the maximum pressure of 182 psi was attainable. Kjellman employed rigid loading platens to apply three normal stresses to the specimens. The effect of the intermediate principal stress on failure condition was demonstrated by performing hydrostatic, one-dimensional, and triaxial tests on dry sand. However, the device was mechanically complex, and therefore, it had only limited usage.

Ko & Scott (1967) first employed flexible membranes in true triaxial testing device. Each surface of the cubical specimen was pressurized by a thin rubber membrane using fluid pressure as the loading mechanism. Therefore, shearing stress would not develop and each face of the cubical specimen could be loaded by a uniform stress. However, the use of a metal spacer frame in the apparatus for dividing sections betweens the pressure cell may have led to the no uniform stress at the edge of the specimen. The apparatus was used to investigate the deformation behavior of sand under hydrostatic compression, shear deformation, and deformation at failure.

Atkinson (1972) developed a cubical test cell for multiaxial testing of rock materials. Flexible membranes were used in the device and had an additional seal for preventing membrane rupture. The material for sealing membranes was selected

differently depending on applied pressure. Atkinson used a proximeter probe system to measure deformation, not monitoring the volume change of pressure fluid. This system contained three probes mounted on each wall and the deformation of each face was obtained from averaging three reading recorded by probes. The pressure was applied to the specimen using a high pressure hydraulic pump.

Janoo (1986) developed a high-pressure computer-controlled true triaxial testing device for measuring drained and undrained behavior of a well graded sand. This system had pore pressure measurements at the surface or at the center of cubical specimen. A Linear Variable Displacement Transducer (LVDT) was used for measuring the deformation of specimen. Similar to Atkinson's probe system, three LVDTs were mounted into each cell wall and the deformation of each face was obtained from averaging three reading recorded by the LVDTs. Pressures necessary for testing was manually provided using a high pressure hydraulic pump. Drained and drained hydrostatic compression, uniaxial compression (K_0), and true triaxial compression tests in different b planes were performed.

Reddy et al. (1992) developed a stress-controlled, flexible boundary, true triaxial testing device to measure the behavior of cemented sand under various stress paths. The deformation of the specimens was measured at four points on each of its six surfaces using 24 LVDTs. This system had drainage and pore water pressure monitoring port machined diagonally through the frame. Tests were carried out along different stress paths containing hydrostatic compression, conventional triaxial compression, and along different directions on octahedral planes.

Hoyos and Macari (2001) developed a computer-driven, mixed-boundary type, stress/suction-controlled true triaxial testing device to investigate the behavior of unsaturated soils, under suction-controlled condition, along multiaxial stress paths. In fact, the device was modified for further testing on silty and clayed soils from that developed by Atkinson (1972) for multiaxial testing of rock materials. The device was a mixed boundary type. The specimen was seated on top of a saturated high-air-entry disk and between five flexible membranes on the remaining sides of the cube. The device had the ability to apply two independent pore-air pressure and pore-water pressure. The axis-translation technique was used to initially induce and constantly maintain matric suction during testing. A series of hydrostatic compression, conventional triaxial compression, triaxial compression, and simple shear test in the first octant of the octahedral stress plane was carried out. Test results showed the nature of principal strain response under multi-axial stress path and the influence of matric suction on the shape, size, and position of the failure envelopes in the octahedral stress plane.

Park (2005) developed a stress-controlled, flexible boundary, true triaxial testing apparatus to investigate the mechanical behaviour of partially saturated silty sand along mutliaxial stress paths. 3-inch cubical samples were prepared at four different moisture content via a dual-mesh pluviation technique. Tests were performed along different stress paths containing hydrostatic compression, conventional triaxial compression, and along different directions on octahedral planes. The results showed that initial soil suction induced by initial water content play an important role in the stress-strain behaviour of partially saturated silty sand.

CHAPTER 3

TRUE TRIAXIAL TESTING APPARATUS

3.1 Introduction

This chapter describes the true triaxial testing device used in this thesis. It has been developed to apply multiaxial stress paths and controlled matric suctions to cubical specimens. The suction-controlled capabilities are beyond the scope of the present work. The core system of the device including main frame, wall assemblies, external water-based pressure hydraulic system, LVDT-based deformation measuring system, and DA/PCS was manufactured at the University of Colorado-Boulder, under direct supervision of Prof. Stein Sture and was assembled at the University of Texas at Arlington, under direct supervision of Professor Laureano Hoyos (Park, 2005).

In the present work, a series of undrained and drained true triaxial tests have been carried out to investigate the mechanical behaviour of kneading-compacted unsaturated silty sand without applying controlled matric suction to the samples.

3.2 Apparatus Description

The true triaxial device is made up of the following nine principal components or modules: (1) a frame, (2) six wall assemblies, (3) a deformation measuring system, (4) a stress-control system, (5) six membranes, (6) a pore-air pressure controlling/monitoring system, (7) a pore-water pressure controlling/monitoring system,

(8) an air/water supply pressure board, and (9) a data acquisition and process control system.

A detailed description of the components was reported by Park (2005). A brief description of the device is presented.

1. Frame: A photograph of the cubical frame is shown in Figure 3.1. Solid aluminum was used for machining the frame. The outside and inner square cavities of the frame were machined to a dimension of 3.07 in and 9.09 in respectively. The function of the frame is to support the top, bottom, and lateral wall assemblies. The narrow inner cavities were machined into each of the six faces of the frame available to accommodate the membranes and shape pressure cavities. The connection bolts were equipped for the each face of the frame to fix the wall assemblies. Drainage and pore-water pressure monitoring ports are machined diagonally through the frame (Reddy et al. 1992).

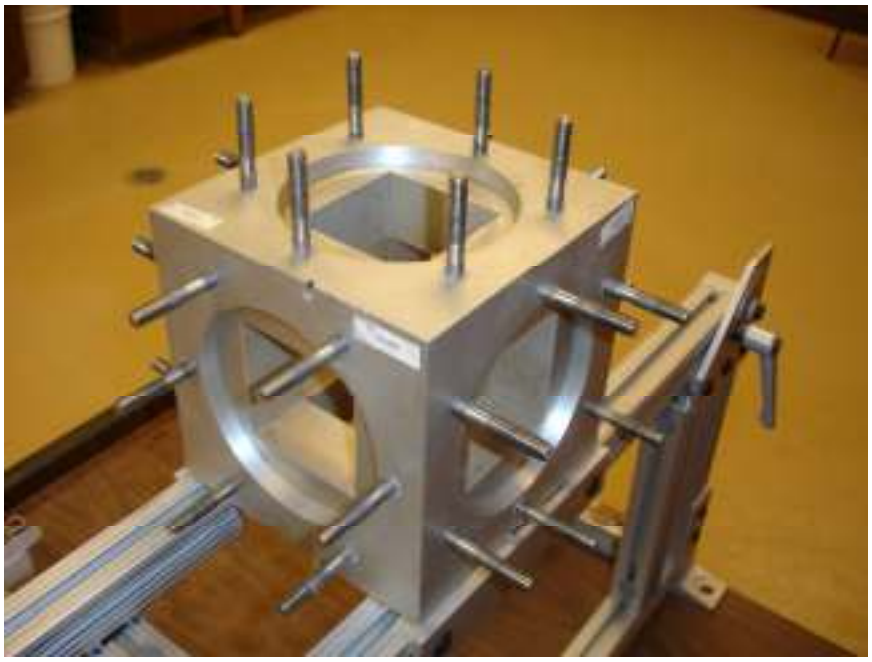

Figure 3.1 Isometric Photograph of the Frame

2. Wall Assemblies: A detailed cross-sectional view of the complete wall assemblies are shown in Park (2005). The wall assemblies were also machined from solid aluminum. Each wall assembly consist of the following three components: (1) a main cover plate equipping interior pressure cavities with the wall seal, (2) a pressure inlet/outlet connection, (3) three threaded holes machined into each cover plate to receive the stainless steel housing of three linear variable differential transformers (LVDT). Figures 3.2 and 3.3 show the cross sectional view and photograph of the wall assembly.

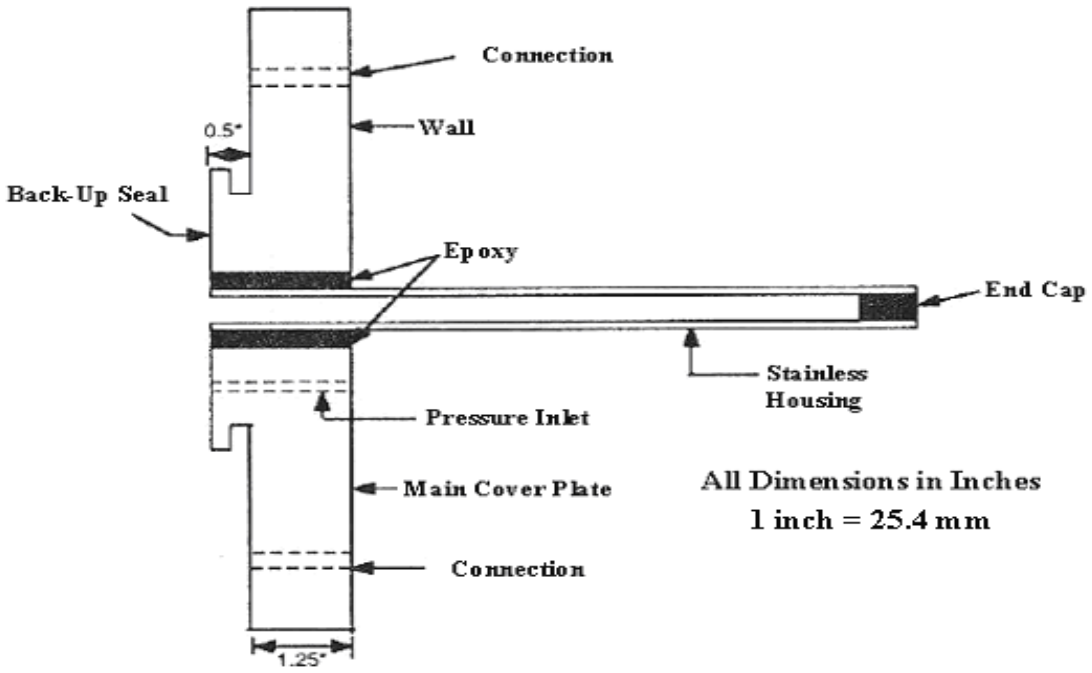

Figure 3.2 Cross-Sectional View of Wall Assembly (Reddy et al. 1992)

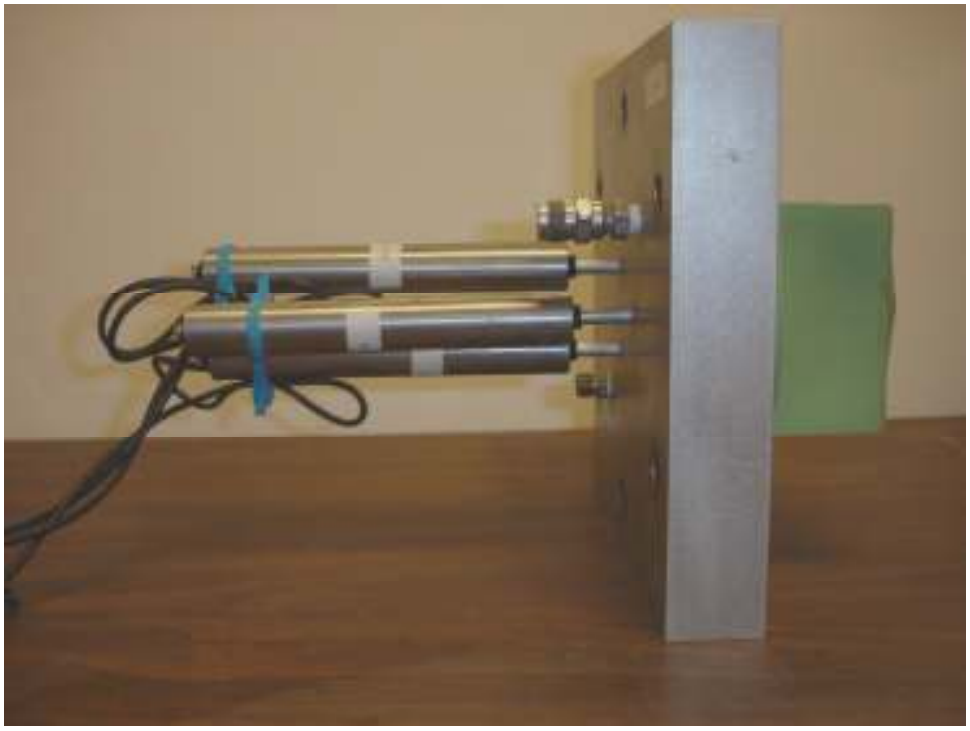

Figure 3.3 Photograph of the Wall Assembly

3. A Deformation Measuring System: 18 high-pressure sealed LVDTs were used for measuring specimen deformations. Three LVDTs are located at three points with a 120° spacing on a 3.18-cm radius on each of the top and lateral faces. A spring allows the core of each LVDT and its extension rod to be thrust into contact with flexible membrane as shown in Figure 3.4. LVDTs' excitation and output are controlled and recorded by means of a data acquisition system. A detail of LVDT calibration is available in Park (2005).

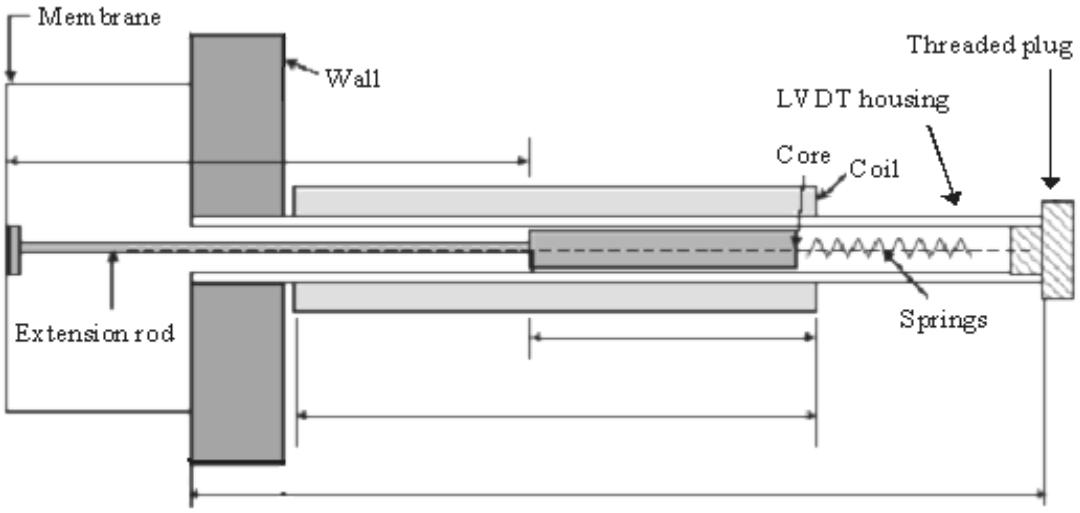

Figure 3.4 Deformation Measuring System (Park, 2005)

4. Stress Application and Control System: The stress control system used in this study is composed of three components: digital pressure gage, valves, and manual precision pressure regulators (Figure 3.5). A schematic of the stress control system is shown in Figure 3.6. The system allows the operator to generate all three independent principal stresses to specimen in the cubical cell. Any desired stress path can be obtained from simultaneous manipulation of the three regulators. The pressure can be measured up to 200 psi (1378 kPa) by three DPG 500 OM, absolute pressure transducers, which were produced by Omega Engineering.

Figure 3.5 Photograph of Stress Control System

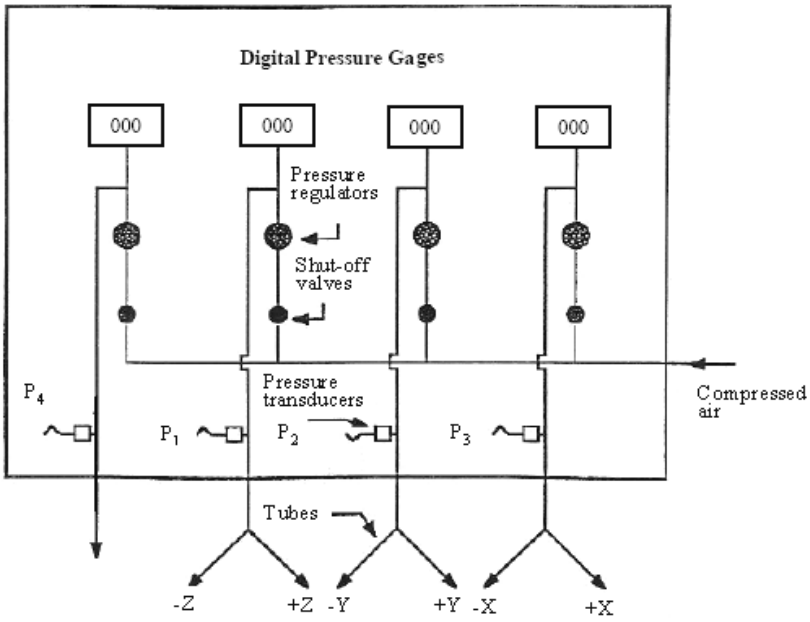

Figure 3.6 Schematic of Stress Application and Control System (Park, 2005)

5. Membranes: The main function of membranes is to uniformly distribute a fluid or pneumatic pressure applied behind membranes to the specimen. Flexible Membranes used in this study were manufactured from the material of Dow Corning silicone rubber which exhibit high tear strength and low stiffness. The dimension of membranes was designed using an assembly containing top and bottom molds machined from aluminum. The procedure of manufacturing membranes is detailed in Park (2005).

6. Data Acquisition and Process Control System (DA/PCS): A schematic of an automated DA/PCS is shown Figure 3.7. The system control the external pressure applied to the specimen and monitor/record its resulting deformation. An analog-to-digital converter (SCB-100 from National Instruments), plugged into the CPU of the PC-based computer, convert the analog input signals (Volt) delivered by the LVDT into digital output signals. DC Power Supply (6303D from Topward), connected to the analog-to-digital converter, was used for signal conditioning. A computer software (Labview 7.0 from National Instruments) makes it possible to record the deformation of specimen.

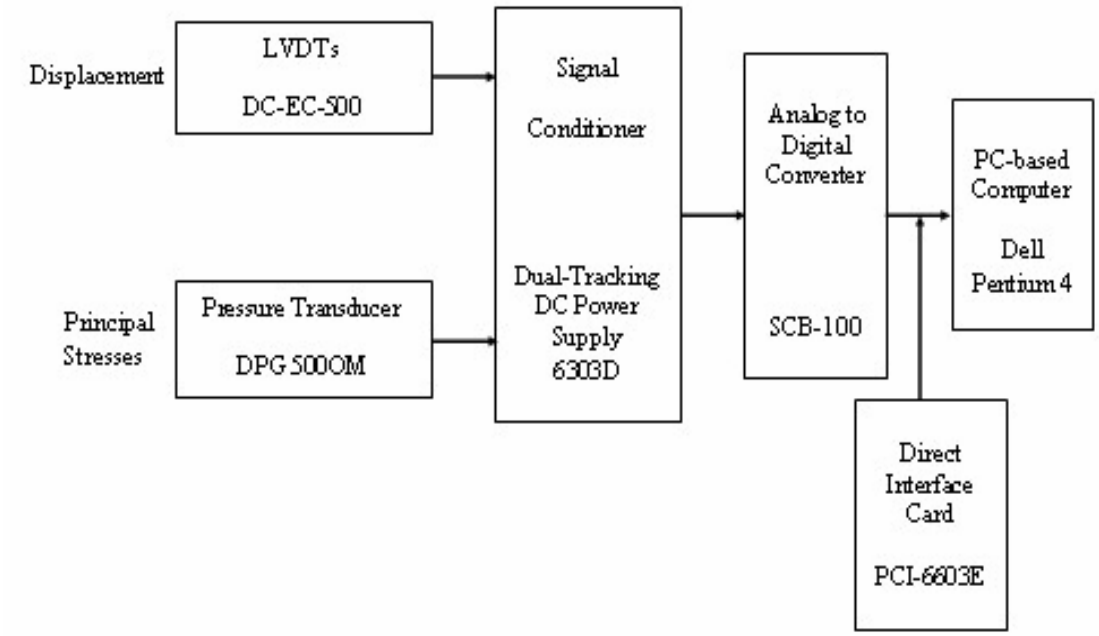

Figure 3.7 Schematic of Data Acquisition System (Park, 2005)

3.3 Step-By-Step Assembling Process

A summary of step-by-step procedure for the entire assemblage of the true triaxial testing setup is described below (Park, 2005).

(1) The bottom wall assembly is first attached at the bottom side of cubic frame in Figure 3.8.

(2) The cubical specimen ready for testing is placed on the top of bottom wall assembly in Figure 3.9.

(3) Four lateral wall assemblies are assembled in Figure 3.10.

(4) The top wall assembly is assembled in Figure 3.11.

(5) After checking all wall assemblies tightened with frame, the inlet/outlet hoses of the pressure system are connected to all six wall assemblies in Figure 3.12.

Figure 3.13 shows a photograph of the complete laboratory testing setup.

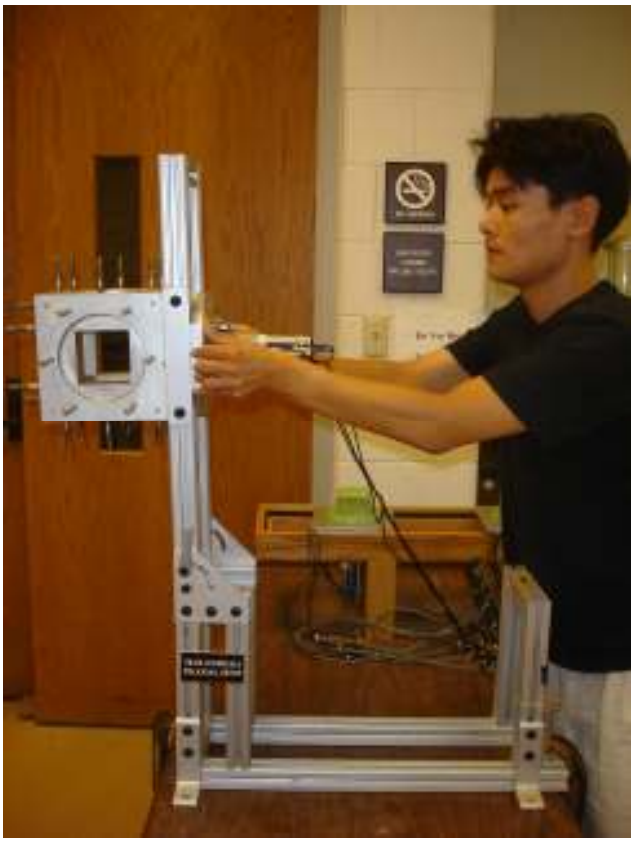

Figure 3.8 Photograph of Bottom Wall Assembling Process

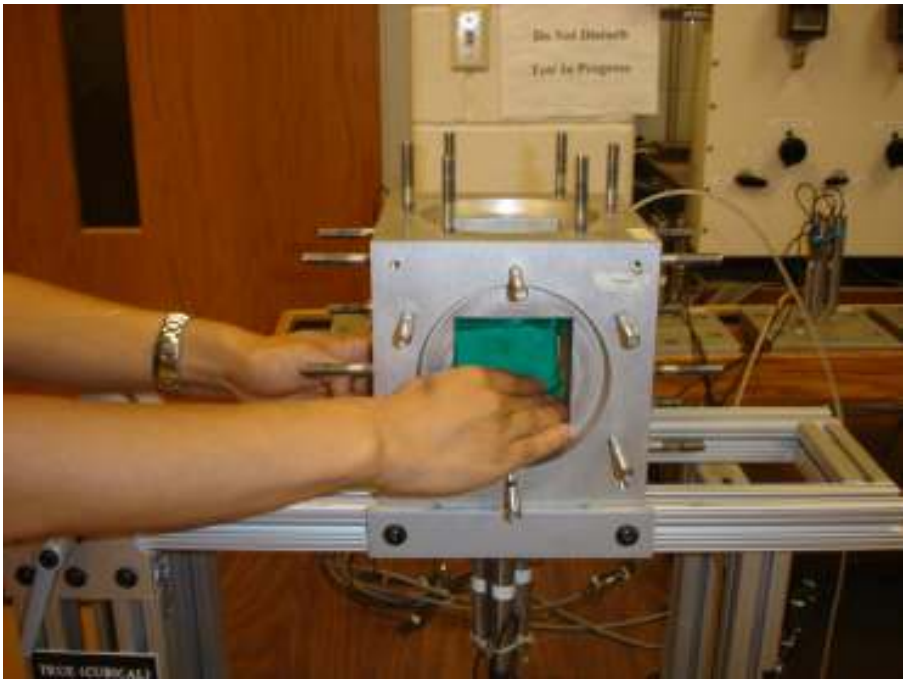

Figure 3.9 Photograph of Specimen Placement Process

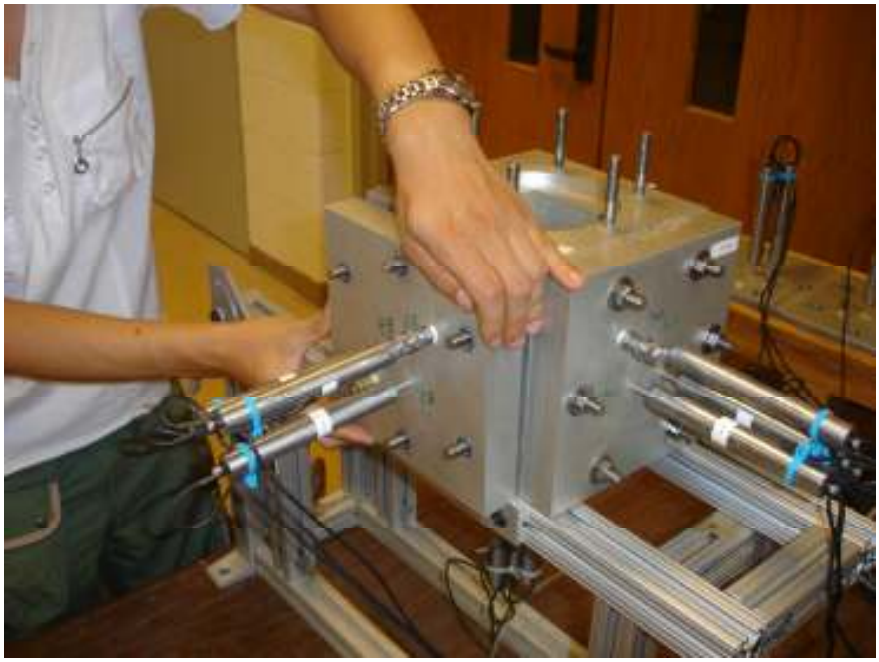

Figure 3.10 Photograph of Lateral Wall Assembling Process

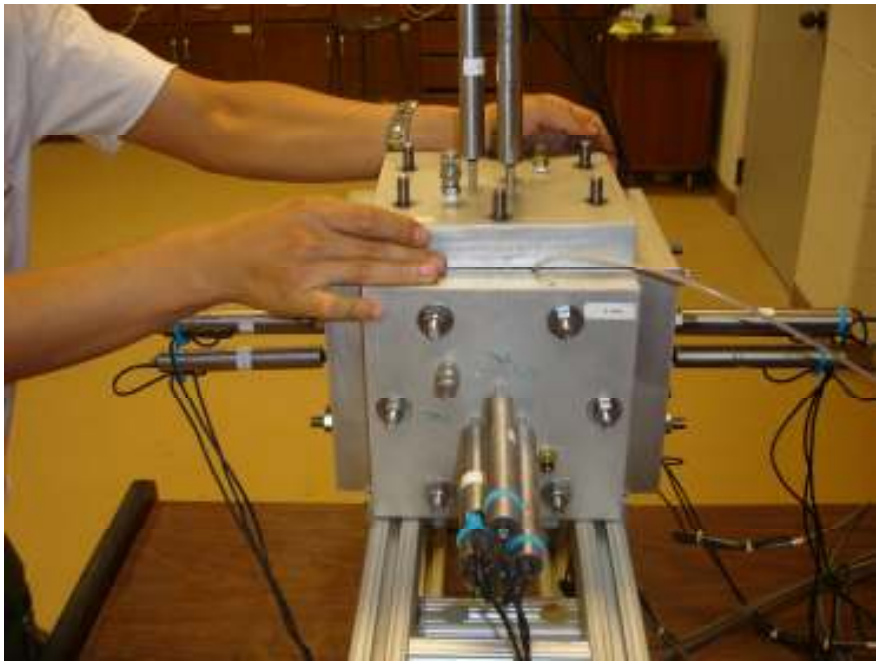

Figure 3.11 Photograph of Top Wall Assembling Process

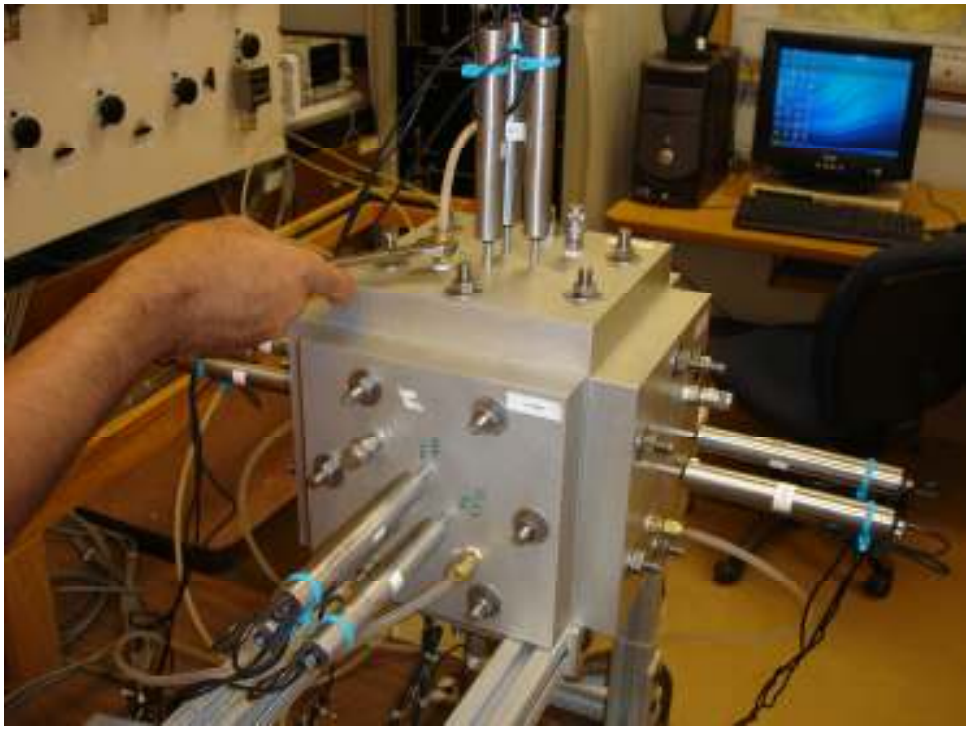

Figure 3.12 Photograph of Inlet/Outlet Assembling Process

Figure 3.13 Photograph of the Complete Testing Setup

CHAPTER 4

EXPERIMENTAL VARIABLES AND TEST PROCEDURES

4.1 Introduction

The experimental program in this thesis is aimed at investigating the stress-strain-strength behaviour of unsaturated silty sand under drained and undrained condition along various multiaxial stress paths. In order to generate initially different soil conditions, unsaturated silty sand samples were prepared at three different water contents.

The following sections provide the description of soil used in this investigation, sample preparation method, initial soil state induced by kneading compaction with spring hammer, soil water characteristic curve (SWCC), experimental variables, and test procedures.

4.2 Soil Description

The soil used in this work was obtained from mixing 30% of silt and 70% of clean sand. The optimum moist content via kneading compaction using a 10-mm diameter spring hammer is approximately 11.5% and results in a maximum dry unit weight of 18.66 kN/m^3. Figure 4.1 shows the results from sieve and hydrometer analyses with a D_{10} of 0.017mm.

The soil is classified as SP-SM according to USCS. The basic engineering properties of testing soil are tabulated in Table 4.1.

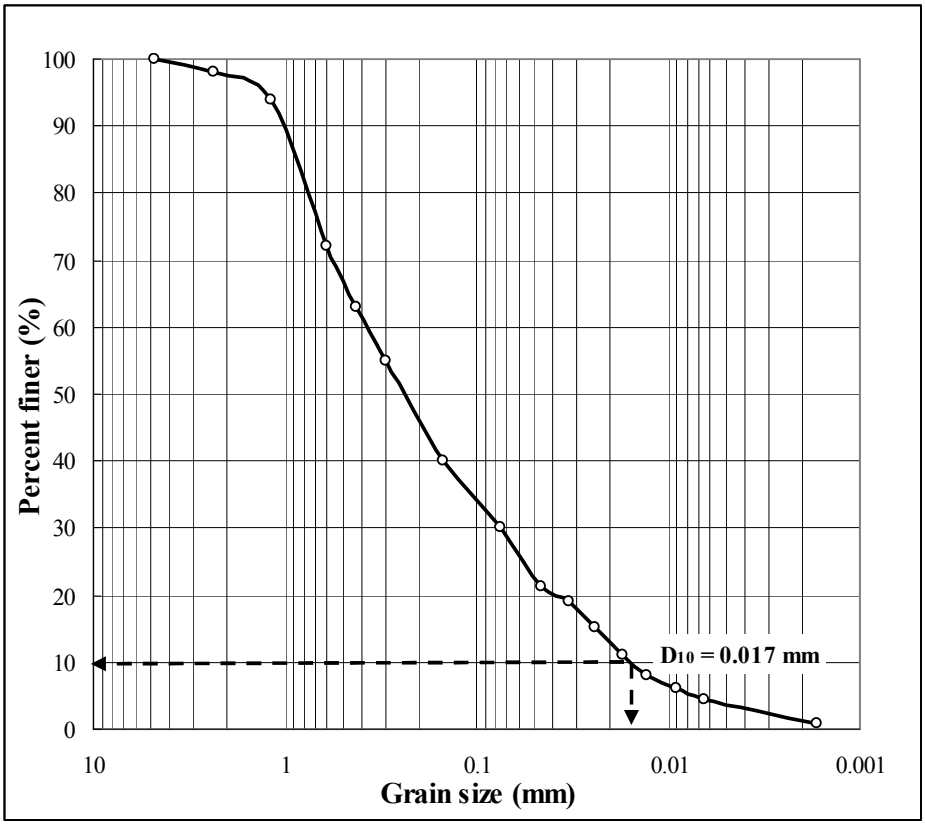

Figure 4.1 Sieve and Hydrometer Analyses for Prepared Silty Sand

Table 4.1 Basic Engineering Properties of Testing Soil

Property	**Result**
Optimum moist content with kneading compaction, w_{opt} (%)	11.5
Maximum dry unit weight with kneading compaction, $\gamma_{d\text{-}max}$ (kN/m^3)	18.66
USCS Classification	SP-SM
D_{10}(mm)	0.017

4.3 Sample Preparation Method

Sample preparation procedure is similar to that reported by Park (2005). However, in this work, kneading compaction by spring hammer was used to ensure uniform density of sample instead of pluviation technique.

Specimens in this work were prepared using compaction of spring hammer at three different initial moist contents. After mixing 30% of silt and 70% of clean sand, the required amount of distilled water was added into soil. The soil was then thoroughly hand mixed. This procedure resulted in a uniform soil-water mixture with little or no soil-water clods. The mixed soil was then compacted in five equal layers into a specially designed, 3-in by 3-in, 3-in in height, transparent specimen preparation mold, as shown in figure 4.2 (a). Each layer was compacted using a 10-mm diameter spring hammer shown in figure 4.2(b) and 4.3. After entire compaction for specimen was completed, a thin nylon tube was inserted through the tope groove of the mold and a filter paper was placed under the inside end of the nylon tube. Further details of the specimen setup procedure are available in Park (2005).

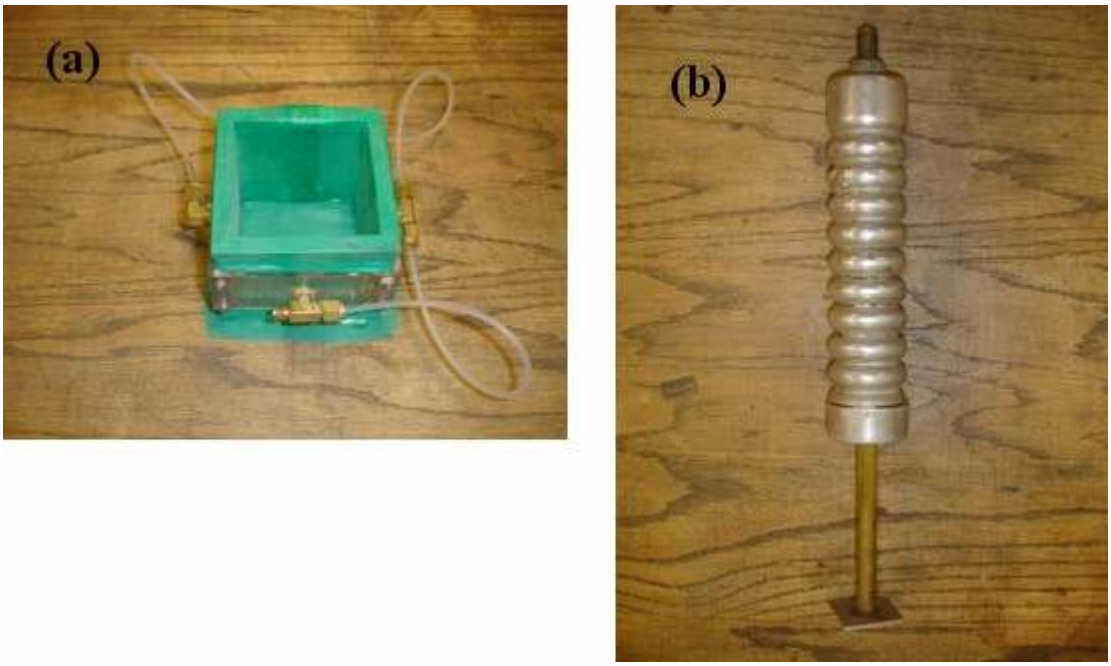

Figure 4.2 Specimen Compaction Device:
(a) Photograph of Specimen Preparation Mold, (b) Photograph of Spring Hammer

Figure 4.3 Photograph of Kneading Compaction for Specimen Preparation

4.4 Initial Sample State and Soil Water Characteristic Curve (SWCC)

The properties of initial sample induced by spring hammer with three different initial water contents are shown in table 4.2.

Table 4.2 Initial Soil States Induced by Kneading Compaction

Initial Soil State	Water Content (%)	Dry Unit Weight (kN/m^3)	Void Ratio	Degree of Saturation (%)	Initial Total Suction * (kPa)
A	6	16.40	0.58	27	1360
B	8	17.73	0.47	45	970
C	10	18.12	0.43	61	550

* Assessed from SWCC.

The selected three initial water contents for testing are also on the dry side of optimum on a standard proctor curve.

After preparing sample, total soil suction was measured using filter paper technique to obtain Soil Water Characteristic Curve (SWCC). The figure 4.4 shows the relationship between water content and soil suction.

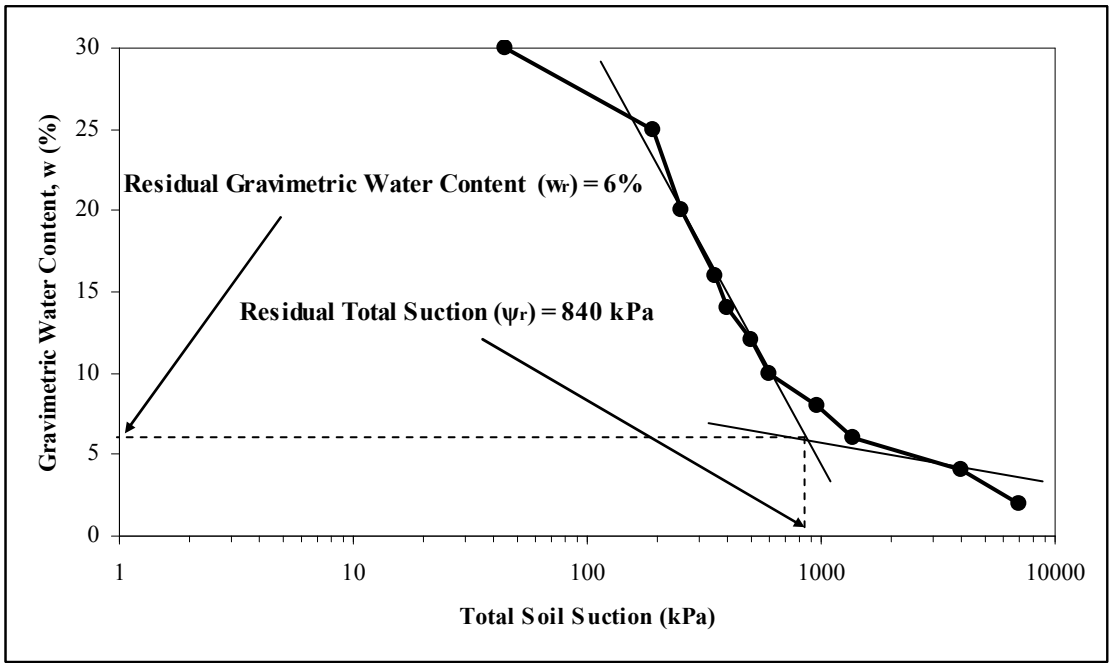

Figure 4.4 Soil Water Characteristic Curve (SWCC) of Testing Soil

4.5 Experimental Variables

Table 4.3 summarizes all the experimental variables used in this thesis work for true triaxial testing. Three different initial water contents (6, 8, and 10%) were selected for investigating the effect of initial soil conditions on unsaturated silty sand. The values of soil suction corresponding to water content of 6, 8, and 10% were 1360, 970, and 550 kPa, respectively. Six different isotropic confining pressures (5, 10, 15, 20, 30, and 40 psi) were applied according to the intended types of stress path. Tests were performed along different stress paths which include conventional triaxial compression (CTC), triaxial compression (TC), triaxial extension (TE), and simple shear (SS).

Table 4.3 Experimental Variables Used for True Triaxial Testing

Description	Number of Variables
Soil type	1. Silty sand (30% of silt and 70% of sand) • Optimum moist content from kneading compaction (w_{opt}) = 11.5% • Maximum dry unit weight from kneading compaction ($\gamma_{d\text{-}max}$) = 18.66 kN/m^3 • USCS classification = SP-SM
Initial water content	1. w = 6% 2. w = 8% 3. w = 10%
Initial compaction-induced suction	1. ψ = 1360 kPa (w = 6%) 2. ψ = 970 kPa (w = 8%) 3. ψ = 550 kPa (w = 10%)
Isotropic confining pressure	1. 5 psi 2. 10 psi 3. 15 psi 4. 20 psi 5. 30 psi 6. 40 psi
Stress path	1. Conventional triaxial compression (CTC) 2. Triaxial Compression (TC) 3. Triaxial Extension (TE) 4. Simple shear (SS)
Drainage	1. Undrained condition 2. Drained condition

4.6 Test Procedures

A similar procedure for testing partially saturated soils under multiaxial stress states and undrained condition in a true triaxial testing device (Park 2005) was followed in this work. However, tests in this program were conducted under drained as well as undrained condition.

After the cubical setup was completely assembled, the specimen was subjected to isotropic confinement and consolidated. The specimen was then loaded for shearing at a constant rate, $\Delta q/\Delta t$ = 1 psi/30min, according to the desired stress path through controlling the three independent pressure regulators. The stress paths imposed on the specimens is as following:

1. Conventional triaxial compression test (CTC)
2. Triaxial compression test (TC)
3. Triaxial extension test (TE)
4. Simple shear test (SS)

Stress paths can be expressed as stress ratio, b. The stress ratio is defined as $(\sigma_2-\sigma_1)/(\sigma_1-\sigma_3)$ where σ_1, σ_2, and σ_3 are the major, intermediate, and minor principal stresses, respectively. Figure 4.5(a) shows stress paths of conventional triaxial compression tests studied in this work. For shearing test on octahedral planes, the specimen were loaded hydrostatically to the octahedral normal stress equal to one of three levels, 20, 30, or 40 psi and then were subjected to shear stress. Stress paths on octahedral plane with a variation of the value of b are shown in Figure 4.5 (b) and (c).

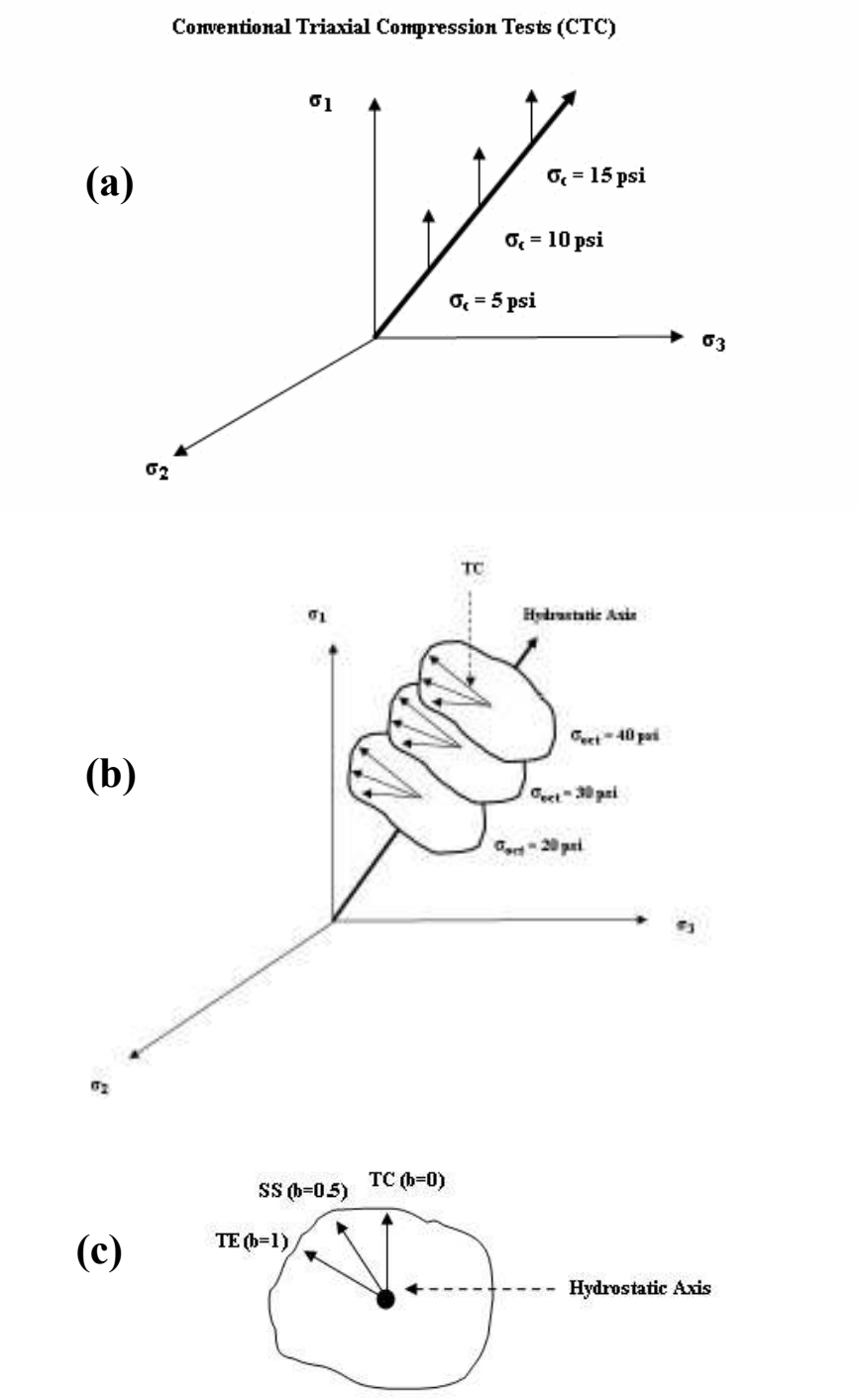

Figure 4.5 Stress Paths Studied: (a) CTC Tests ; (b) and (c) TC, TE, and SS Tests

CHAPTER 5

ANALYSIS OF TEST RESULTS

5.1 Introduction

This chapter presents all the results from the series of 36 drained and 36 undrained true triaxial tests. Results are analyzed to study the stress-strain-strength behaviour of kneading-compacted unsaturated silty sand under different confining pressures and initial compaction-induced suction states.

5.2 Notation Symbols

Notation symbols used in this thesis work are shown in Table 5.1. It was tabulated to facilitate the reading of variables such as stress paths, strains, and stresses which are used to present the stress-strain-strength behaviour of specimens.

5.3 Drained Testing

5.3.1 Introduction

The results of a series of 36 drained true triaxial tests are presented and discussed in the following sections. In section 5.3.2, the influence of octahedral stress on the stress-strain behaviour of unsaturated silty sand is presented. The influence of initial soil state on the stress-strain behaviour of unsaturated silty sand is presented in

section 5.3.3. In section 5.3.4, failure envelops on octahedral plane and critical state response on p-q diagram is presented.

5.3.2 Influence of Octahedral Stress

5.3.2.1 Conventional Triaxial Compression (CTC) Tests.

A series of 9 drained CTC tests were carried out under effective confining pressures of 5, 10, and 15 psi on silty sand at three initial moist contents: 6%, 8%, and 10%. During the tests, the intermediate and minor principal stresses were kept constant while major principal stress increased. The results of these testings are presented in Figures 5.1 to 5.3. The measured principal strains versus deviatoric stress and major principal strain versus volumetric strain are plotted in the figures respectively. As shown in the figures, the principal strains in x and y direction are much equally expansive, while the major principal strain in z direction is significantly compressive. It can be clearly seen from Figures 5.1 to 5.3 that the strength and stiffness of soil increases with an increase in octahedral normal stress. The volumetric strains (w = 6 and 8%) is predominantly compressive while the volumetric strain (w = 10%) is slightly dilative.

Table 5.1 Notation Symbols Used in This Thesis Work

Symbol	Description
CTC	Conventional Triaxial Compression
TC	Triaxial Compression
TE	Triaxial Extension
SS	Simple Shear
p	Net Mean Stress = $(1/3)(\sigma_1 + \sigma_2 + \sigma_3)$
q	Deviatoric Stress = $(\sigma_1 - \sigma_3)$
ϵ_1	Major Principal Strain
ϵ_2	Intermediate Principal Strain
ϵ_3	Minor Principal Strain
ϵ_v	Volumetric Strain = $(1/3)(\epsilon_1 + \epsilon_2 + \epsilon_3)$
σ_1	Major Principal Stress
σ_2	Intermediate Principal Stress
σ_3	Minor Principal Stress
σ_{oct}	Octahedral Normal Stress = $(1/3)(\sigma_1 + \sigma_2 + \sigma_3)$
τ_{oct}	Octahedral Shear Stress = $(1/3)\{(\sigma_1 - \sigma_2)^2 + (\sigma_2 - \sigma_3)^2 + (\sigma_3 - \sigma_1)^2\}^{1/2}$
b	Stress Ratio = $(\sigma_2 - \sigma_3) / (\sigma_1 - \sigma_3)$

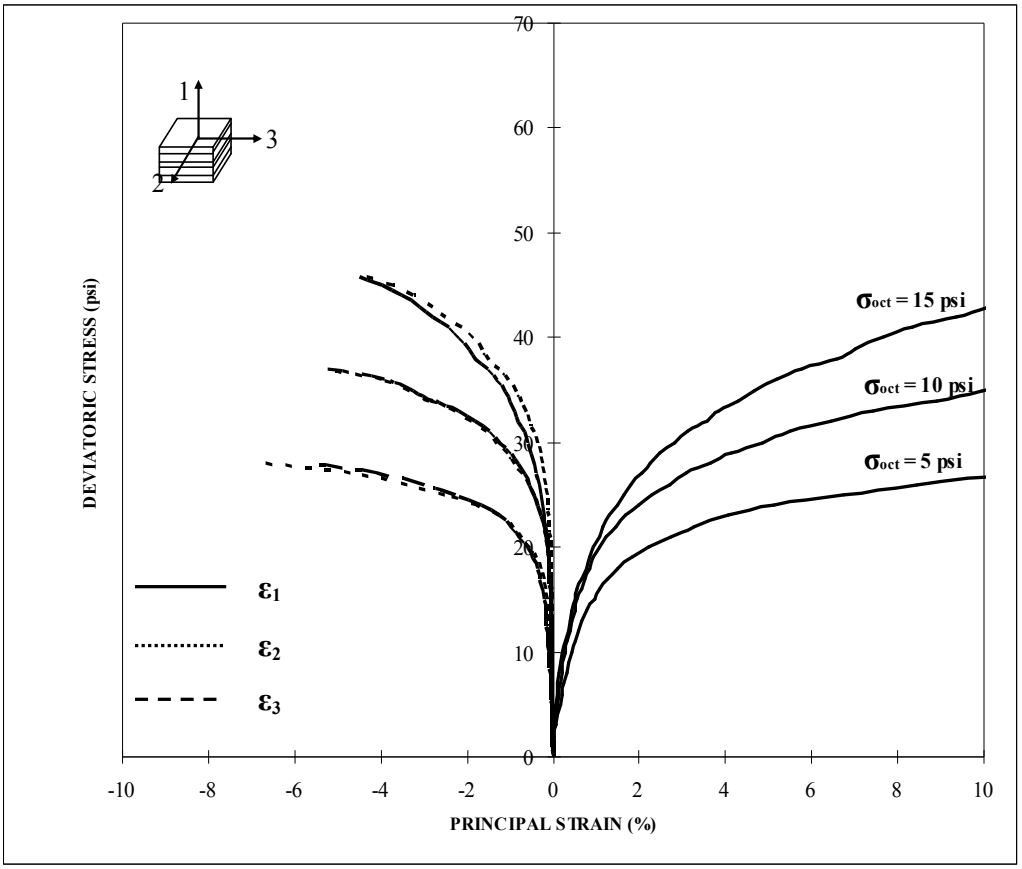

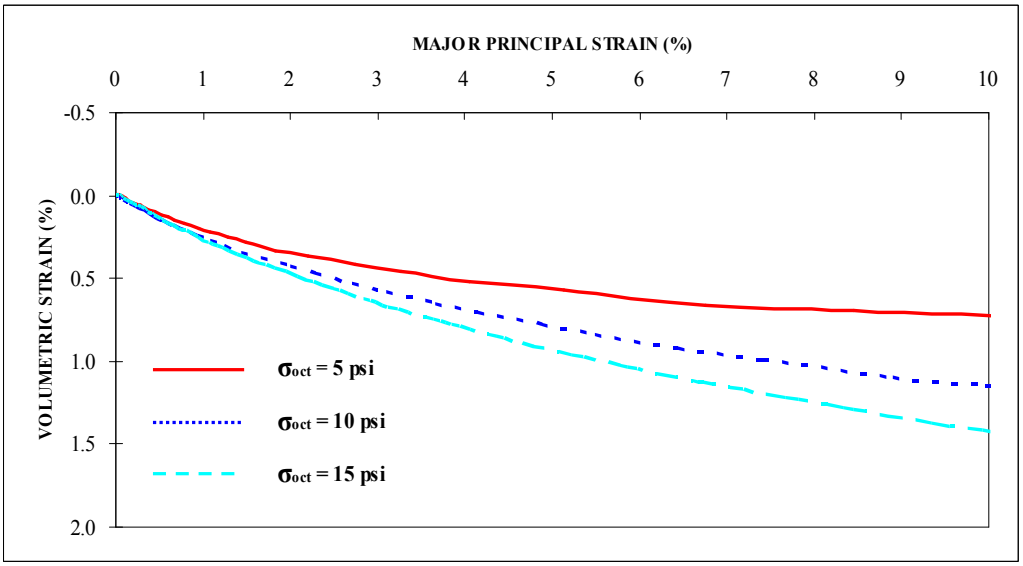

Figure 5.1 CTC Test Results under Drained Loading (w = 6%)

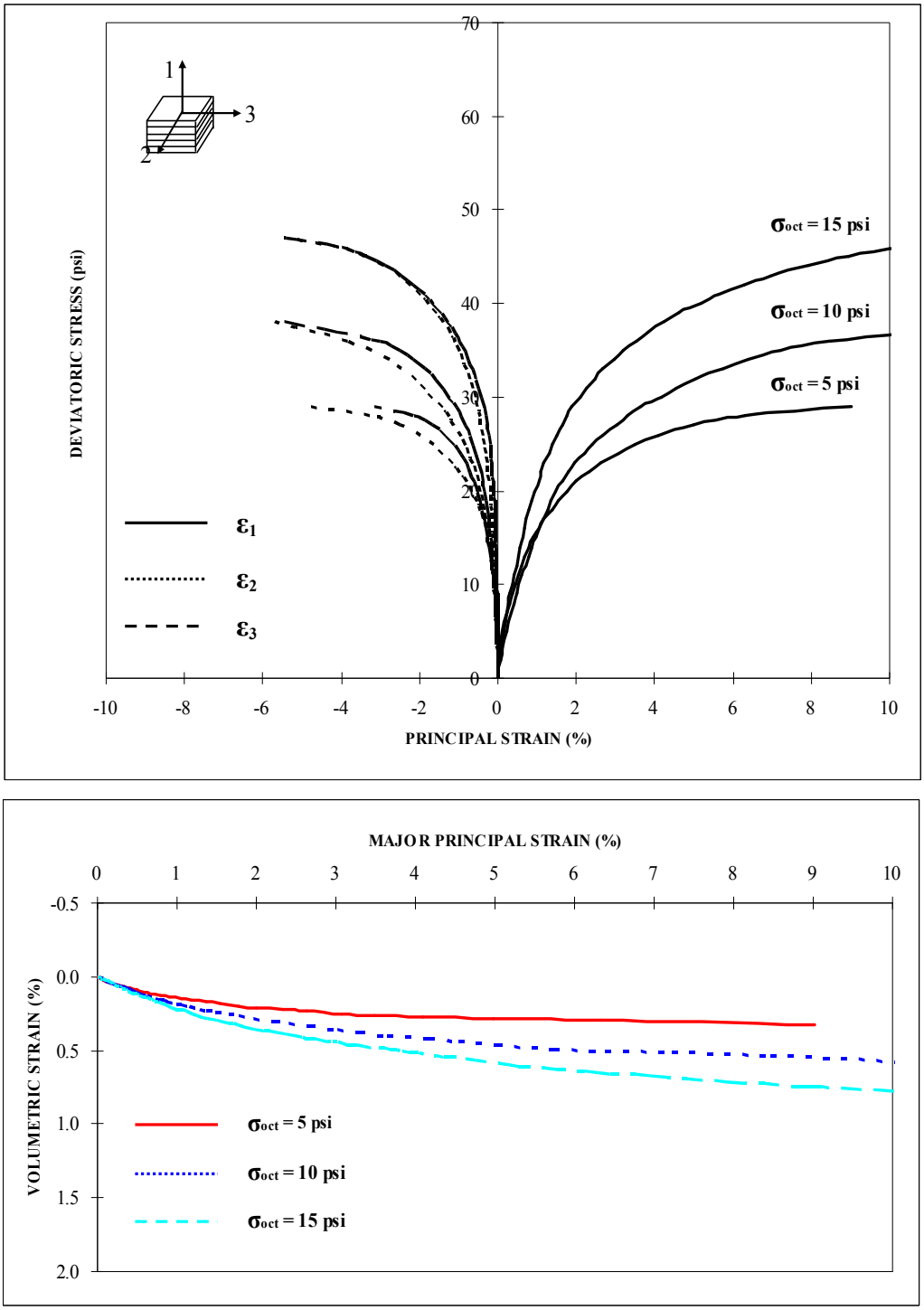

Figure 5.2 CTC Test Results under Drained Loading (w = 8%)

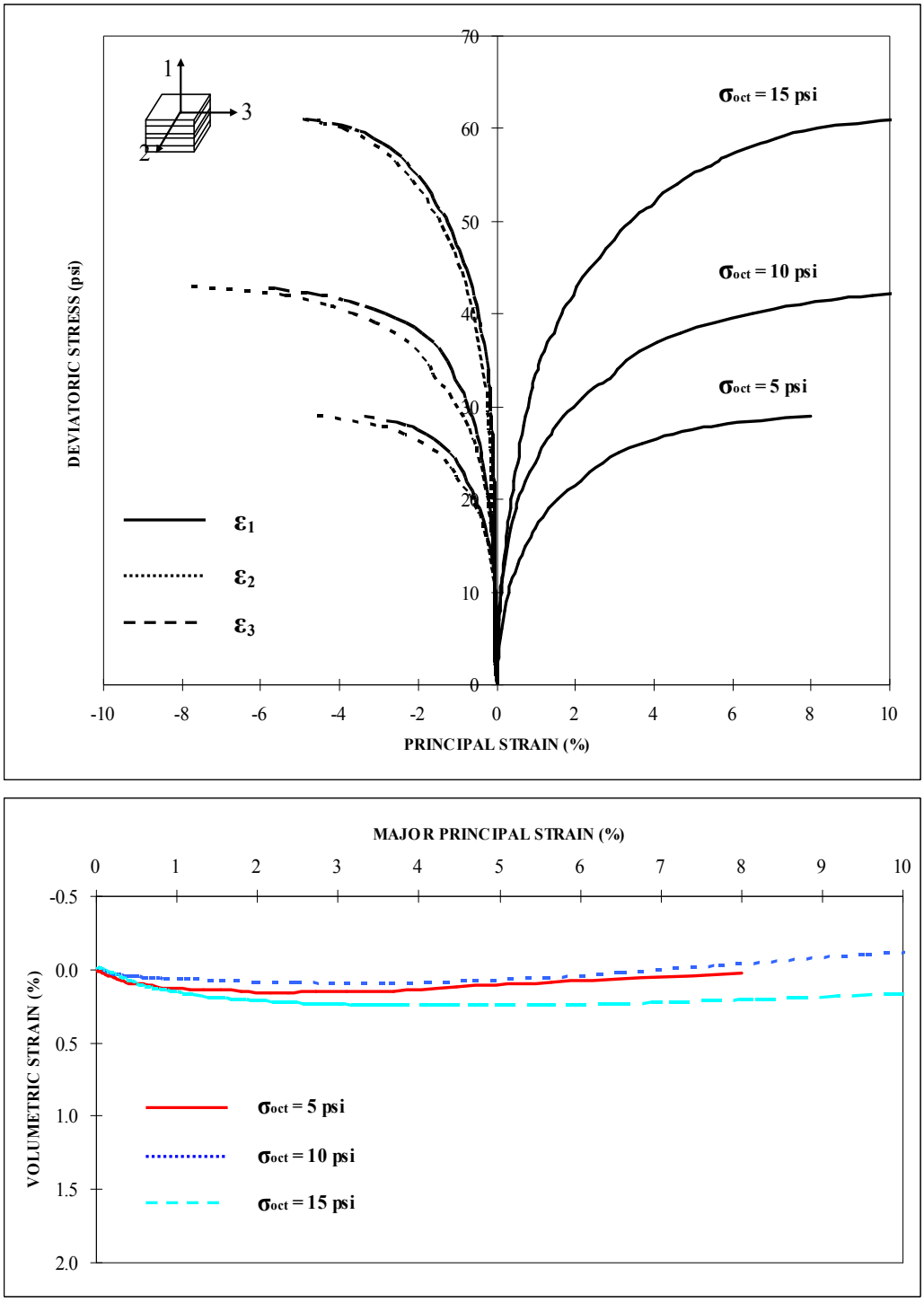

Figure 5.3 CTC Test Results under Drained Loading (w = 10%)

5.3.2.2 Triaxial Compression (TC) Tests

A series of 9 drained TC tests were carried out under effective confining pressures of 20, 30, and 40 psi on silty sand at three initial moist contents: 6%, 8%, and 10%. During the tests, the intermediate and minor principal stresses were equally decreased while the major principal stress increased, in order to keep octahedral normal stress constant. The results of these testings are presented in Figures 5.4 to 5.6. The measured principal strains versus octahedral shear stress and major principal strain versus volumetric strain are plotted in the figures respectively. As shown in the figures, the principal strains in x and y direction is expansive, while the major principal strain in z direction is significantly compressive. It can be clearly seen from Figures 5.4 to 5.6 that the shear strength and stiffness of soil increases with an increase in octahedral normal stress. The volumetric strain is predominantly compressive.

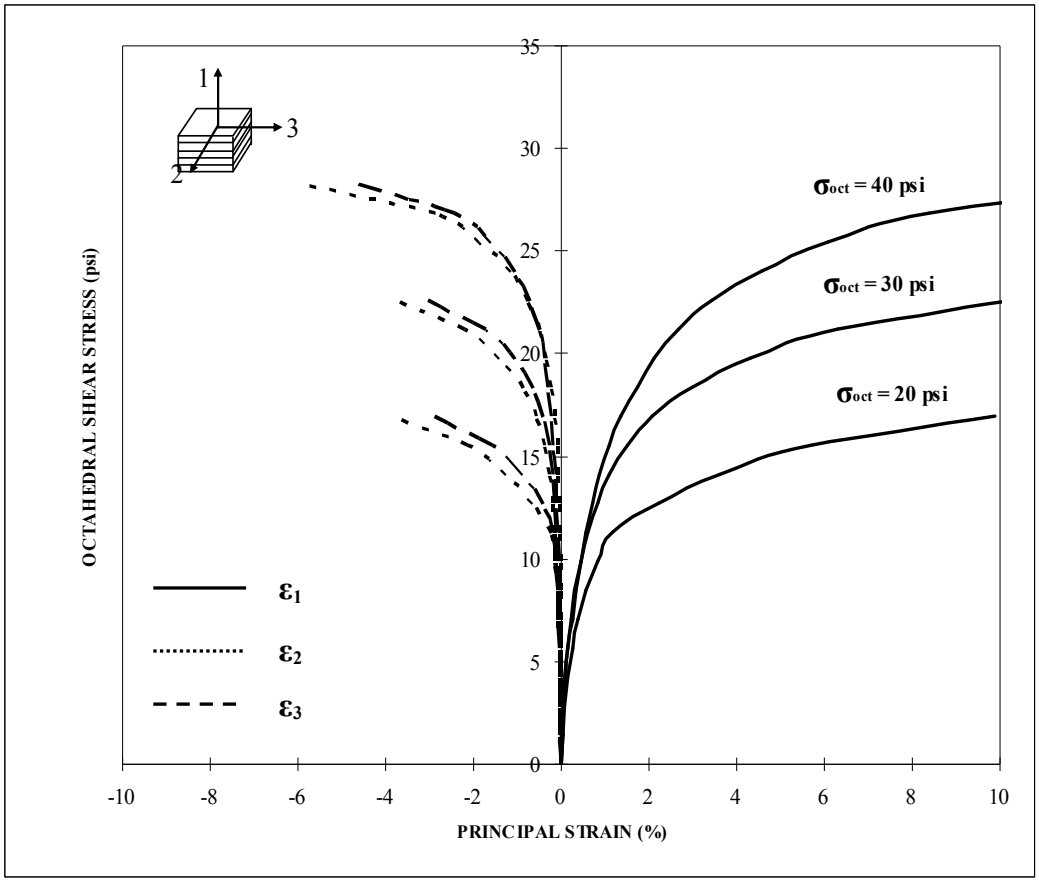

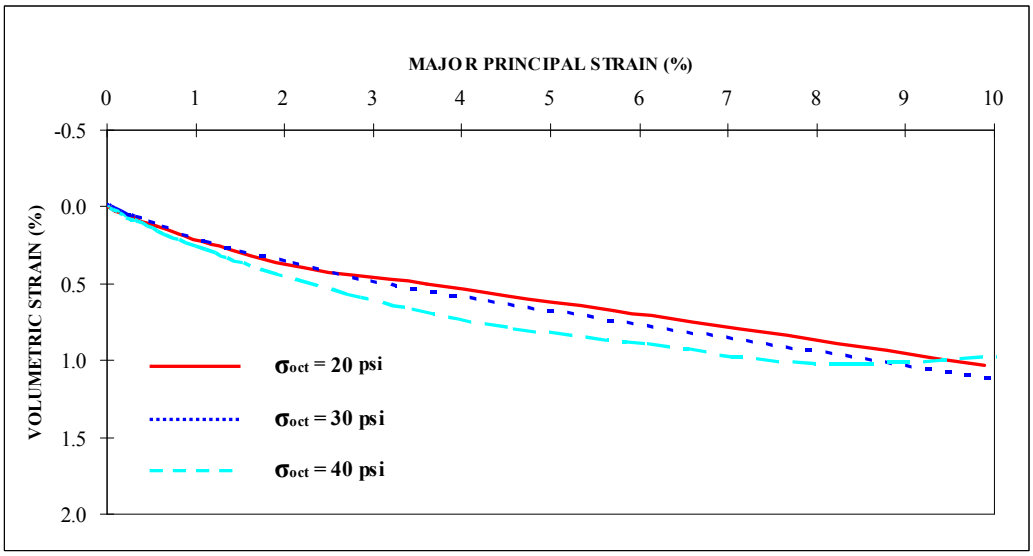

Figure 5.4 TC Test Results under Drained Loading (w = 6%)

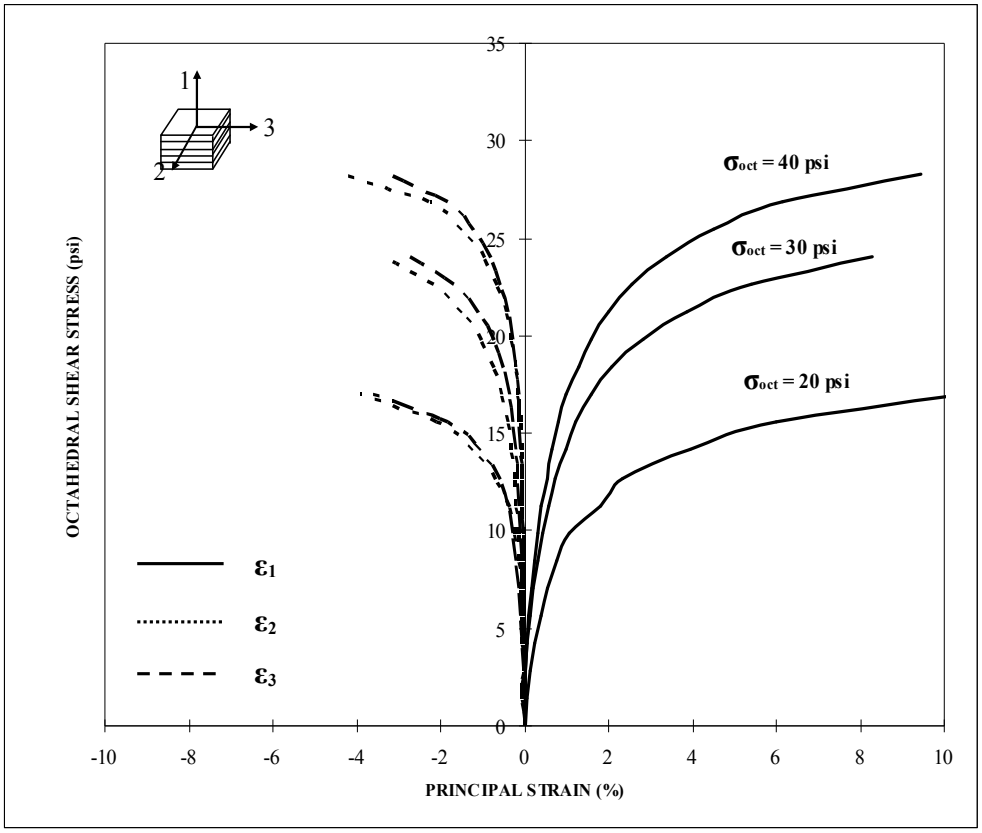

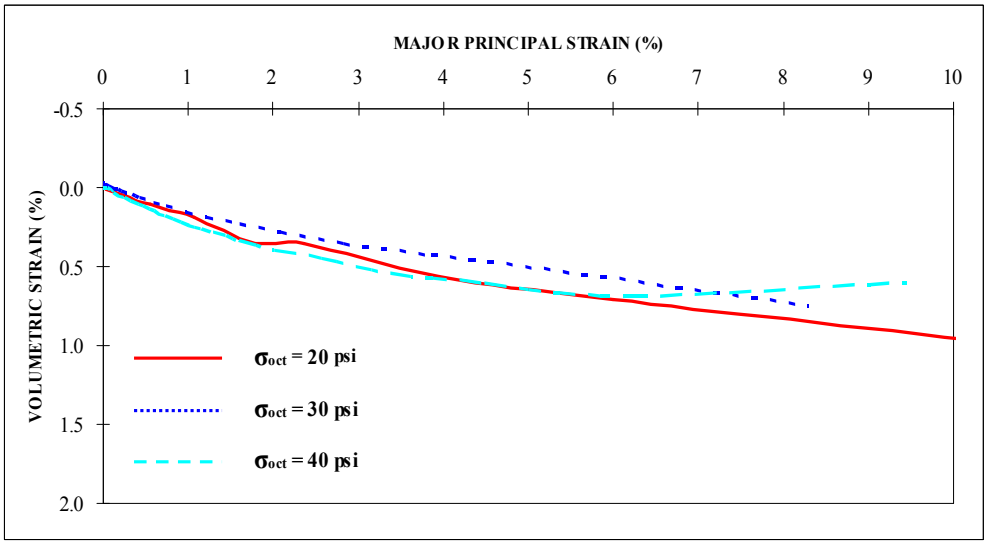

Figure 5.5 TC Test Results under Drained Loading (w = 8%)

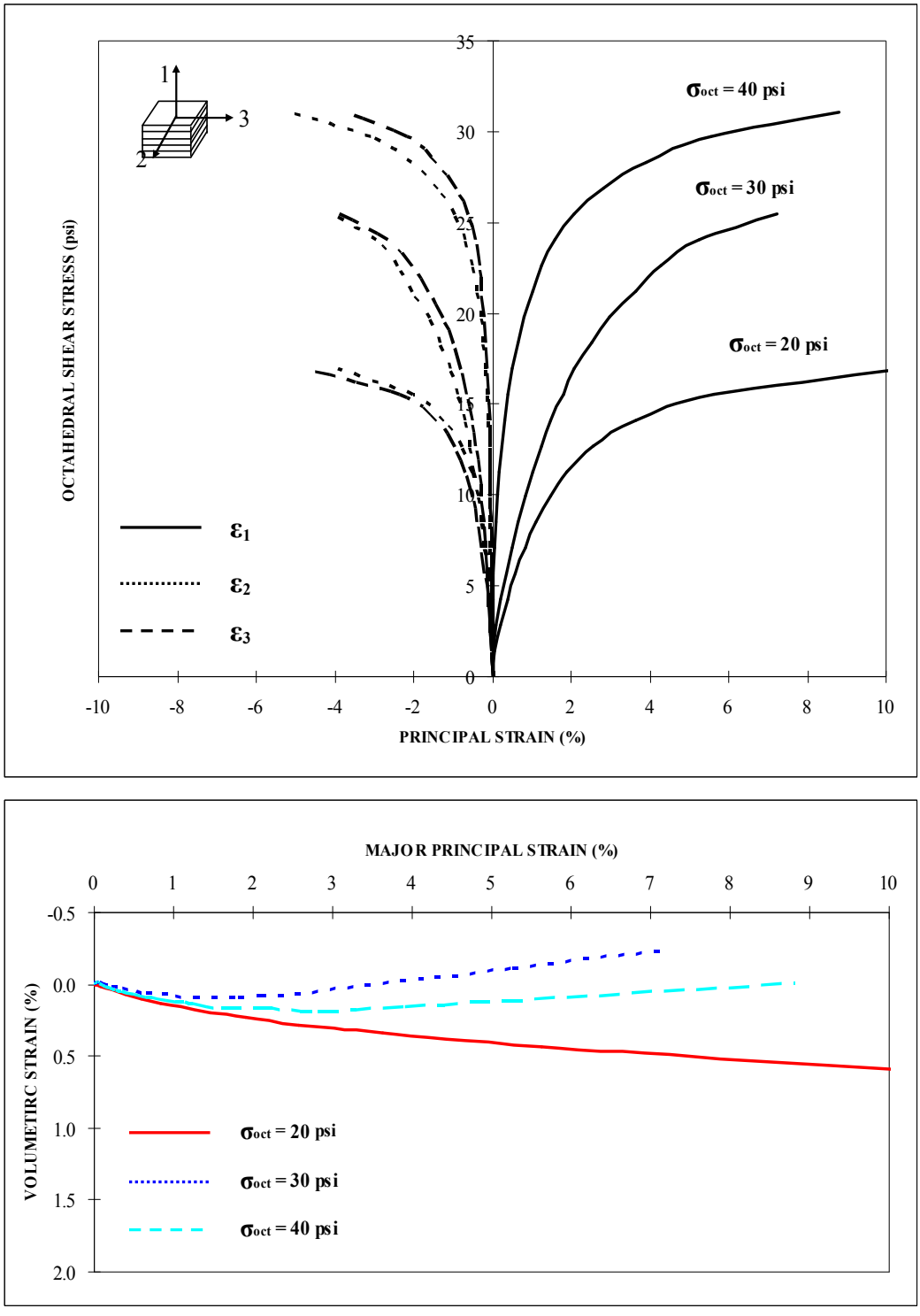

Figure 5.6 TC Test Results under Drained Loading (w = 10%)

5.3.2.3 Triaxial Extension (TE) Tests

A series of 9 drained TE tests were carried out under effective confining pressures of 20, 30, and 40 psi on silty sand at three initial moist contents: 6%, 8%, and 10%. During the tests, the major and intermediate principal stresses were equally increased while the minor principal stress decreased, in order to keep octahedral normal stress constant. The results of these testings are presented in Figures 5.7 to 5.9. The measured principal strains versus octahedral shear stress and major principal strain versus volumetric strain are plotted in the figures respectively. As shown in the figures, the principal strains in y and z direction is compressive, while the minor principal strain in x direction is expansive. It can be clearly seen from Figures 5.7 to 5.9 that the shear strength and stiffness of soil increases with an increase in octahedral normal stress. The volumetric strains (w = 6 and 8%) are slightly compressive while the volumetric strain (w = 10%) is slightly dilative.

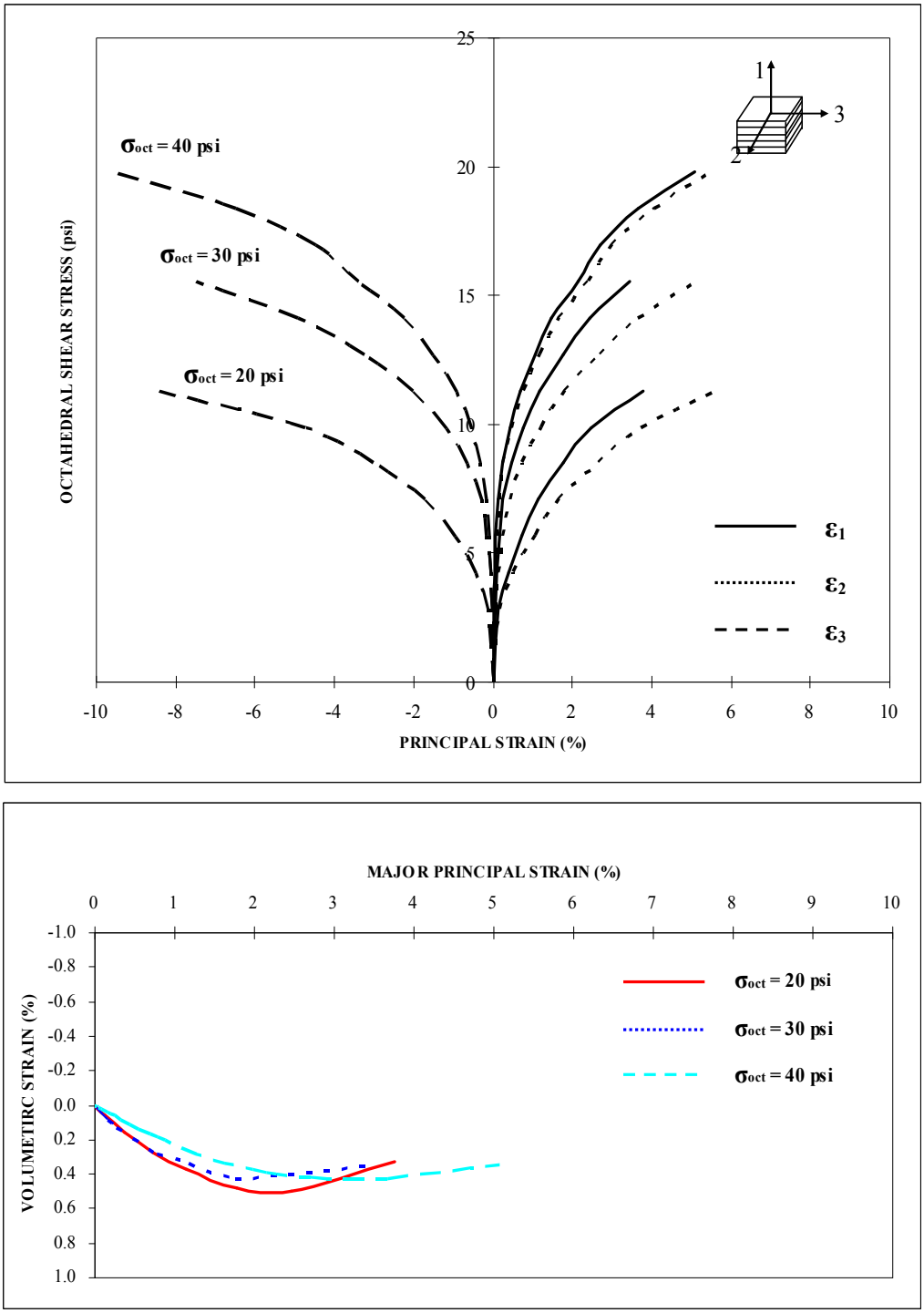

Figure 5.7 TE Test Results under Drained Loading (w = 6%)

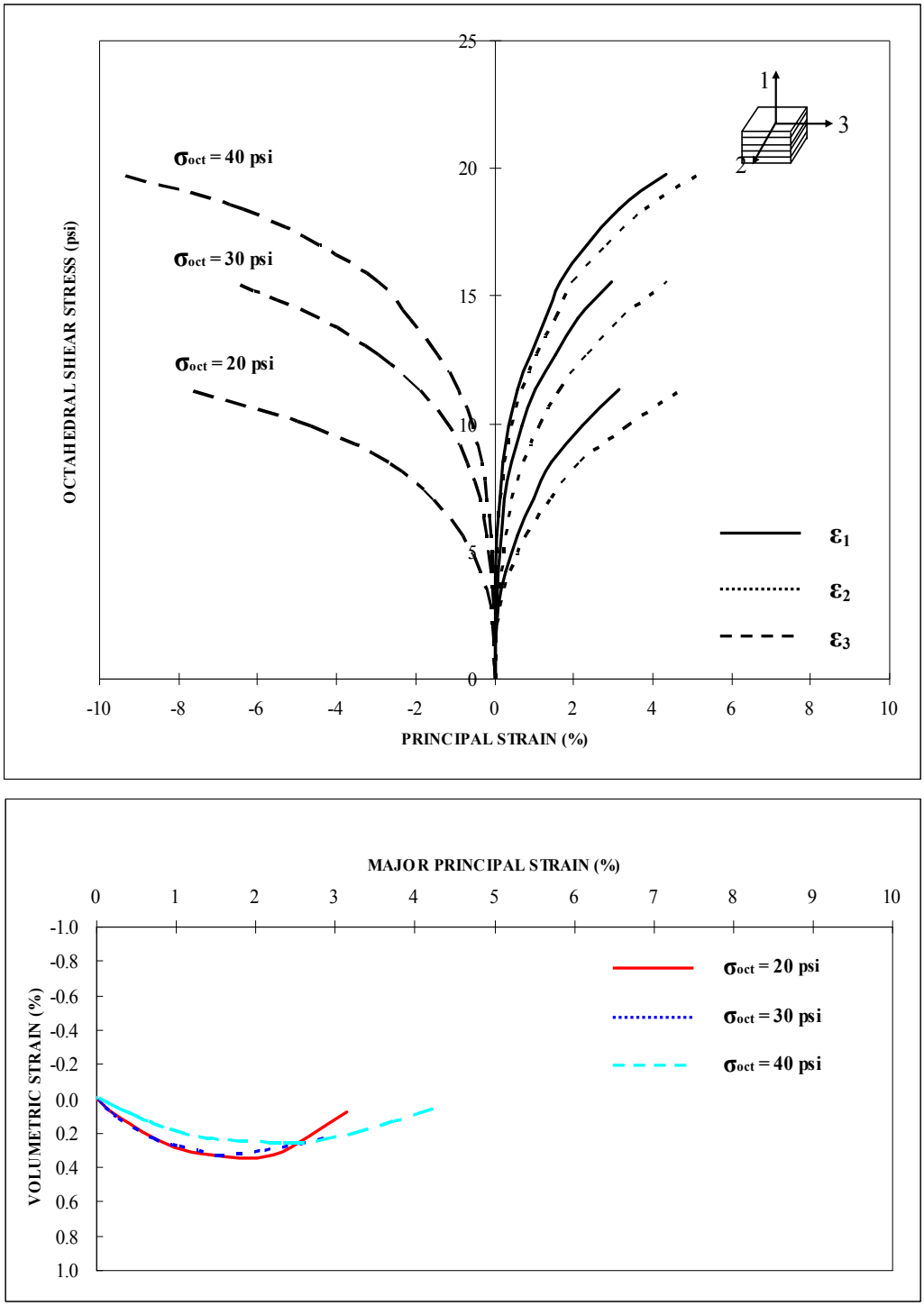

Figure 5.8 TE Test Results under Drained Loading (w = 8%)

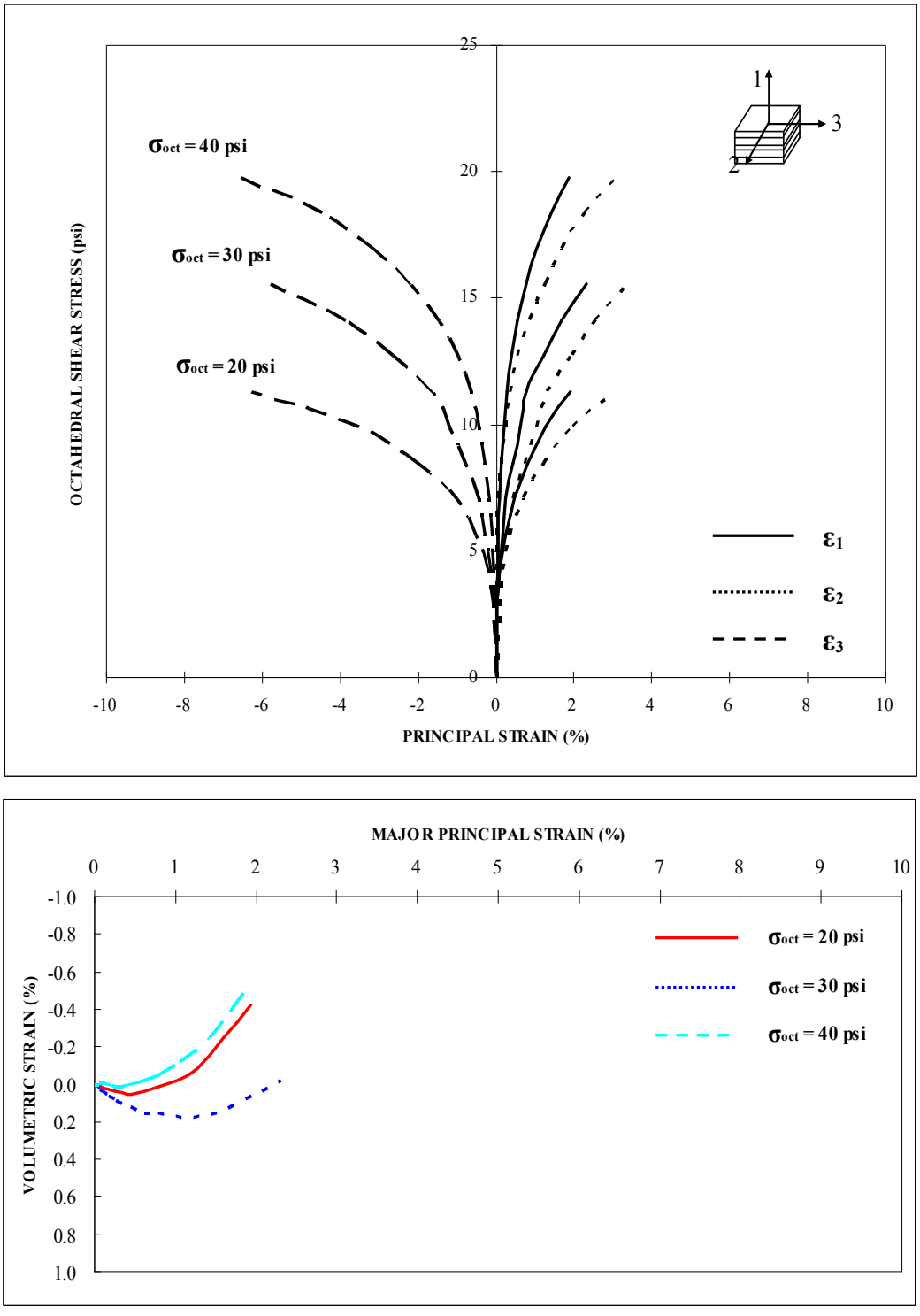

Figure 5.9 TE Test Results under Drained Loading (w = 10%)

5.3.2.4 Simple Shear (SS) Tests

A series of 9 drained SS tests were carried out under effective confining pressures of 20, 30, and 40 psi on silty sand at three initial moist contents: 6%, 8%, and 10%. During the tests, the intermediate principal stress was kept constant while the major principal stress increased and at the same time the minor principal stress was decreased in the same magnitude, in order to keep octahedral normal stress constant. The results of these testings are presented in Figures 5.10 to 5.12. The measured principal strains versus octahedral shear stress and major principal strain versus volumetric strain are plotted in the figures respectively. As shown in the figures, the principal strains in y direction is very small, while the major principal strain in z direction is compressive and the minor principal strain in x direction is expansive. It can be clearly seen from Figures 5.10 to 5.12 that the shear strength and stiffness of soil increases with an increase in octahedral normal stress. The volumetric strain (w = 10%) is predominately dilative.

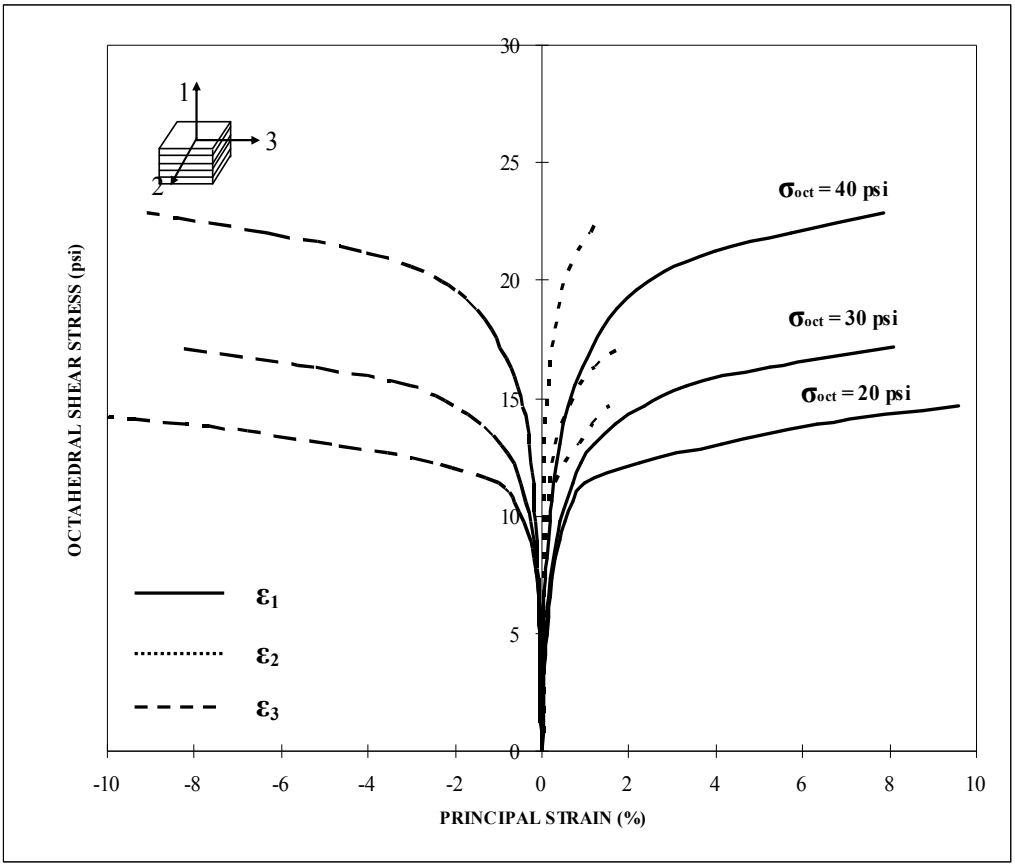

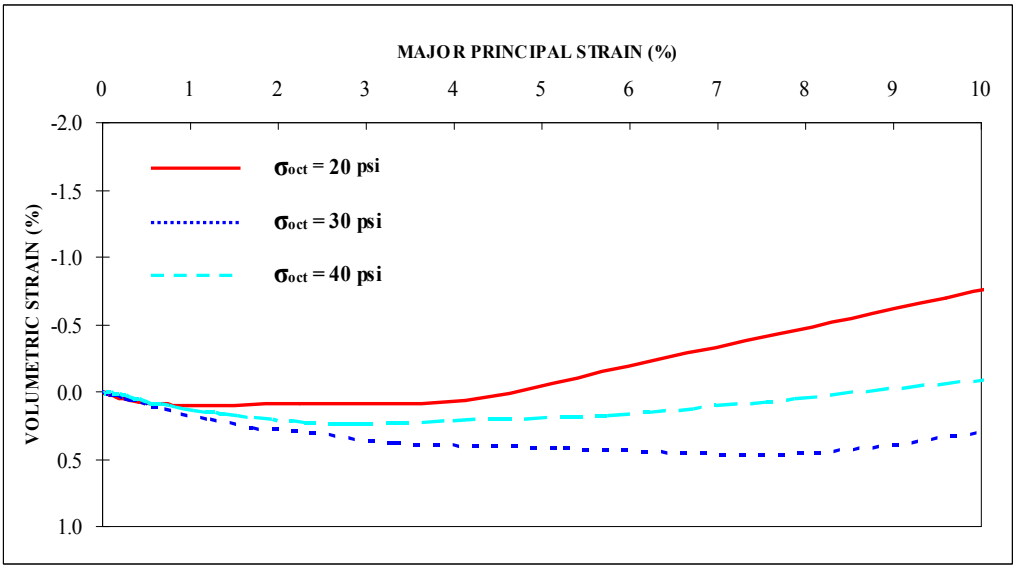

Figure 5.10 SS Test Results under Drained Loading (w = 6%)

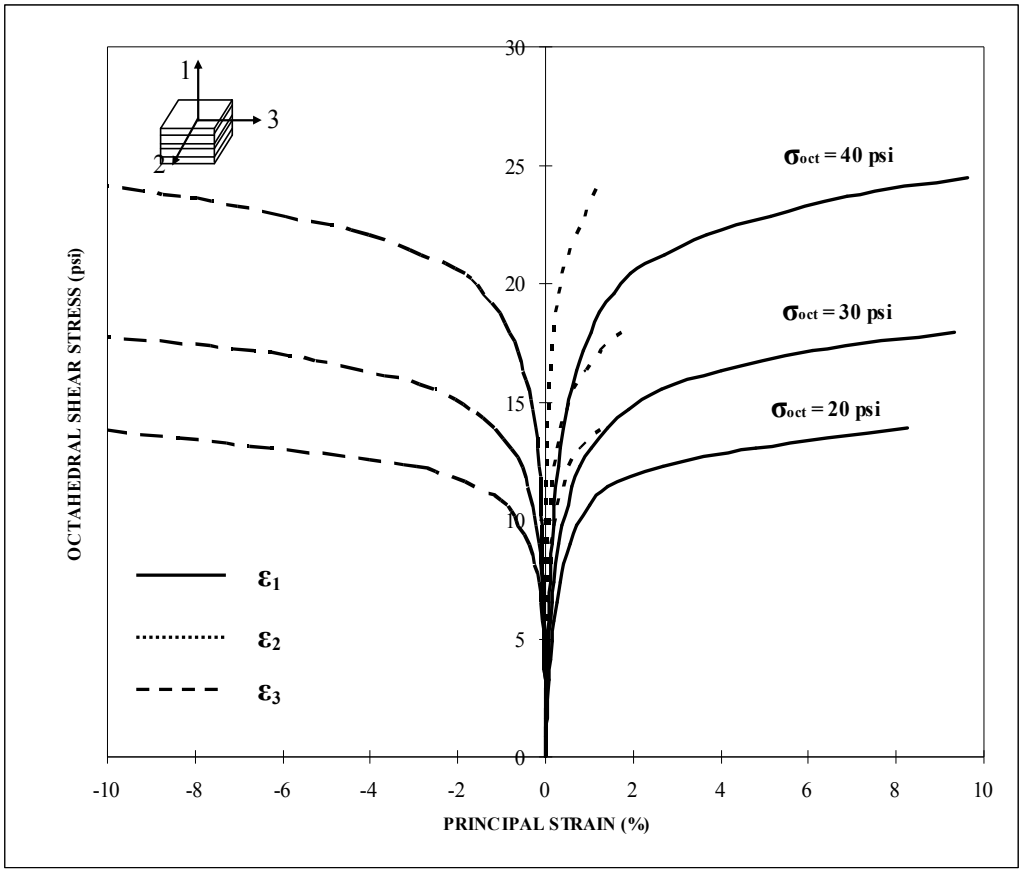

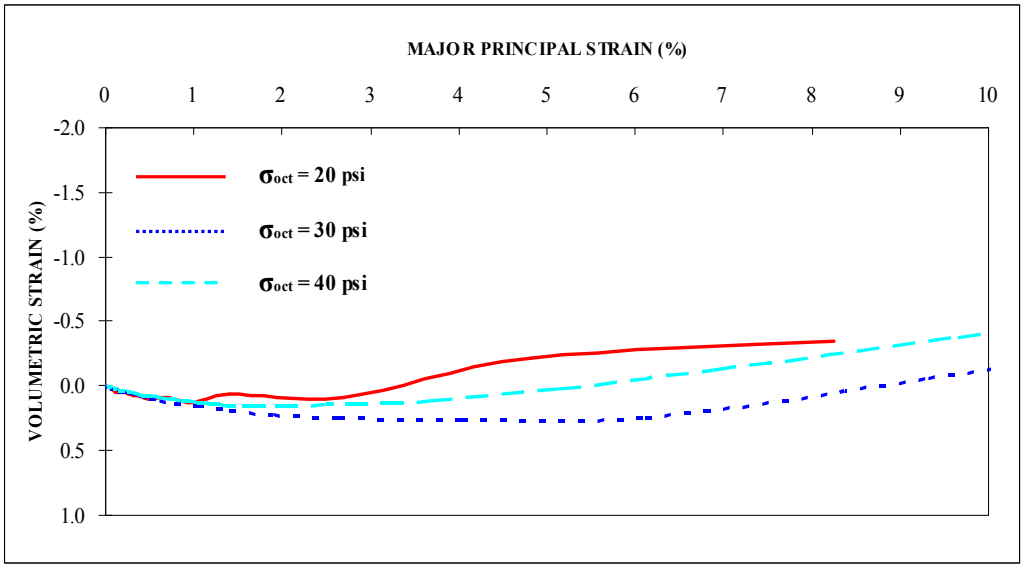

Figure 5.11 SS Test Results under Drained Loading (w = 8%)

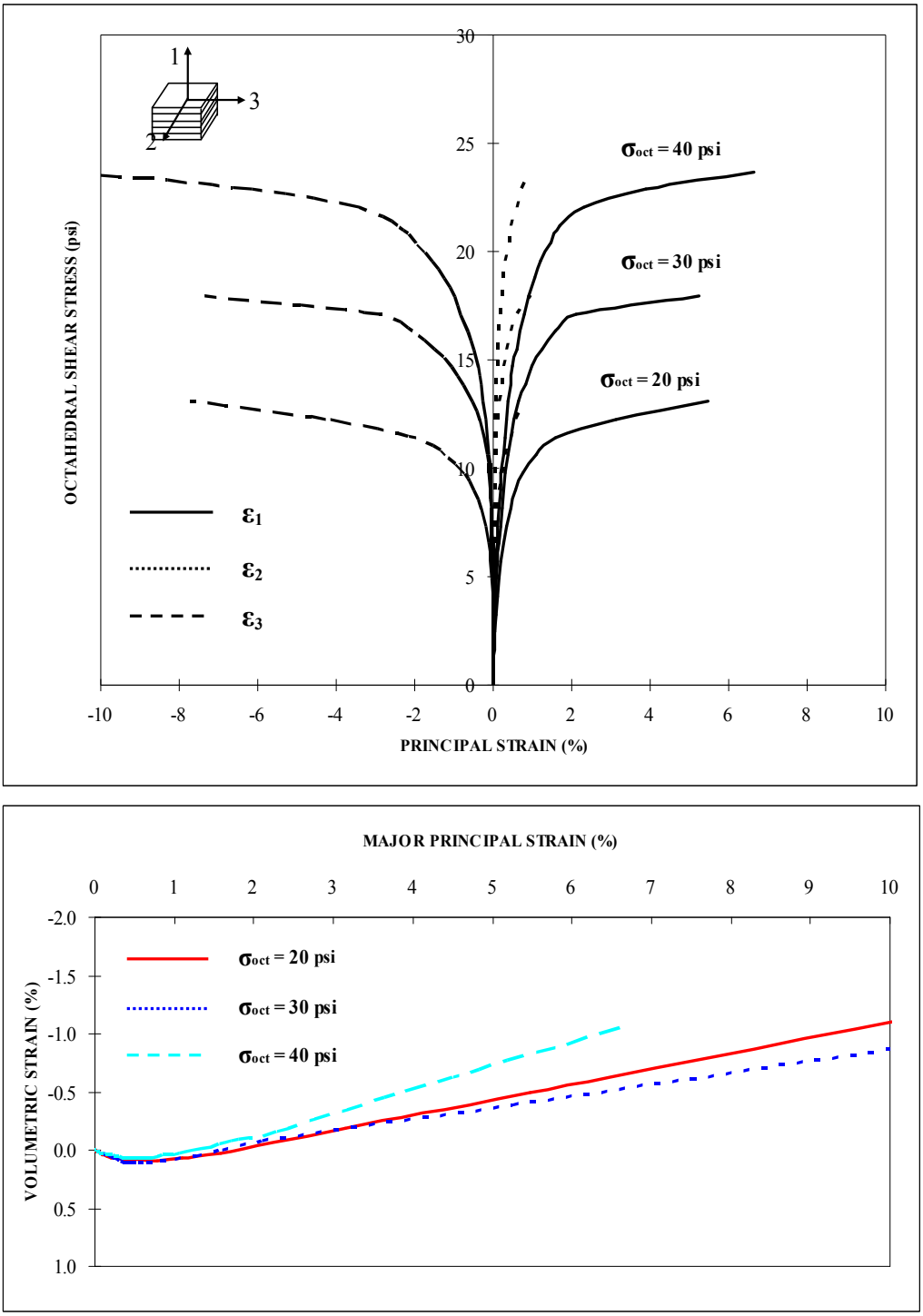

Figure 5.12 SS Test Results under Drained Loading (w = 10%)

5.3.3 Influence of Initial Soil State on Unsaturated Soil Strength

The influence of initial soil state on the strength of unsaturated soil is presented from Figures 5.13 to 5.24. Soil strength increases as initial degree of saturation increases from 27 to 61% and initial dry density increases from 16.40 to 18.12 kN/m^3, in spite of initial suction decreasing from 1360 to 550 kPa. It has been known that as suction increase soil strength increases. However, as shown in Figures 5.13 to 5.24, the measured results demonstrate that the contribution of the initial degree of saturation and initial dry density in soil strength under drained condition is much higher than that of soil suction induced by water menisci.

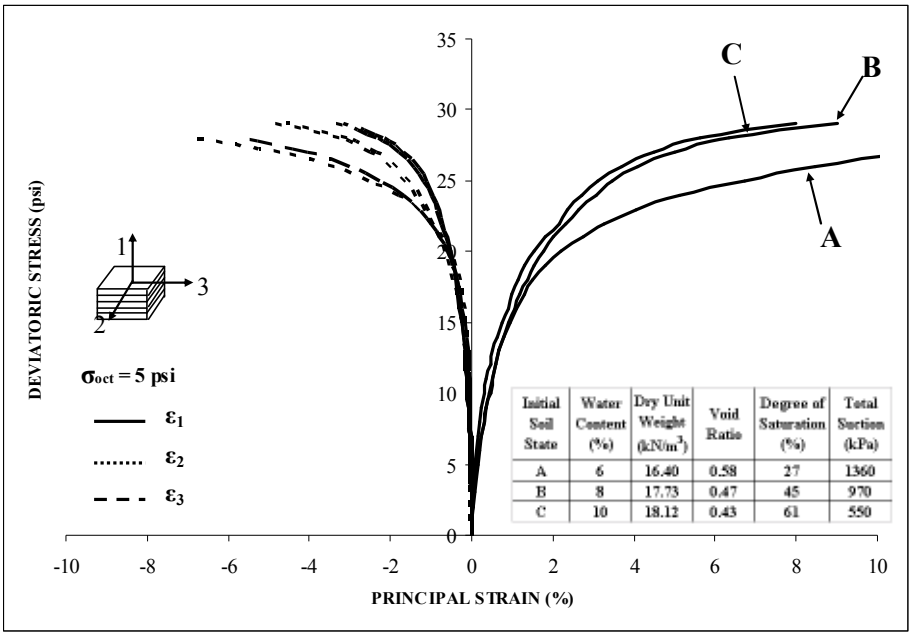

Figure 5.13 CTC Test Results for Silty Sand with Three Different Initial Conditions under Drained Loading (σ_{oct} = 5 psi)

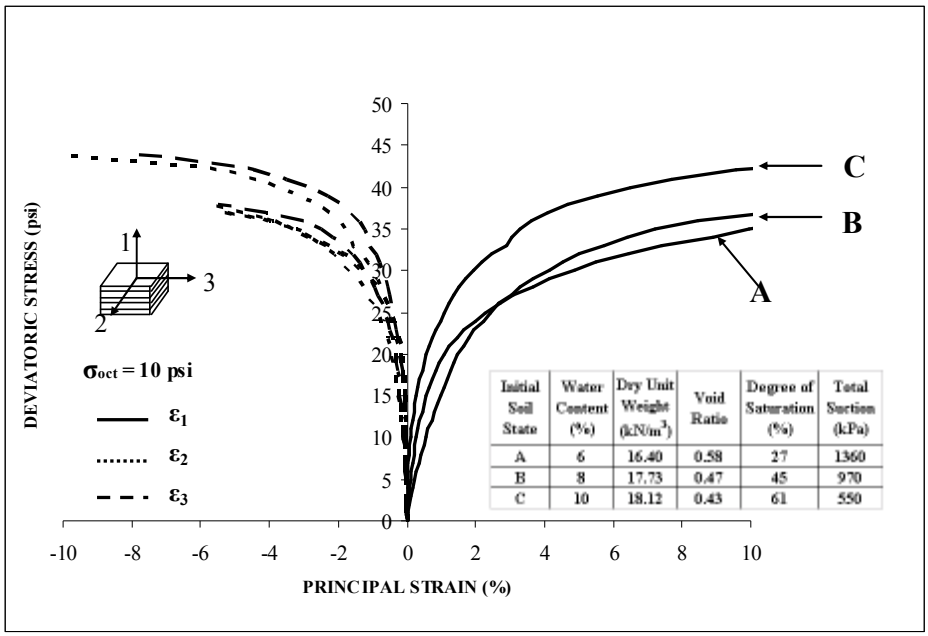

Figure 5.14 CTC Test Results for Silty Sand with Three Different Initial Conditions under Drained Loading (σ_{oct} = 10 psi)

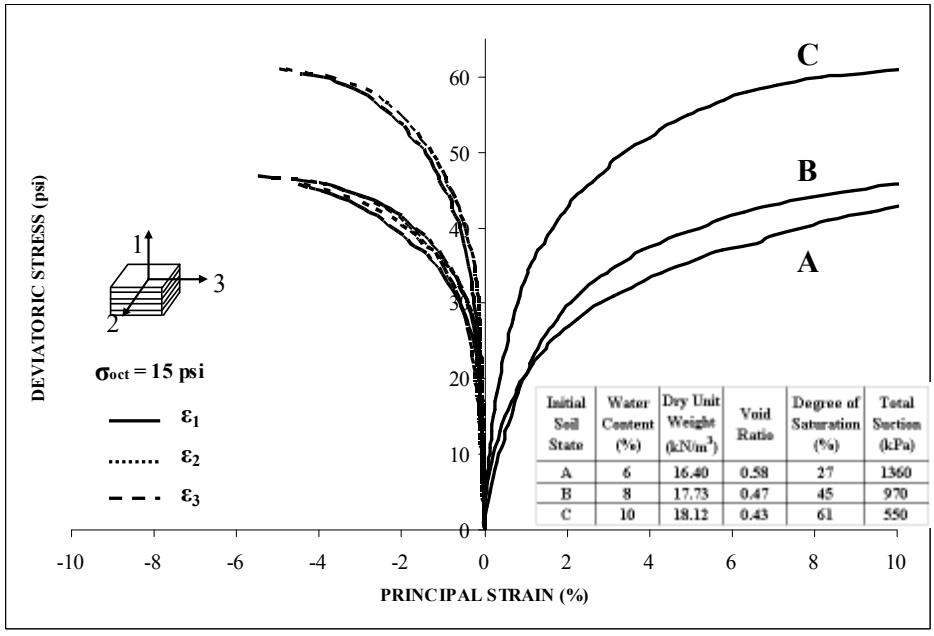

Figure 5.15 CTC Test Results for Silty Sand with Three Different Initial Conditions under Drained Loading (σ_{oct} = 15 psi)

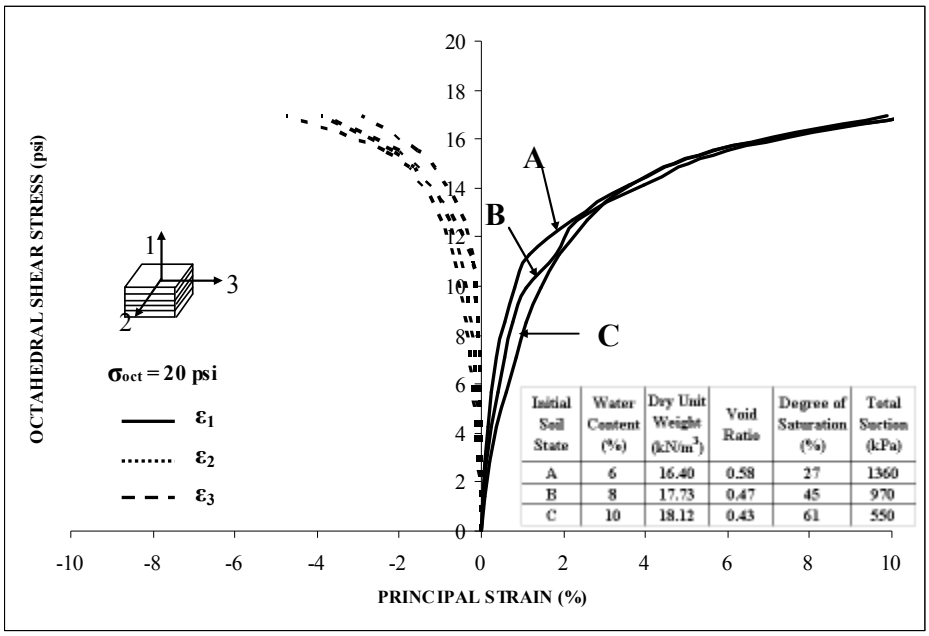

Figure 5.16 TC Test Results for Silty Sand with Three Different Initial Conditions under Drained Loading (σ_{oct} = 20 psi)

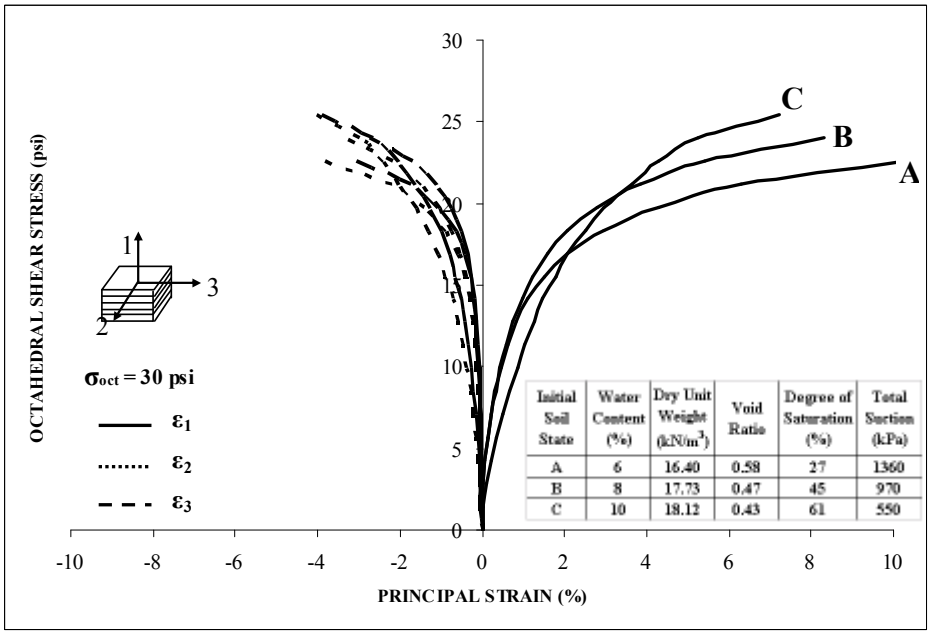

Figure 5.17 TC Test Results for Silty Sand with Three Different Initial Conditions under Drained Loading (σ_{oct} = 30 psi)

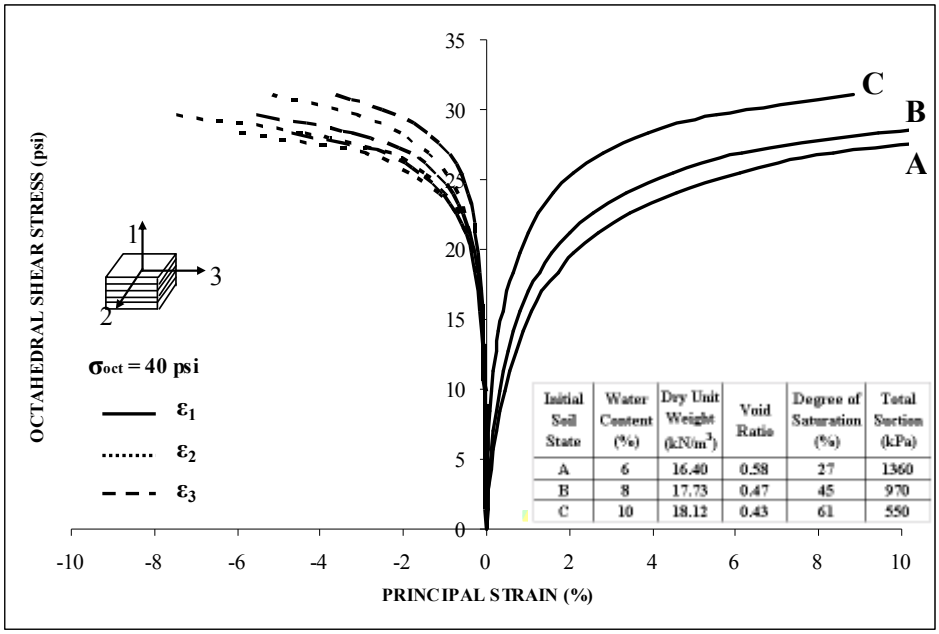

Figure 5.18 TC Test Results for Silty Sand with Three Different Initial Conditions under Drained Loading (σ_{oct} = 40 psi)

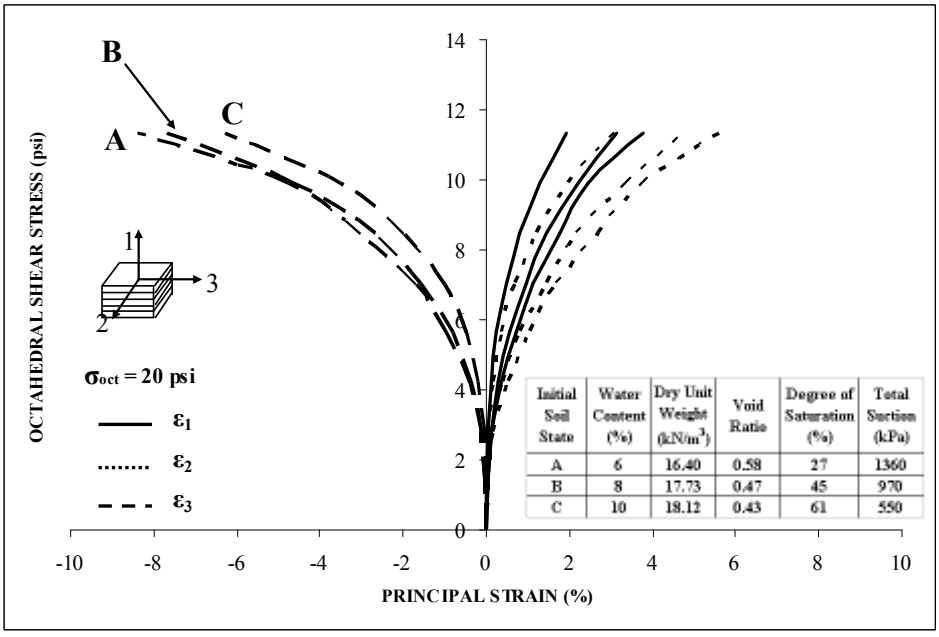

Figure 5.19 TE Test Results for Silty Sand with Three Different Initial Conditions under Drained Loading (σ_{oct} = 20 psi)

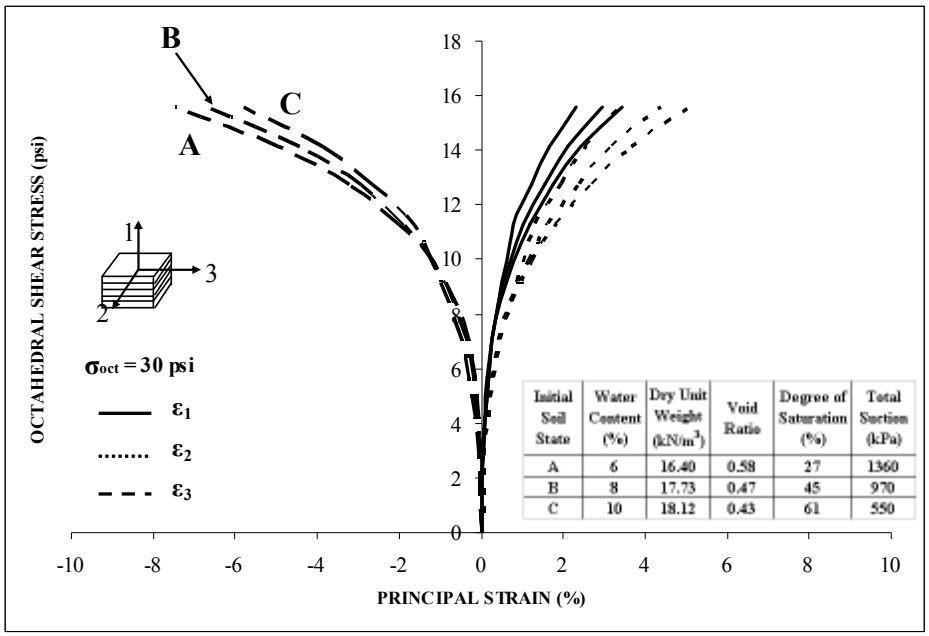

Initial Soil State	Water Content (%)	Dry Unit Weight (kN/m^3)	Void Ratio	Degree of Saturation (%)	Total Suction (kPa)
A	6	16.40	0.58	27	1360
B	8	17.73	0.47	45	970
C	10	18.12	0.43	61	550

Figure 5.20 TE Test Results for Silty Sand with Three Different Initial Conditions under Drained Loading (σ_{oct} = 30 psi)

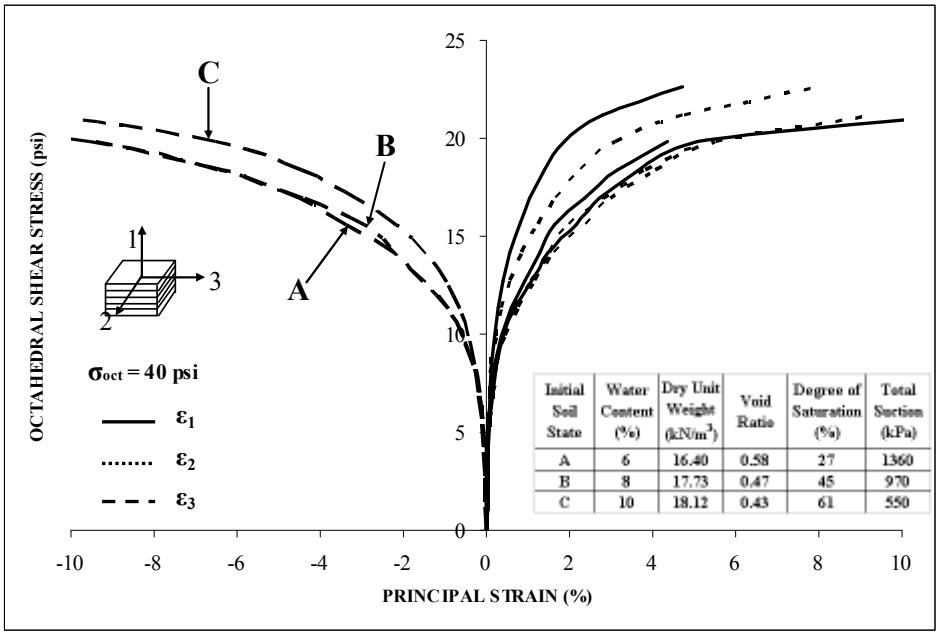

Initial Soil State	Water Content (%)	Dry Unit Weight (kN/m^3)	Void Ratio	Degree of Saturation (%)	Total Suction (kPa)
A	6	16.40	0.58	27	1360
B	8	17.73	0.47	45	970
C	10	18.12	0.43	61	550

Figure 5.21 TE Test Results for Silty Sand with Three Different Initial Conditions under Drained Loading (σ_{oct} = 40 psi)

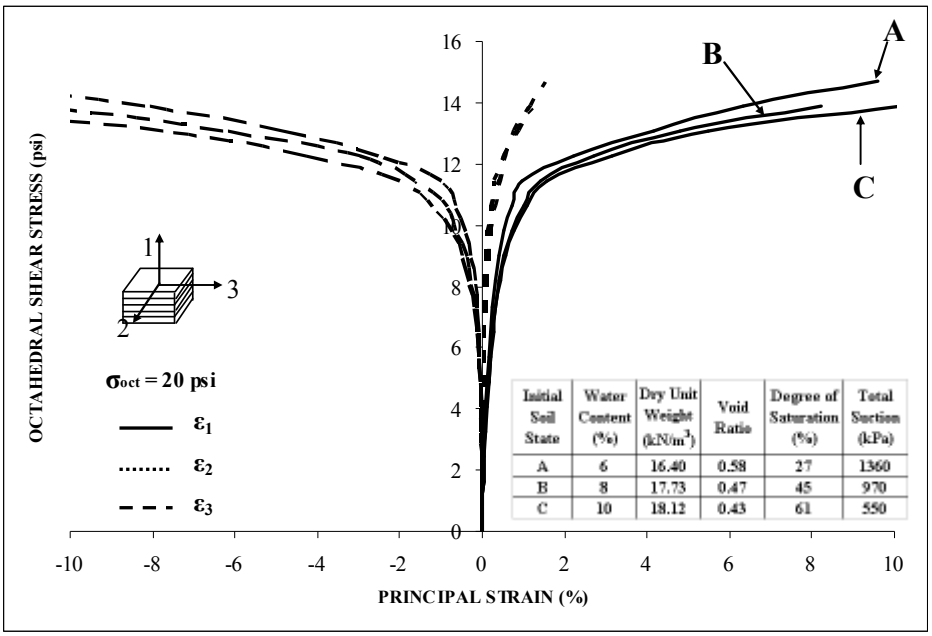

Figure 5.22 SS Test Results for Silty Sand with Three Different Initial Conditions under Drained Loading (σ_{oct} = 20 psi)

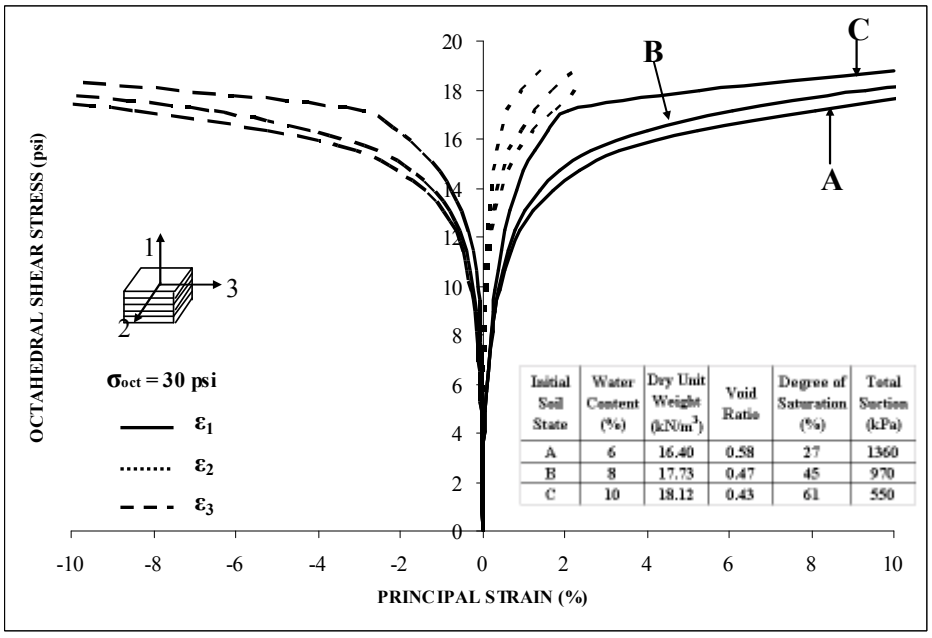

Figure 5.23 SS Test Results for Silty Sand with Three Different Initial Conditions under Drained Loading (σ_{oct} = 30 psi)

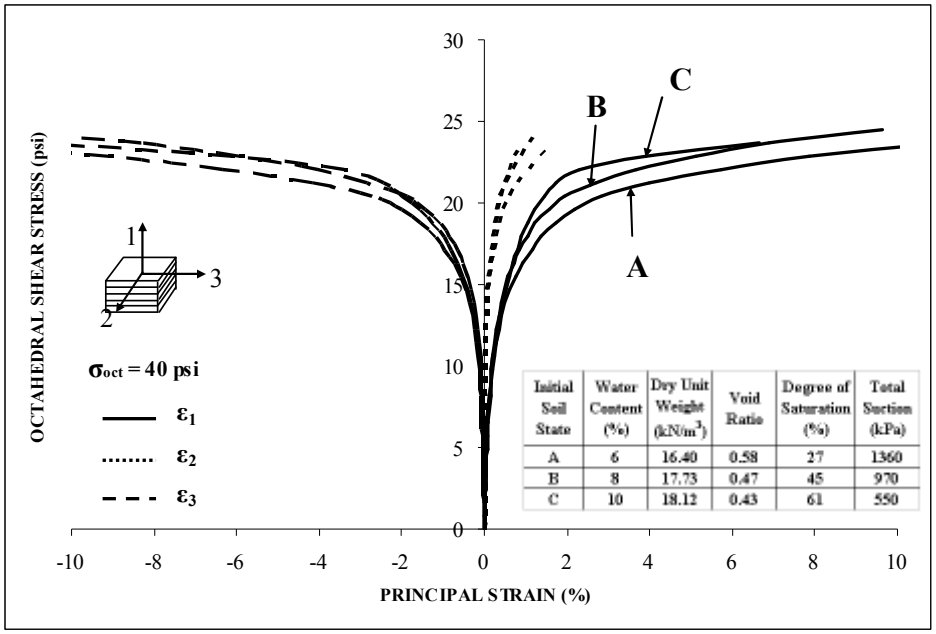

Figure 5.24 SS Test Results for Silty Sand with Three Different Initial Conditions under Drained Loading (σ_{oct} = 40 psi)

5.3.4 Failure Envelopes on Octahedral Plane and Critical State Line

The projection of failure envelopes obtained from drained true triaxial tests onto the octahedral plane is shown in Figure 5.25. It is based on three types of soil (A, B, and C) containing different initial conditions and three different octahedral normal stresses (σ_{oct} = 20, 30, and 40 psi). It can be concluded that the shape, size, and position of the failure envelope are significantly affected by initial degree of saturation and initial density. In other word, soil with higher initial dry density and degree of saturation exhibits more expanded failure envelope.

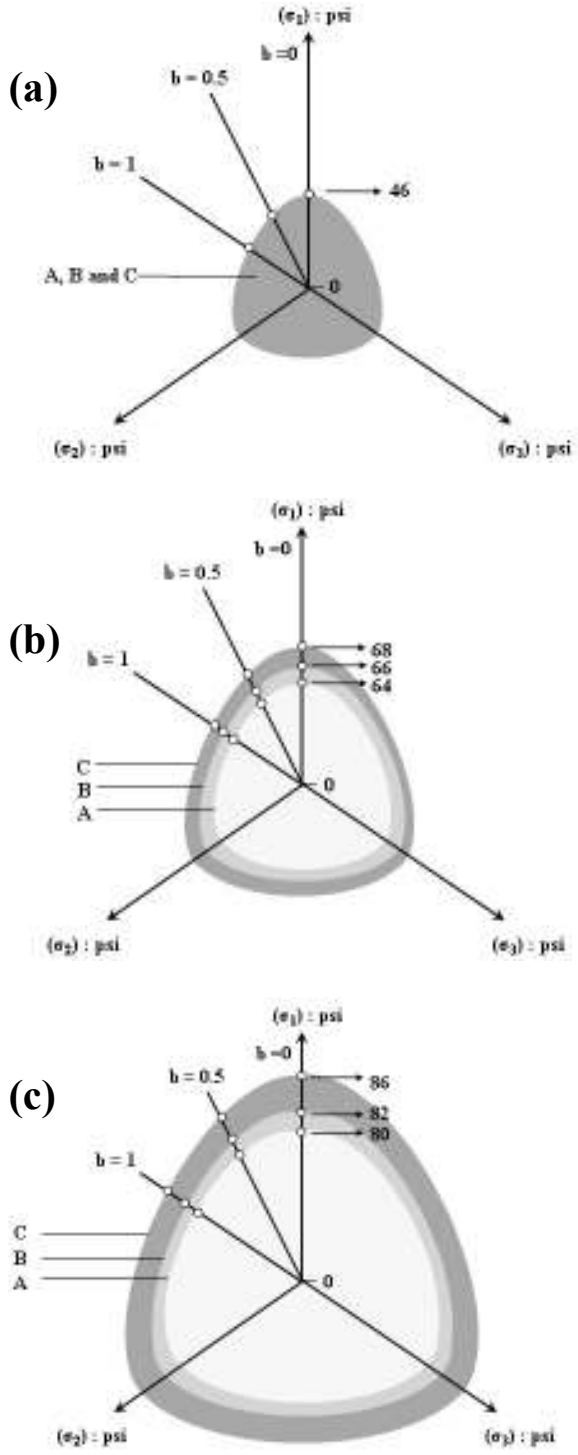

Initial Soil State	Water Content (%)	Dry Unit Weight (kN/m^3)	Void Ratio	Degree of Saturation (%)	Total Suction (kPa)
A	6	16.40	0.58	27	1360
B	8	17.73	0.47	45	970
C	10	18.12	0.43	61	550

Figure 5.25 Projection of Failure Envelopes on Octahedral Plane under Drained Loading: (a) σ_{oct} = 20 psi, (b) σ_{oct} = 30 psi, (c) σ_{oct} = 40 psi.

In addition, best-fit critical state lines are presented in terms of net mean stress, p and deviatoric stress, q (Figure 5.26). It seems that the slope of critical state line, M is nearly constant and is independent of initial degree of saturation and dry density.

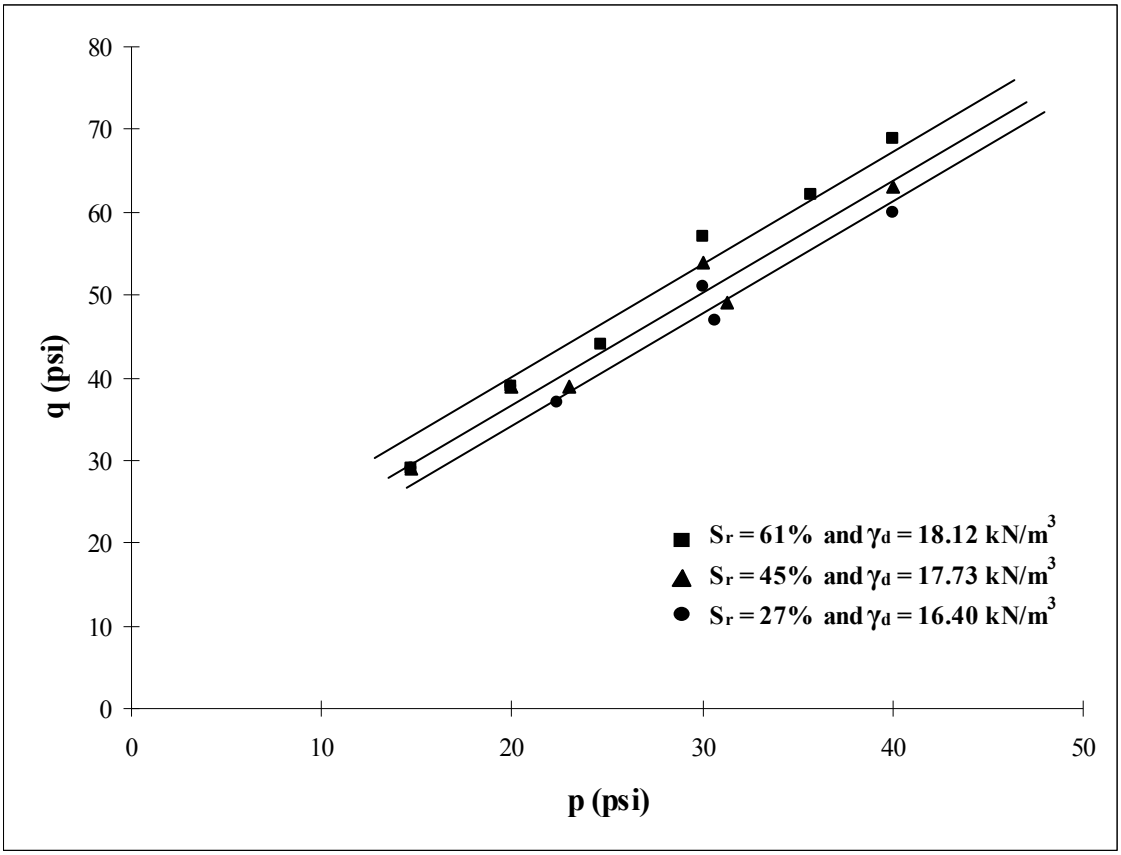

Figure 5.26 P-q Diagram for Kneading-Compacted Unsaturated Silty Sand under Drained Loading

5.4 Undrained Testing

5.4.1 Introduction

The results of a series of 36 undrained true triaxial tests are presented in the following sections. During these tests, the drainage port was sealed using silicon to prevent water drainage from specimens. The organization of the following sections is in same order as that of previous drain testing section.

5.4.2 Influence of Octahedral Stress

5.4.2.1 Conventional Triaxial Compression (CTC) Tests

A series of 9 undrained CTC tests were performed with same confining pressures and water contents as drained CTC testings. The results of these testings are presented in Figures 5.27 to 5.29. The measured results show similar to those of drained testings. The principal strains in x and y direction are much equally expansive, while the major principal strain in z direction is significantly compressive. The strength and stiffness of soil increase with an increase in octahedral normal stress. The volumetric strains (w = 6 and 8%) is predominantly compressive while the volumetric strain (w = 10%) is slightly dilative.

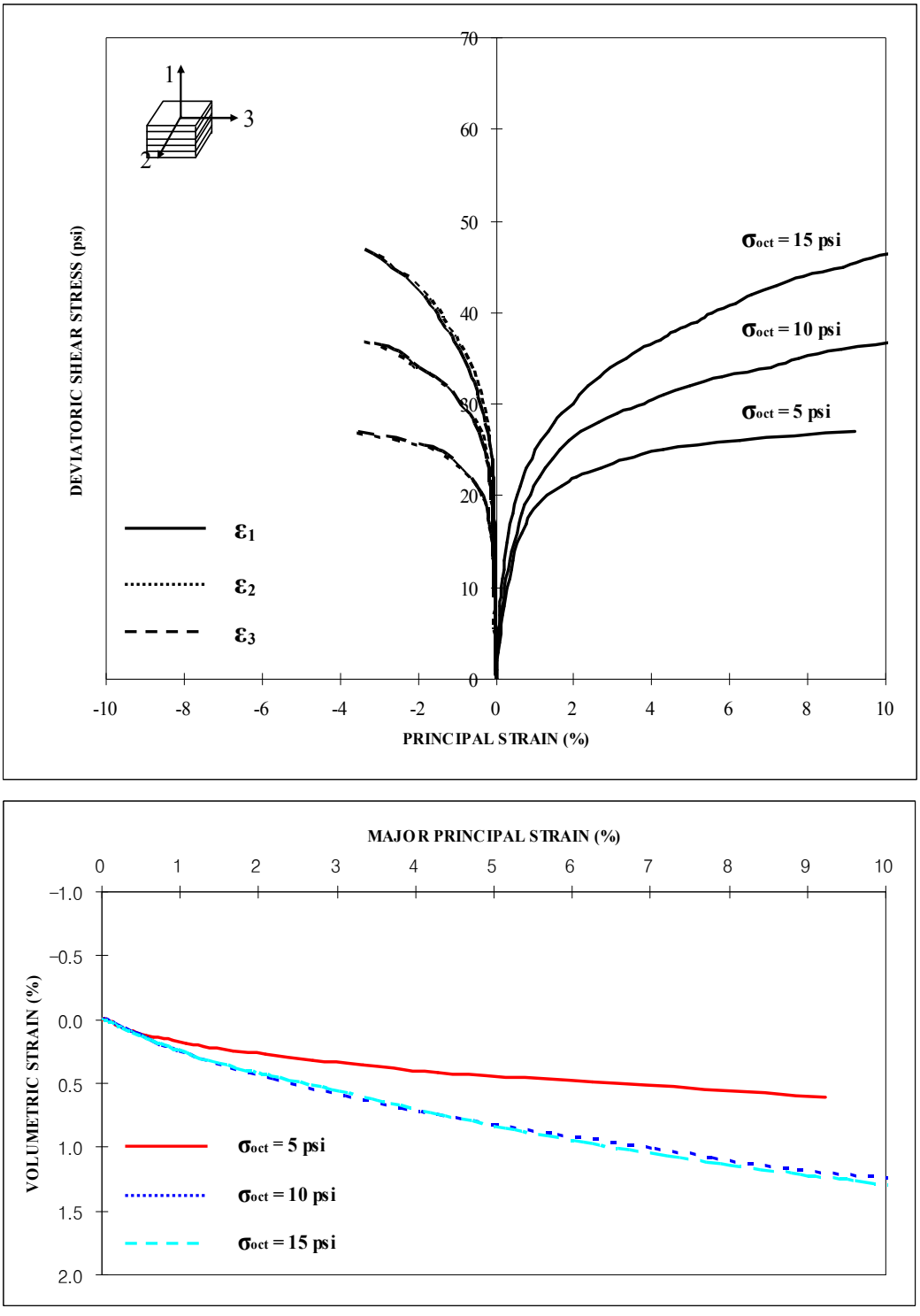

Figure 5.27 CTC Test Results under Undrained Loading (w = 6%)

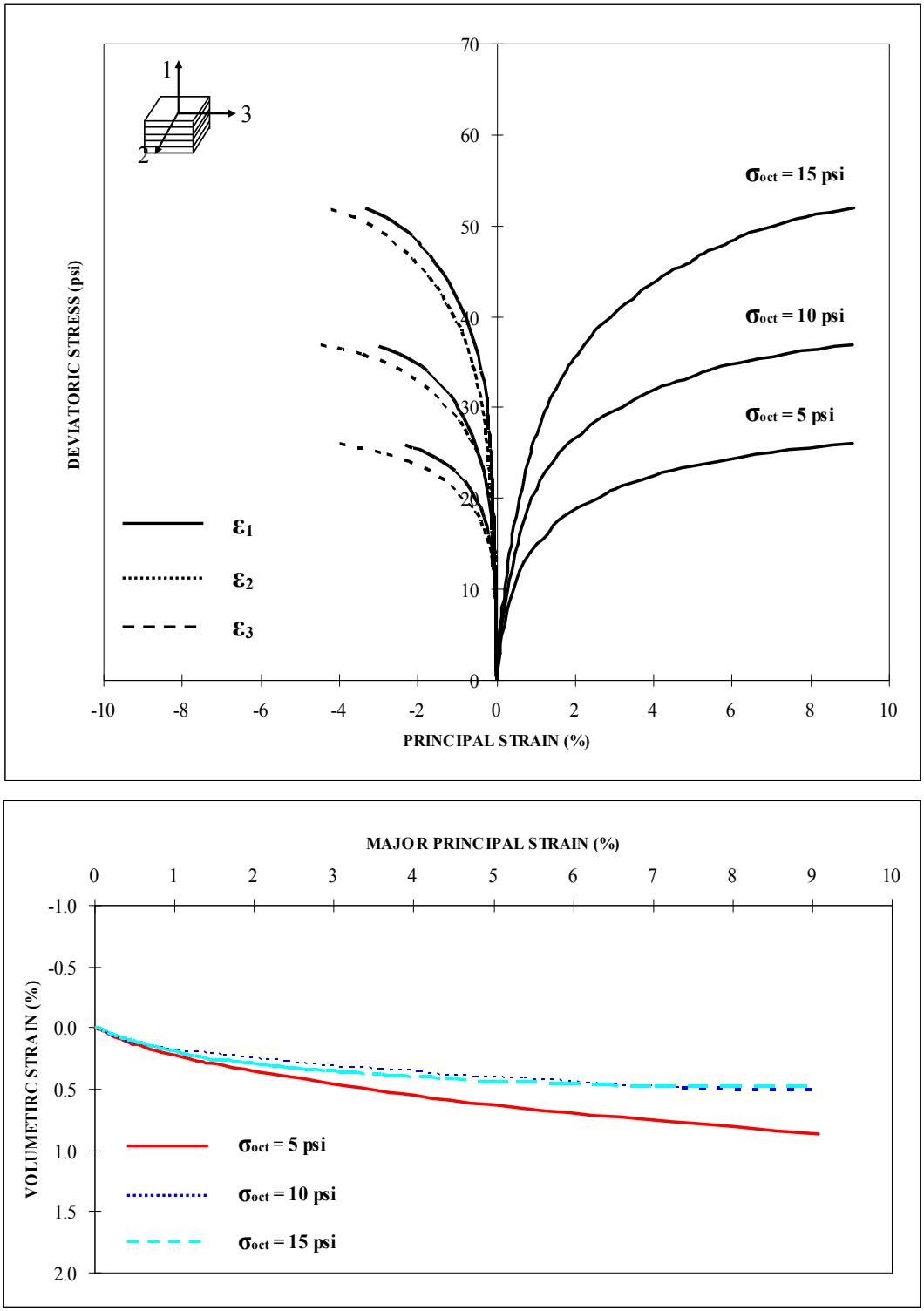

Figure 5.28 CTC Test Results under Undrained Loading (w = 8%)

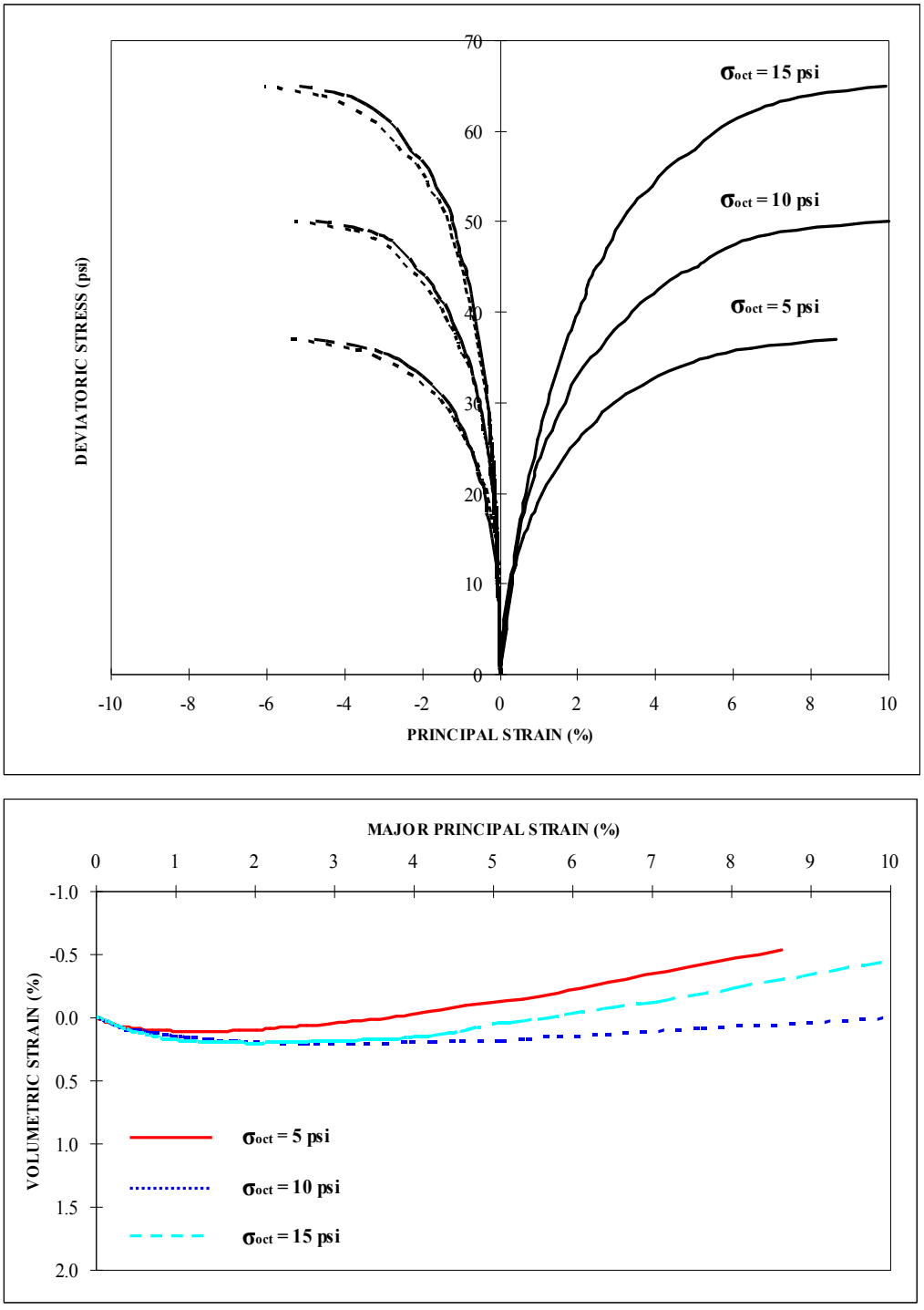

Figure 5.29 CTC Test Results under Undrained Loading (w = 10%)

5.4.2.2 Triaxial Compression (TC) Tests

A series of 9 undrained TC tests were carried out with same confining pressures and water contents as drained TC testings. The results of these testings are presented in Figures 5.30 to 5.32. The measured results show similar to those of drained testings. The principal strains in x and y direction is expansive, while the major principal strain in z direction is significantly compressive. The strength of soil increases with an increase in octahedral normal stress. The volumetric strain (w = 6 and 8%) is predominantly compressive.

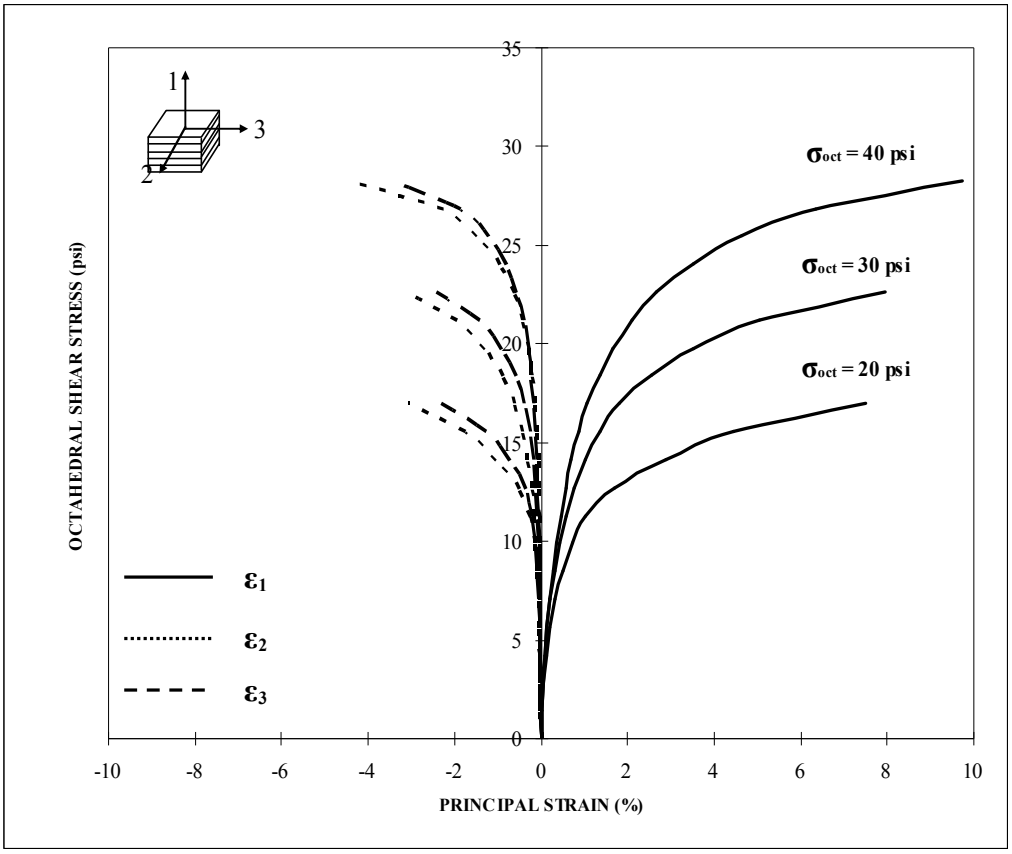

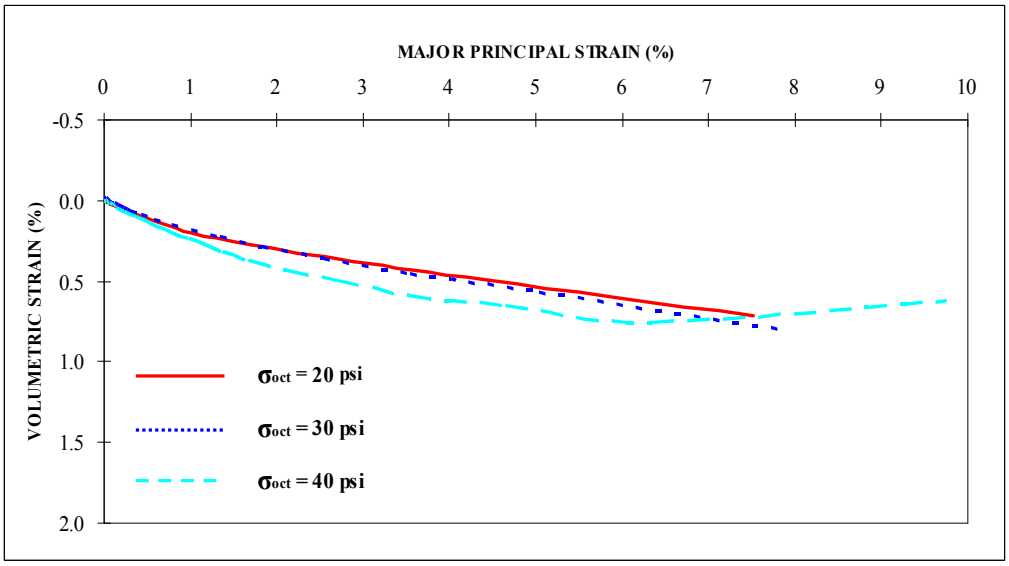

Figure 5.30 TC Test Results under Undrained Loading (w = 6%)

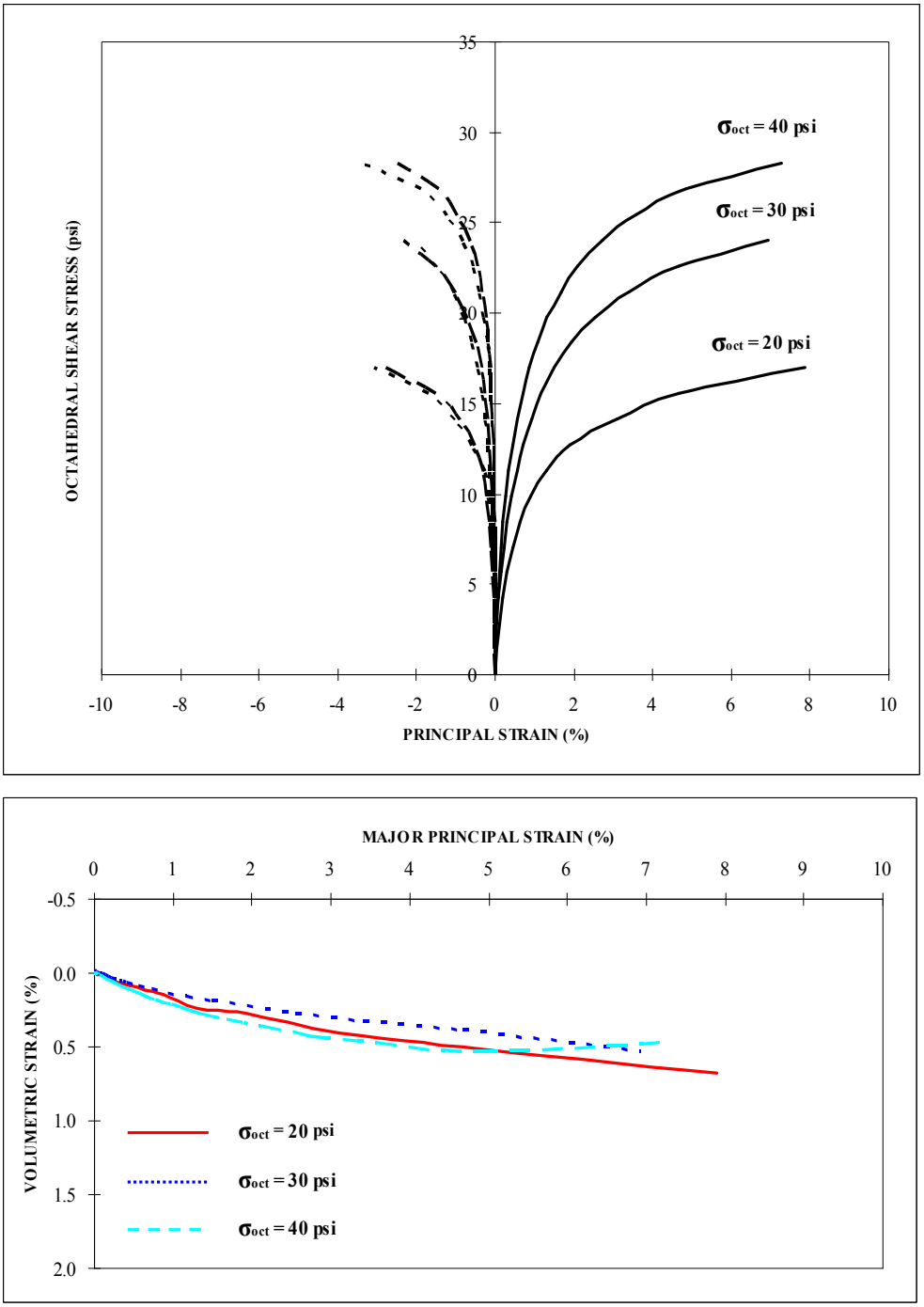

Figure 5.31 TC Test Results under Undrained Loading (w = 8%)

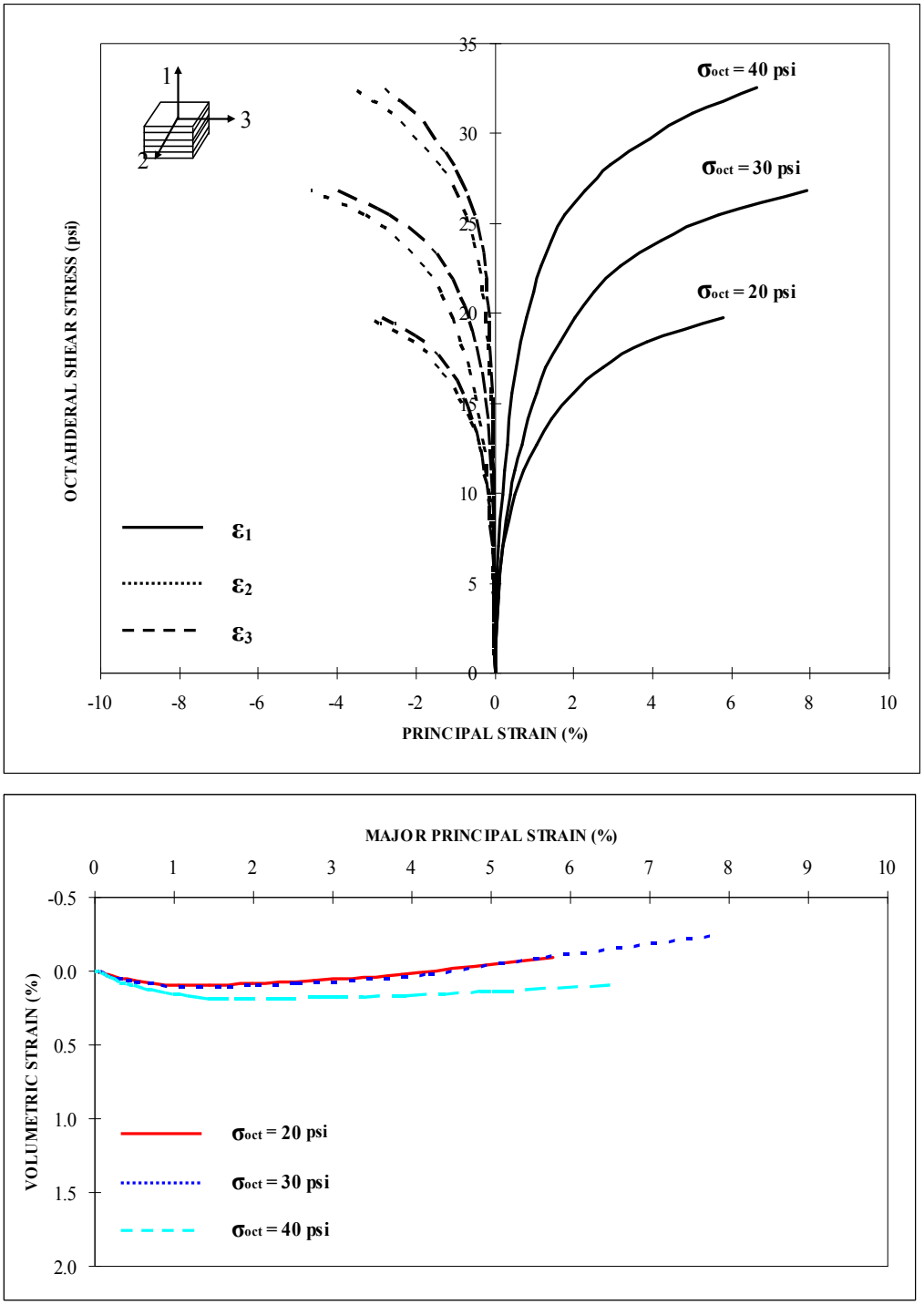

Figure 5.32 TC Test Results under Undrained Loading (w = 10%)

5.4.2.3 Triaxial Extension (TE) Tests

A series of 9 undrained TE tests were carried out with same confining pressures and water contents as drained TE testings. The results of these testings are presented in Figures 5.33 to 5.35. The measured results show similar to those of drained testings. The principal strains in y and z direction is compressive, while the minor principal strain in x direction is expansive. The strength of soil increases with an increase in octahedral normal stress. The volumetric strain (w = 10%) is predominately dilative.

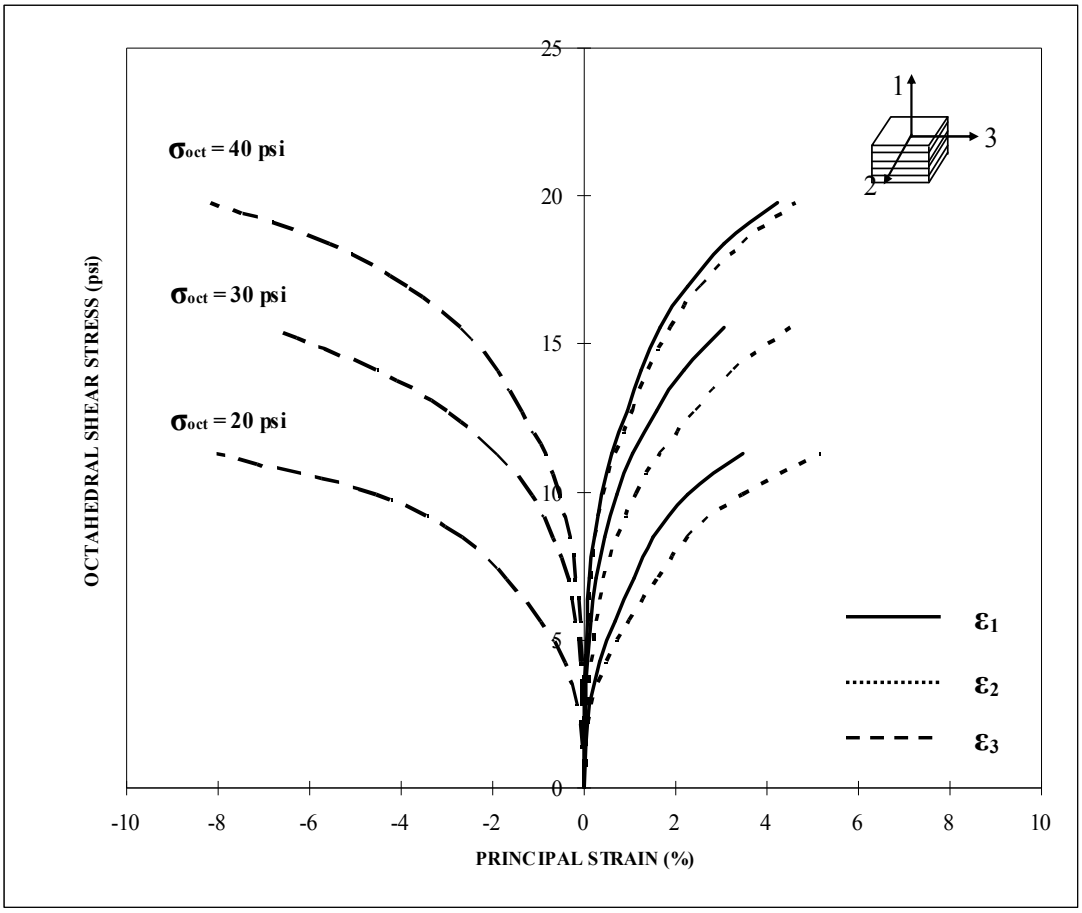

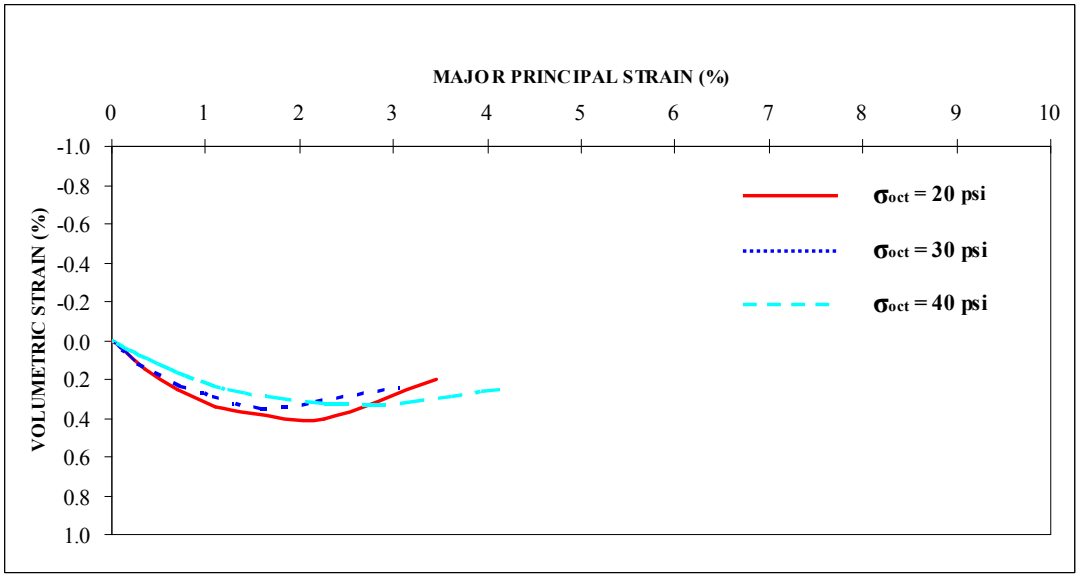

Figure 5.33 TE Test Results under Undrained Loading (w = 6%)

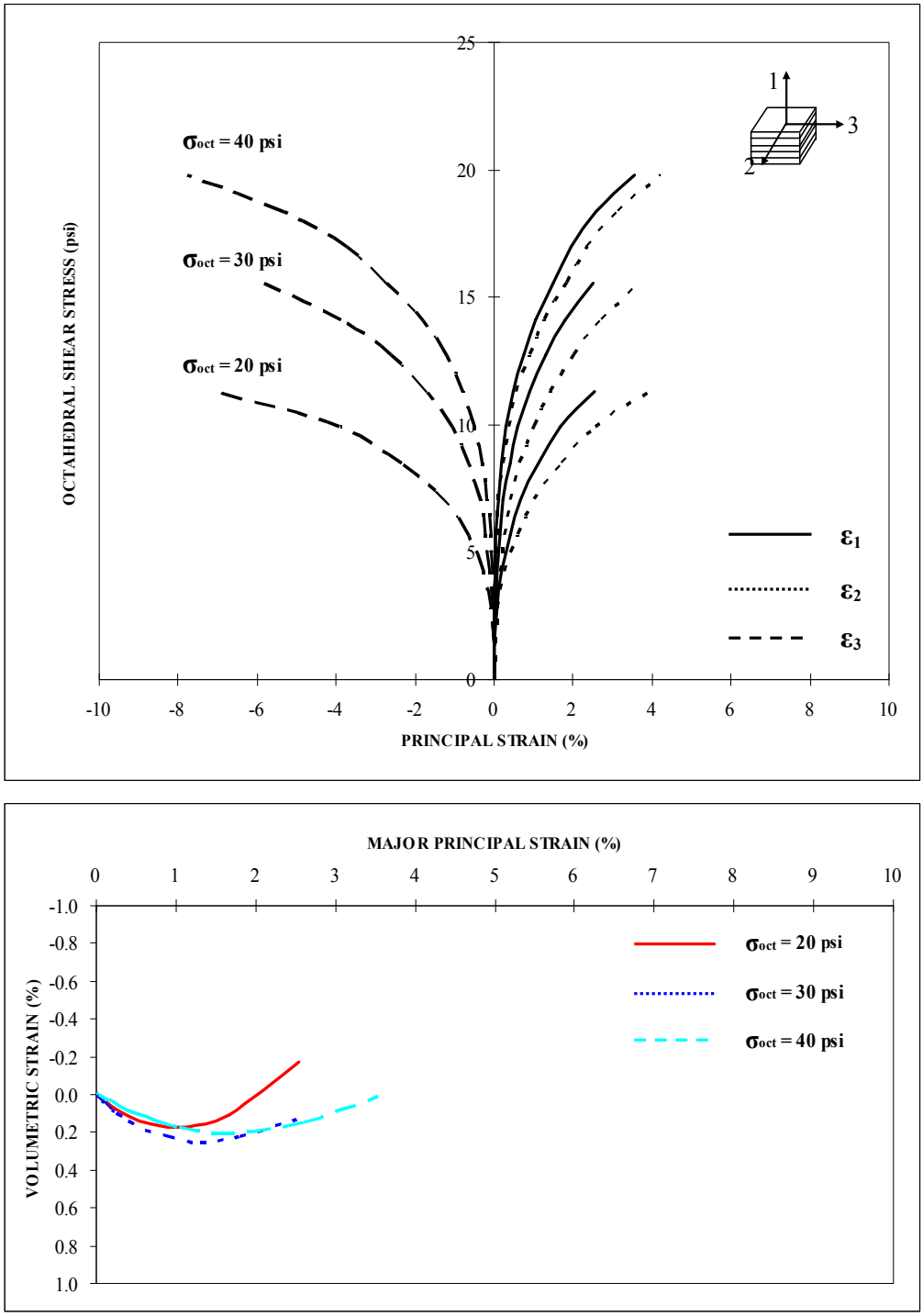

Figure 5.34 TE Test Results under Undrained Loading (w = 8%)

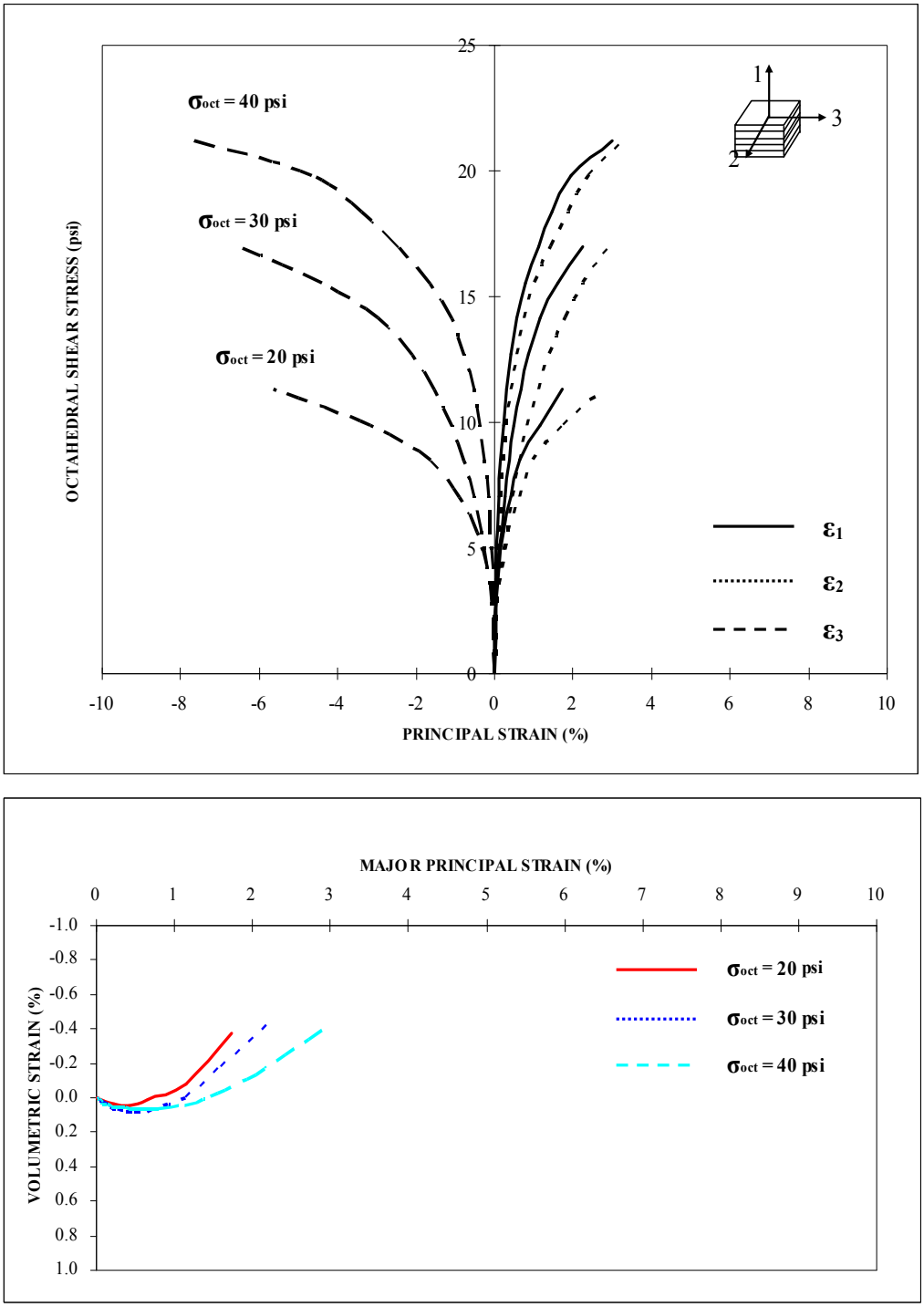

Figure 5.35 TE Test Results under Undrained Loading (w = 10%)

5.4.2.4 Simple Shear (SS) Tests

A series of 9 undrained SS tests were carried out at the same confining pressures and water contents as drained SS testings. The results of these testings are presented in Figures 5.36 to 5.38. In general, the experimental results are similar to those from drained testings. The principal strain in y direction is very small, while the major principal strain in z direction is compressive and the minor principal strain in x direction is expansive. The strength and stiffness of soil increase with an increase in octahedral normal stress. The volumetric strain is generally dilative.

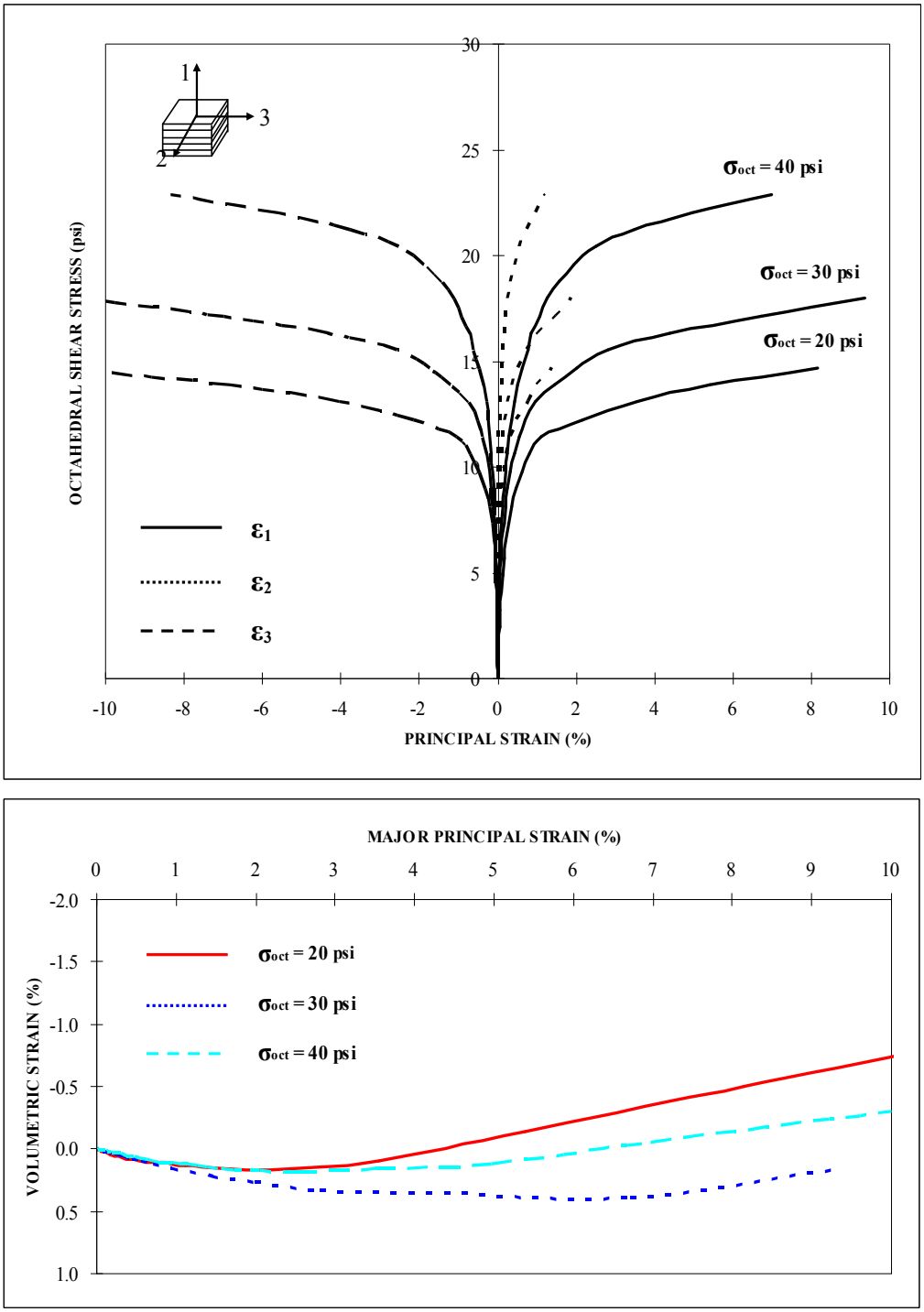

Figure 5.36 SS Test Results under Undrained Loading (w = 6%)

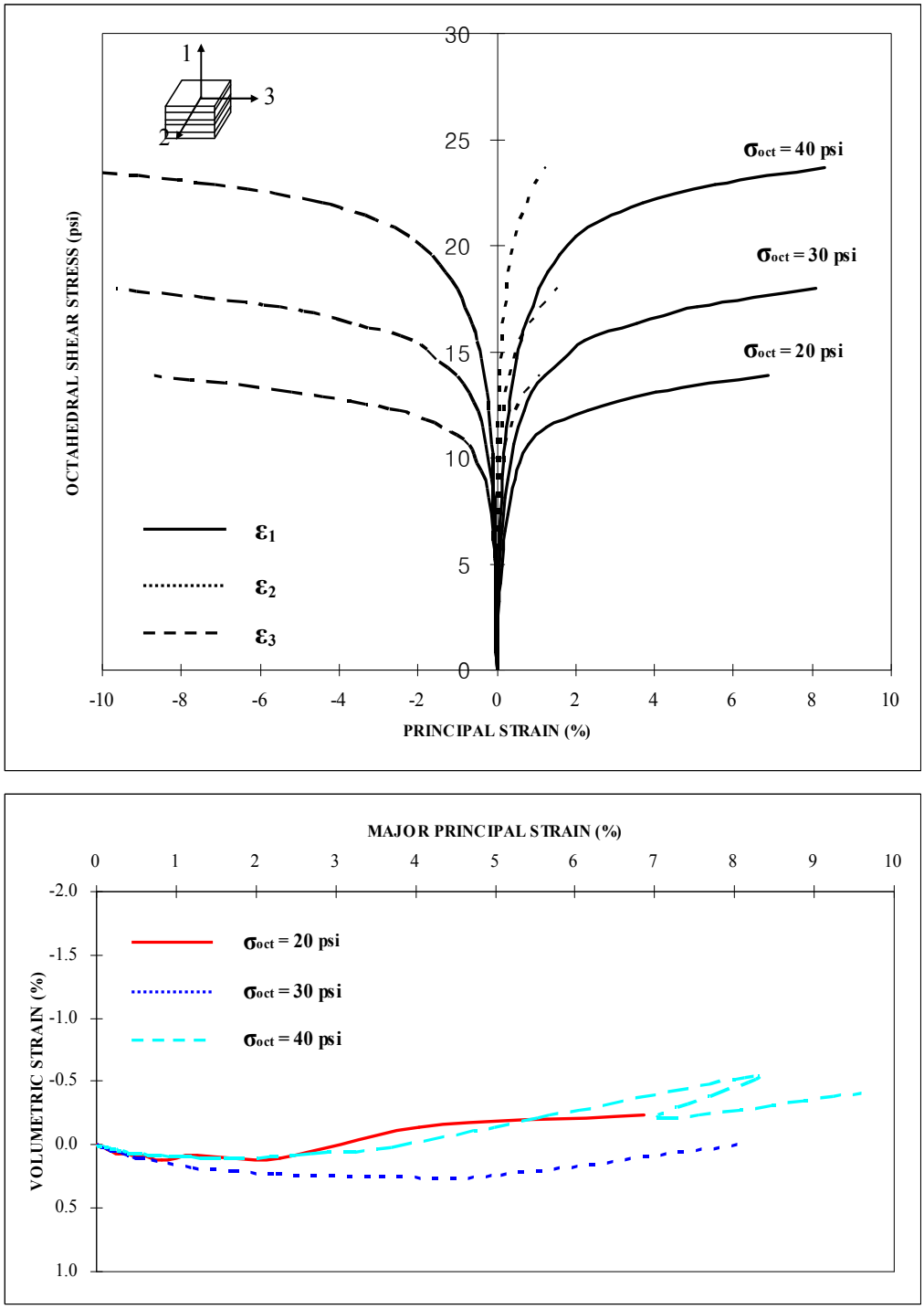

Figure 5.37 SS Test Results under Undrained Loading (w = 8%)

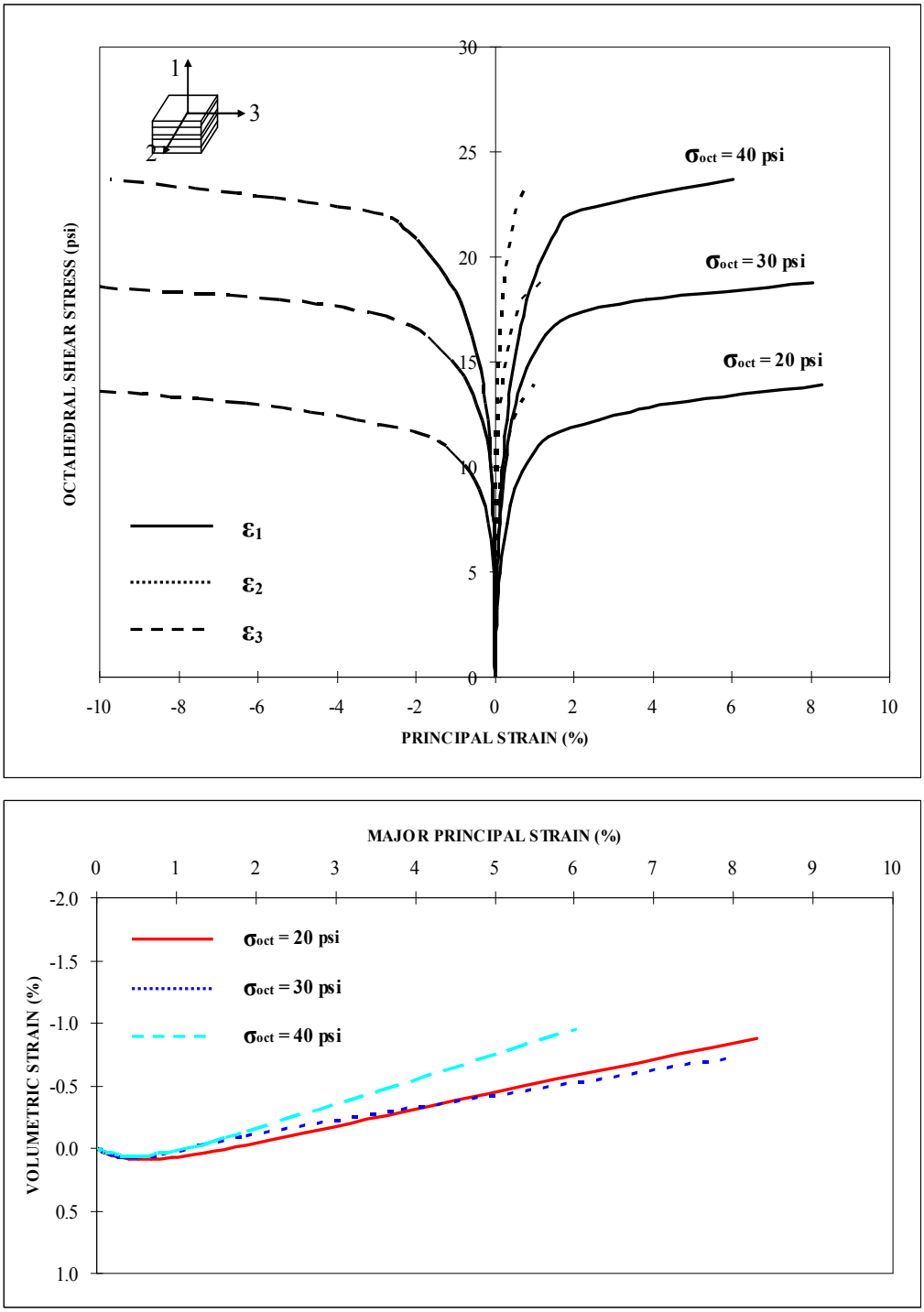

Figure 5.38 SS Test Results under Undrained Loading (w = 10%)

5.4.3 Influence of Initial Soil State on Unsaturated Soil Strength

The influence of initial soil state on the strength of unsaturated soil is presented from figures 5.39 to 5.50. The results show similar to those of drained testings. The strength of soil increases as degree of saturation increases from 27 to 61% and initial dry density increases from 16.40 to 18.12 kN/m^3, in spite of initial suction decreasing from 1360 to 550 kPa. The measured results demonstrate that the contribution of the initial degree of saturation and initial dry density in soil strength under undrained condition is much higher than that of soil suction induced by water menisci.

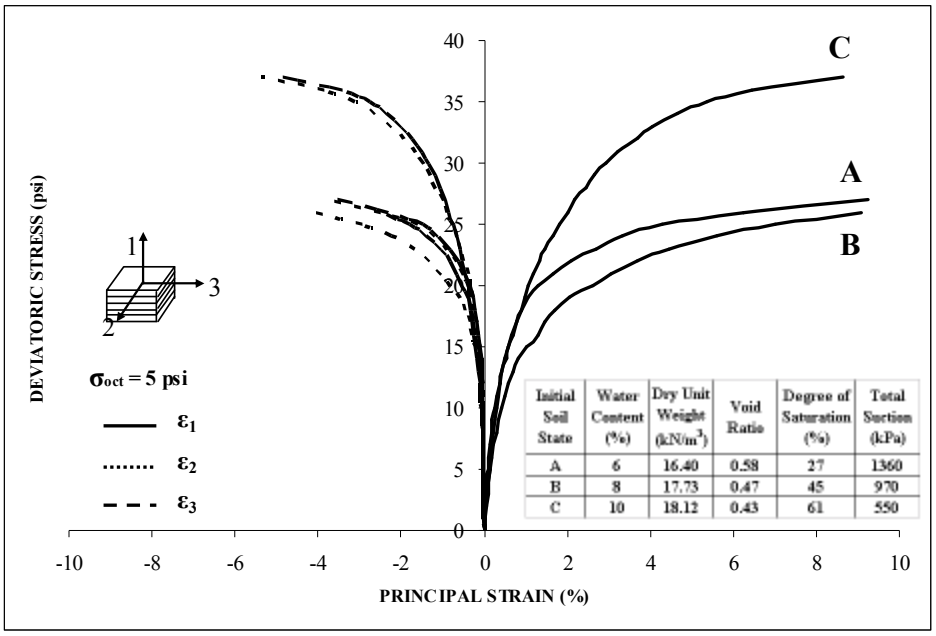

Initial Soil State	Water Content (%)	Dry Unit Weight (kN/m^3)	Void Ratio	Degree of Saturation (%)	Total Suction (kPa)
A	6	16.40	0.58	27	1360
B	8	17.73	0.47	45	970
C	10	18.12	0.43	61	550

Figure 5.39 CTC Test Results for Silty Sand with Three Different Initial Conditions under Undrained Loading (σ_{oct} = 5 psi)

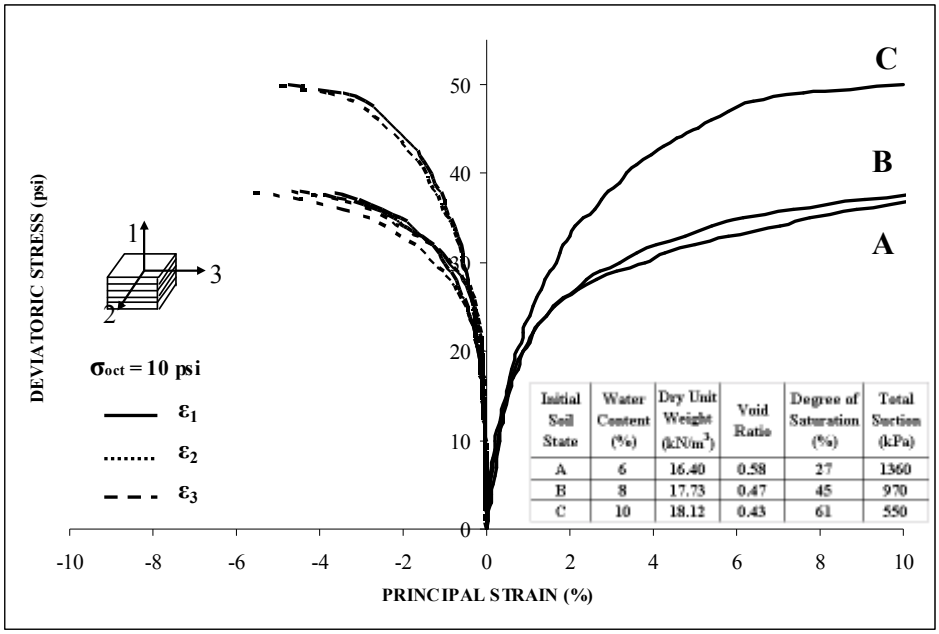

Figure 5.40 CTC Test Results for Silty Sand with Three Different Initial Conditions under Undrained Loading (σ_{oct} = 10 psi)

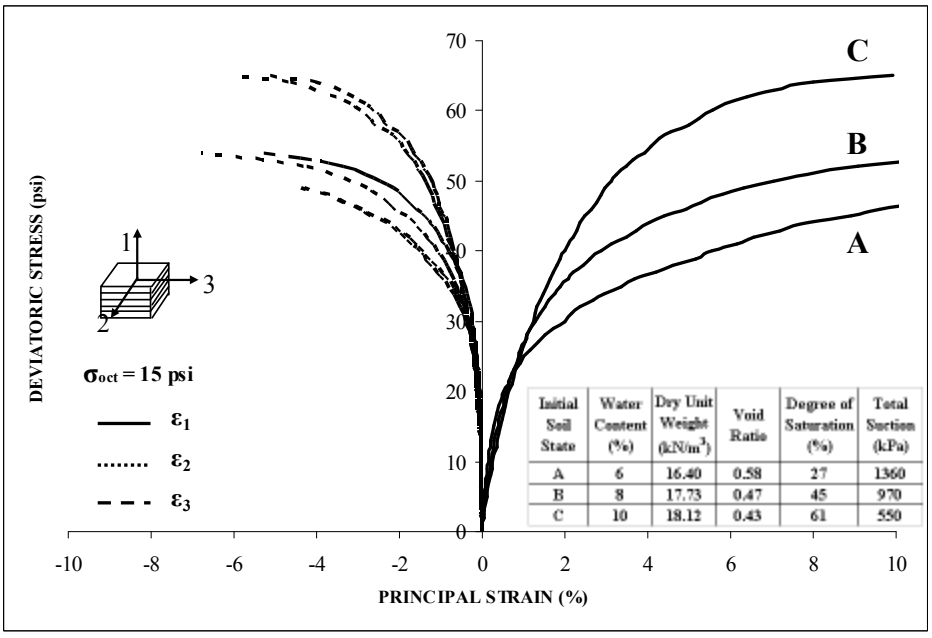

Figure 5.41 CTC Test Results for Silty Sand with Three Different Initial Conditions under Undrained Loading (σ_{oct} = 15 psi)

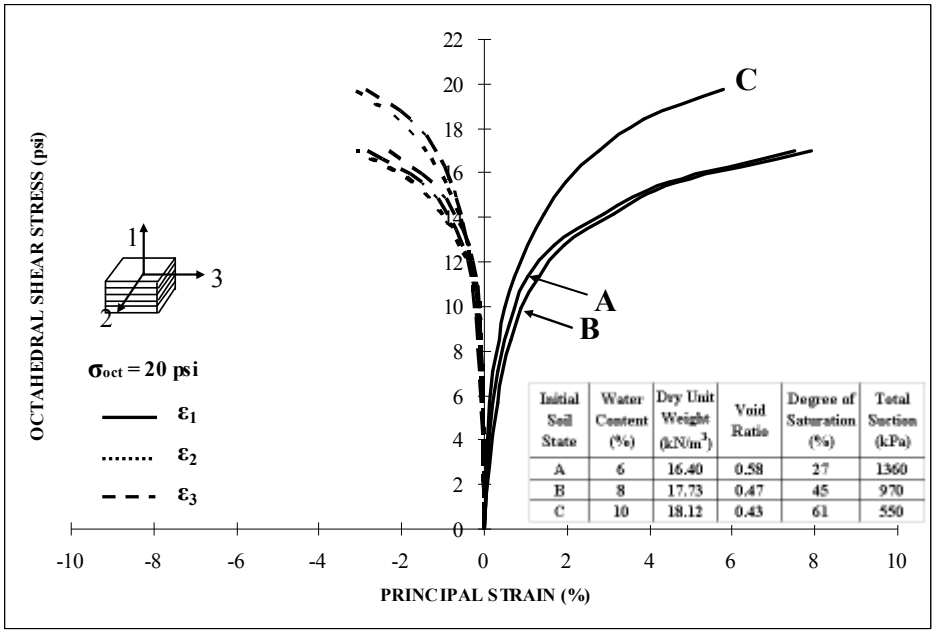

Figure 5.42 TC Test Results for Silty Sand with Three Different Initial Conditions under Undrained Loading (σ_{oct} = 20 psi)

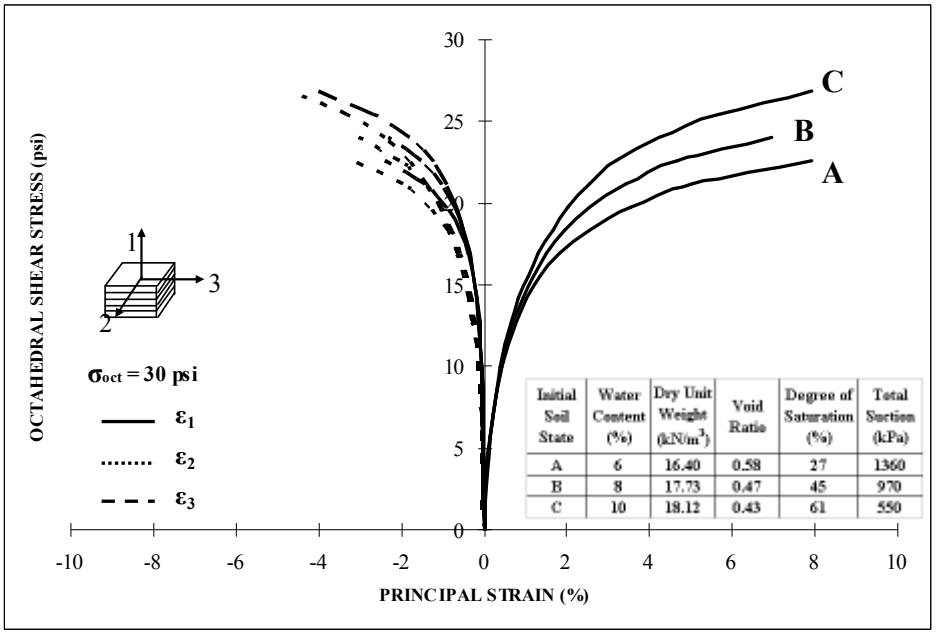

Figure 5.43 TC Test Results for Silty Sand with Three Different Initial Conditions under Undrained Loading (σ_{oct} = 30 psi)

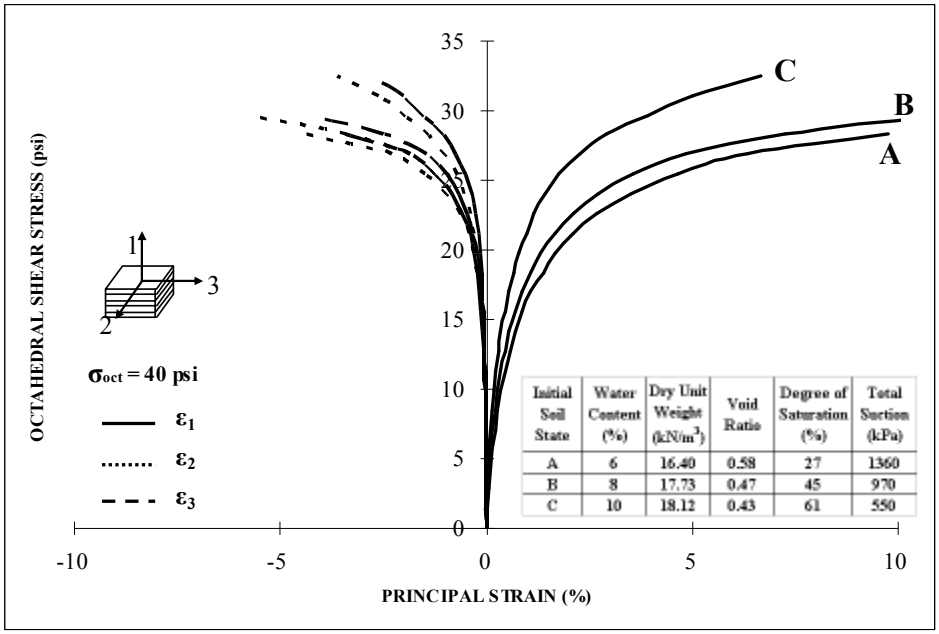

Figure 5.44 TC Test Results for Silty Sand with Three Different Initial Conditions under Undrained Loading (σ_{oct} = 40 psi)

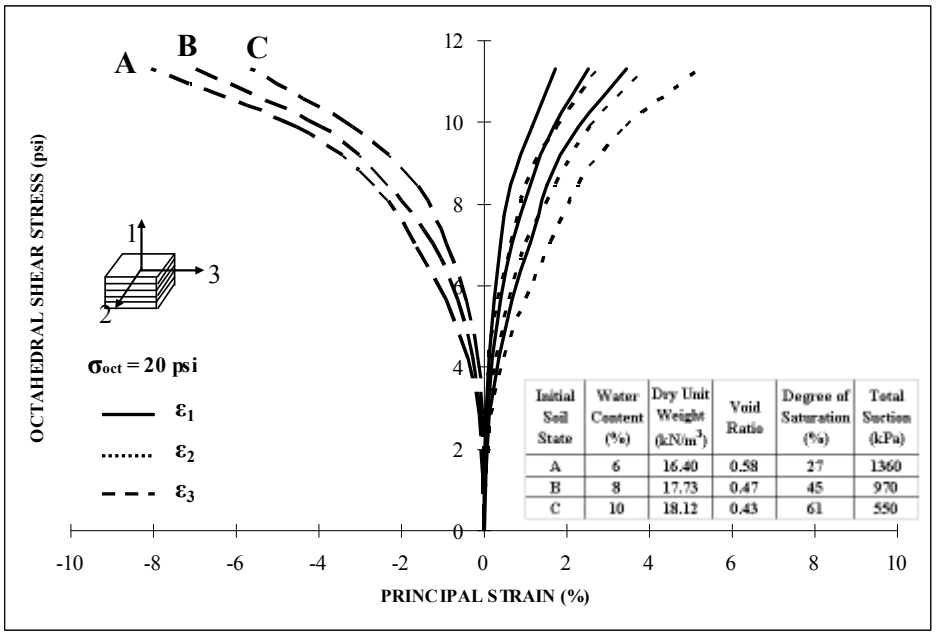

Figure 5.45 TE Test Results for Silty Sand with Three Different Initial Conditions under Undrained Loading (σ_{oct} = 20 psi)

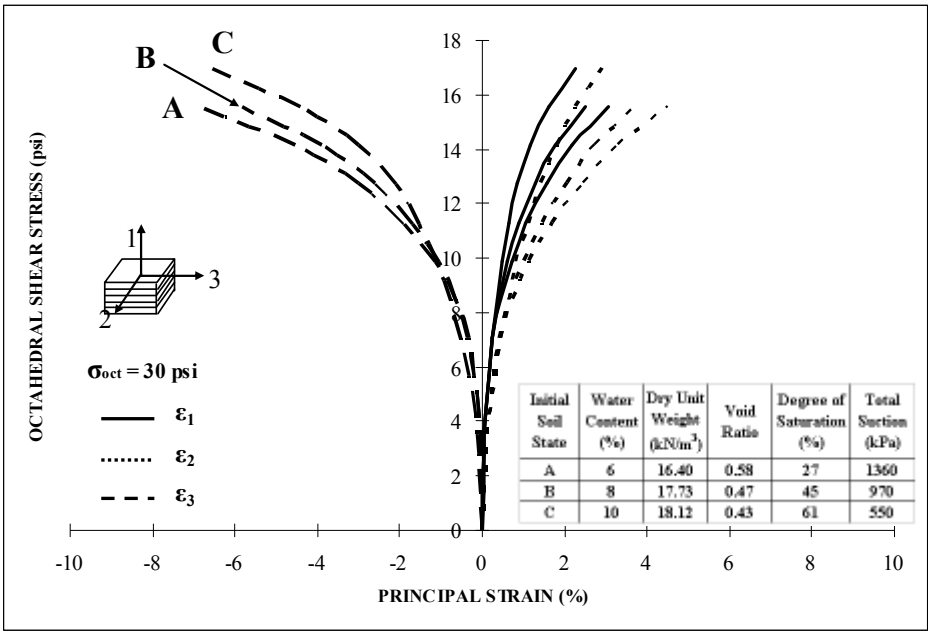

Figure 5.46 TE Test Results for Silty Sand with Three Different Initial Conditions under Undrained Loading (σ_{oct} = 30 psi)

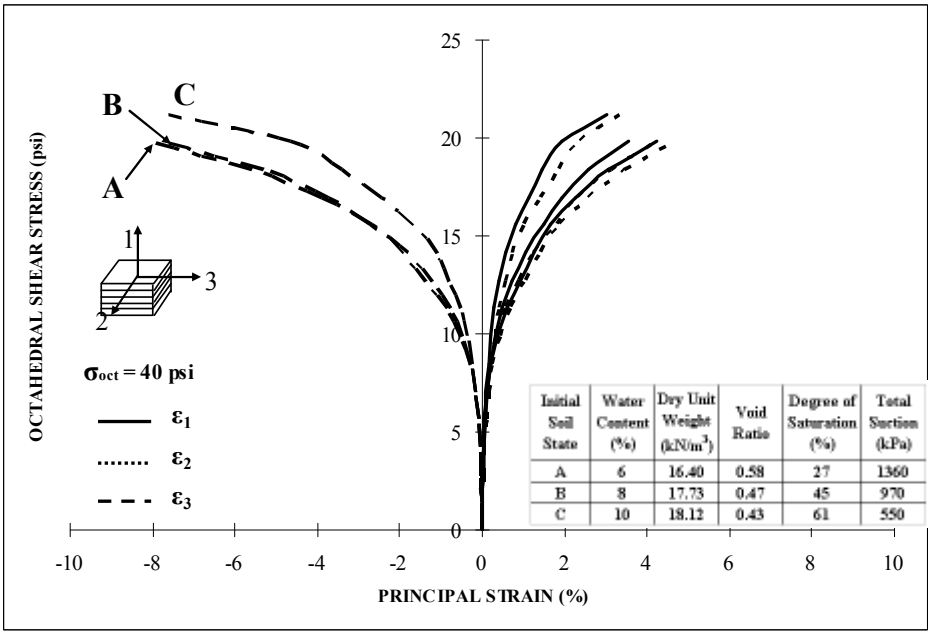

Figure 5.47 TE Test Results for Silty Sand with Three Different Initial Conditions under Undrained Loading (σ_{oct} = 40 psi)

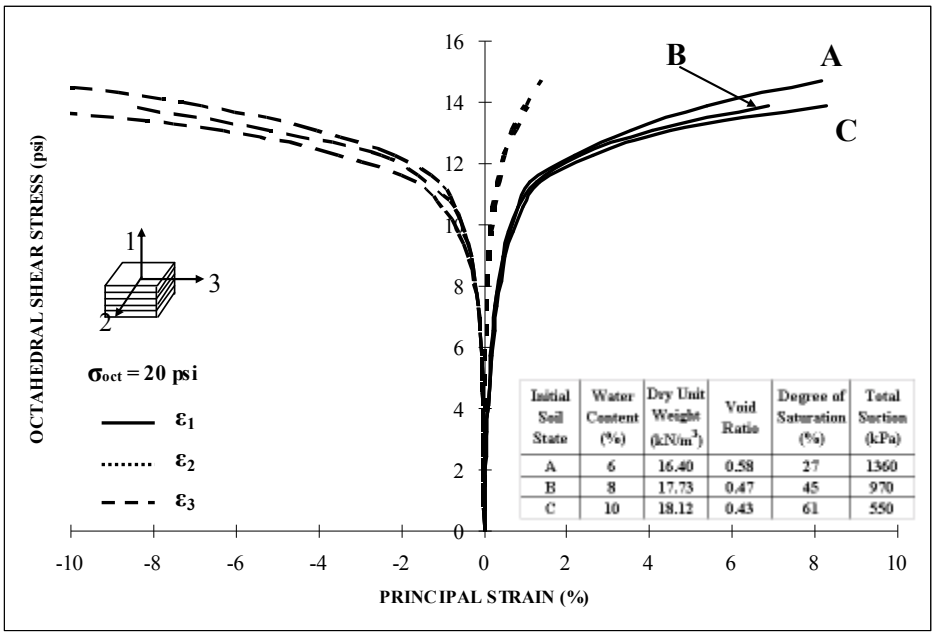

Figure 5.48 SS Test Results for Silty Sand with Three Different Initial Conditions under Undrained Loading (σ_{oct} = 20 psi)

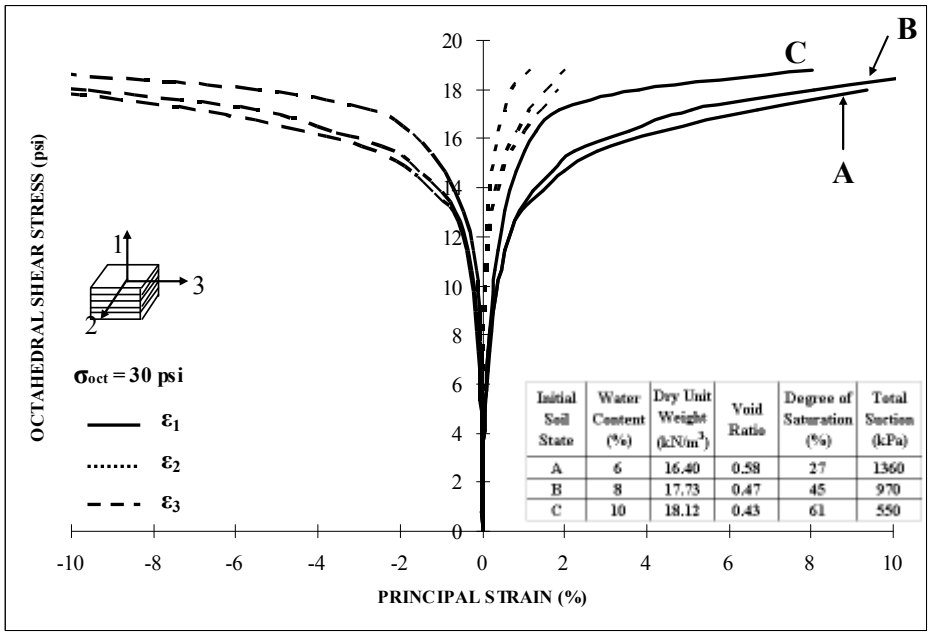

Figure 5.49 SS Test Results for Silty Sand with Three Different Initial Conditions under Undrained Loading (σ_{oct} = 30 psi)

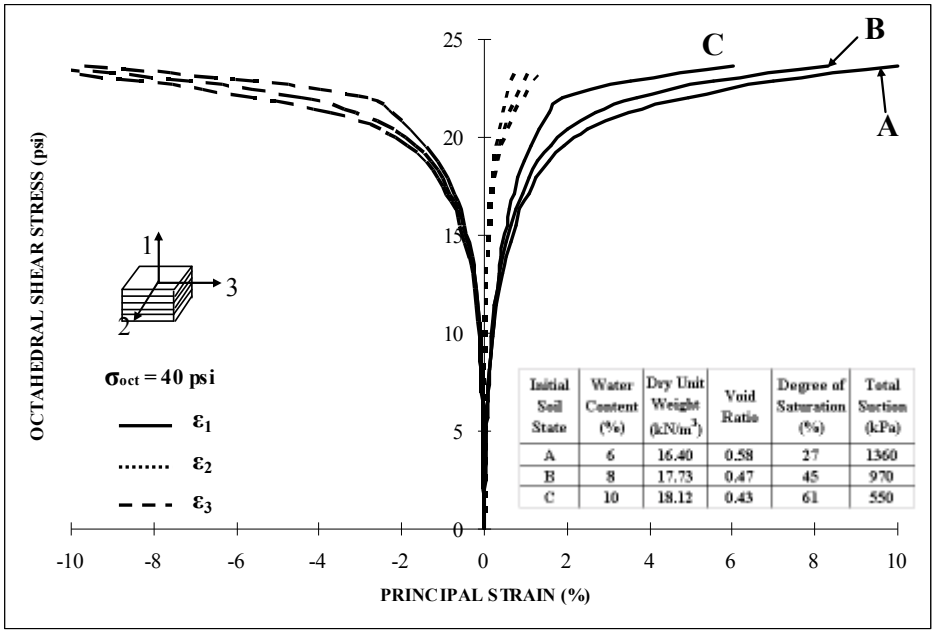

Figure 5.50 SS Test Results for Silty Sand with Three Different Initial Conditions under Undrained Loading (σ_{oct} = 40 psi)

5.4.4 Failure Envelopes on Octahedral Plane and Critical State Line

The projection of failure envelopes obtained from undrained true triaxial tests onto the octahedral plane is shown in Figure 5.51. It is based on three types of soil (A, B, and C) containing different initial conditions and three different octahedral normal stresses (σ_{oct} = 20, 30, and 40 psi). The results are similar to those of drained testings which show the shape, size, and position of the failure envelope are significantly affected by initial degree of saturation and initial dry density. However, the size of failure envelope is equal or slightly bigger than that under drained testing.

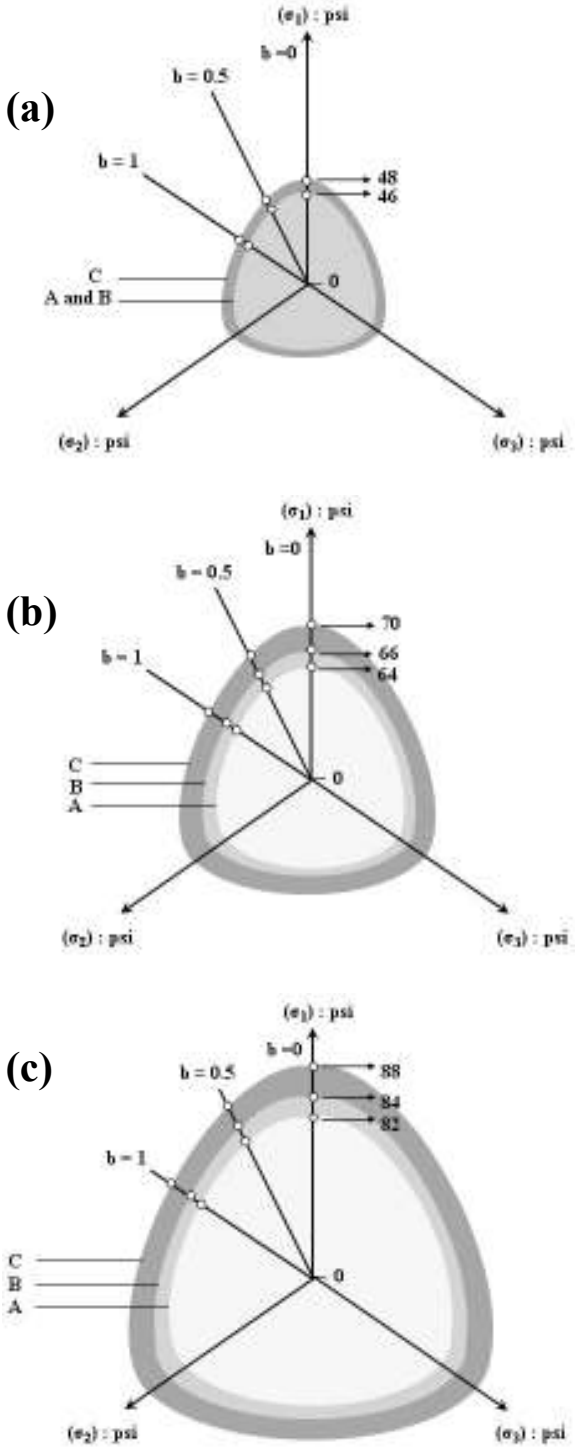

Initial Soil State	Water Content (%)	Dry Unit Weight (kN/m^3)	Void Ratio	Degree of Saturation (%)	Total Suction (kPa)
A	6	16.40	0.58	27	1360
B	8	17.73	0.47	45	970
C	10	18.12	0.43	61	550

Figure 5.51 Projection of Failure Envelopes on Octahedral Plane under Undrained Loading: (a) σ_{oct} = 20 psi, (b) σ_{oct} = 30 psi, (c) σ_{oct} = 40 psi.

In addition, best-fit critical state lines are presented in terms of net mean stress, p and deviatoric stress, q (Figure 5.52). It seems that the slope of critical state line, M is nearly constant and is independent of initial degree of saturation and dry density.

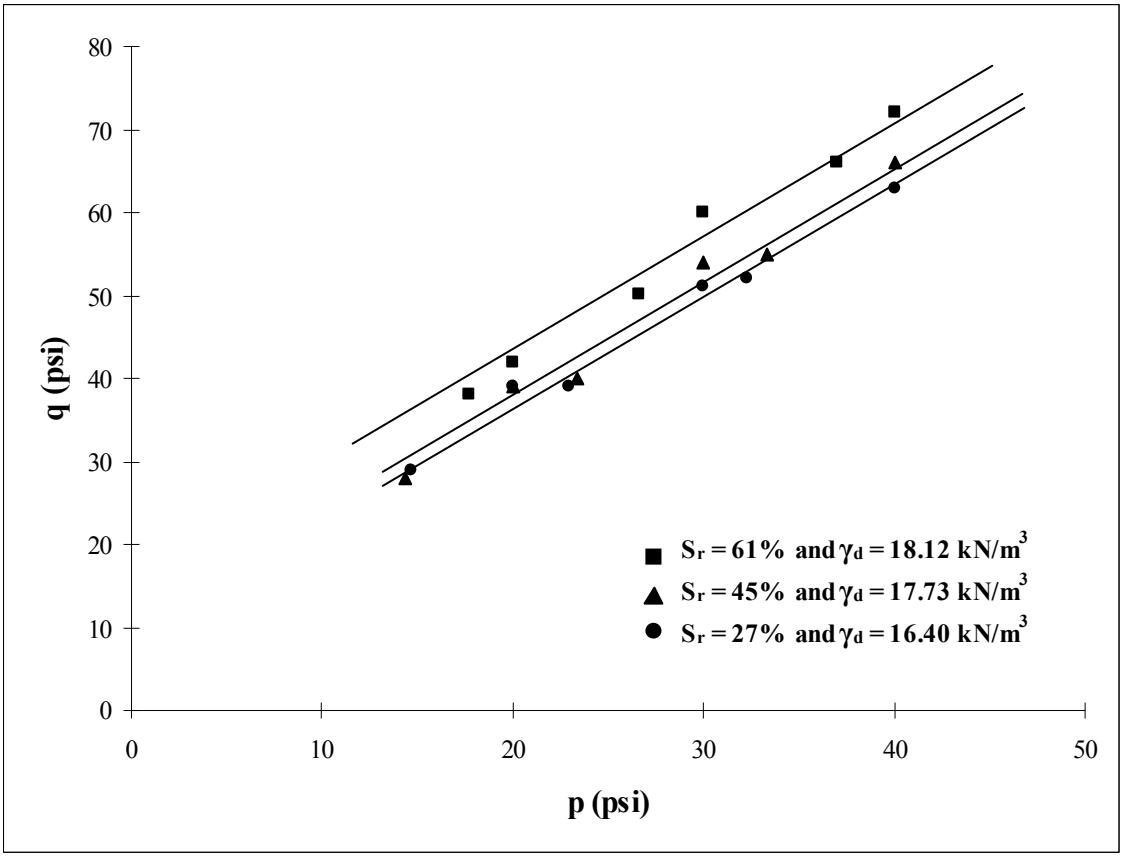

Figure 5.52 P-q Diagram for Kneading-Compacted Unsaturated Silty Sand under Undrained Loading

5.5 Comparison of Drained and Undrained Soil Behaviors

Figures 5.53 to 5.88 show the comparison between results from drained and undrained loading. In general, the strength of soil under drained condition in saturated soil is higher than that under undrained condition. However, in these tests performed on unsaturated soils, the undrained strength of soil shows slightly higher value than the drained strength. There are two possible reasons to explain this behaviour. According to section 2.4.1 under Literature Review, starting from a low degree of saturation, the soil strength increases with an increase in degree of saturation up to a certain optimum value, beyond which the strength drops due to further increase in degree of saturation. In general, the degree of saturation in unsaturated soil increases slightly during undrained loading and on the contrary, decreases slightly during drained loading (Rahardjo 1990). According to Figures 5.53 to 5.88, for the unsaturated specimens containing initially same degree of saturation before tests, the results generally show that the strength of soil under undrained condition is slightly greater than that under drained condition. Therefore, it can be concluded that the three values of degree of saturation (27, 45, and 61%) undertaken in this thesis work are below a certain optimum value. Another possible reason is that water menisci in soil under drained loading can be easily broken up and therefore the contribution of suction on soil strength is lost, whereas under undrained loading the compaction-induced menisci can be better kept due to the help of pore-air pressure buildup to hold them.

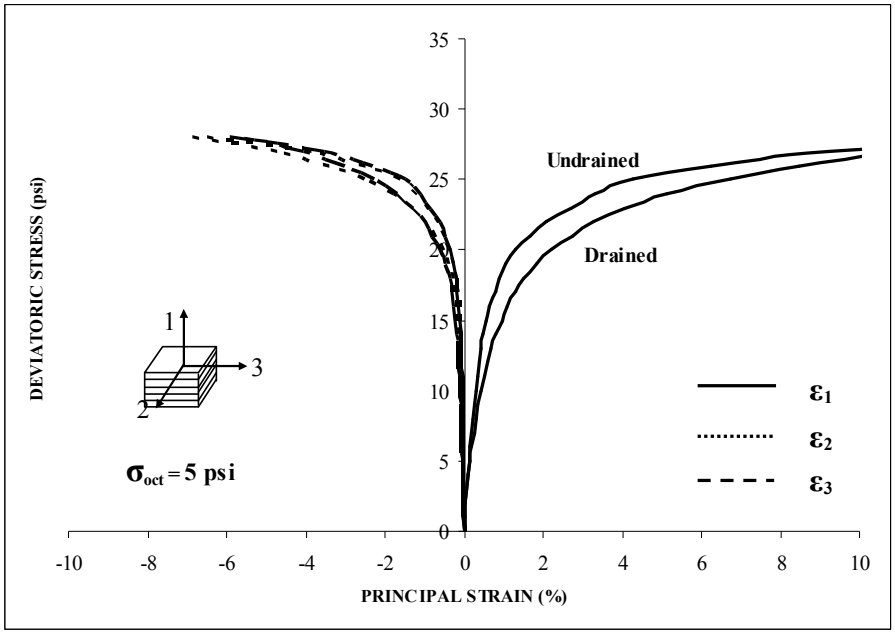

Figure 5.53 Comparison between Drained and Undrained CTC Test Results ($w = 6\%$, $\sigma_{oct} = 5$ psi)

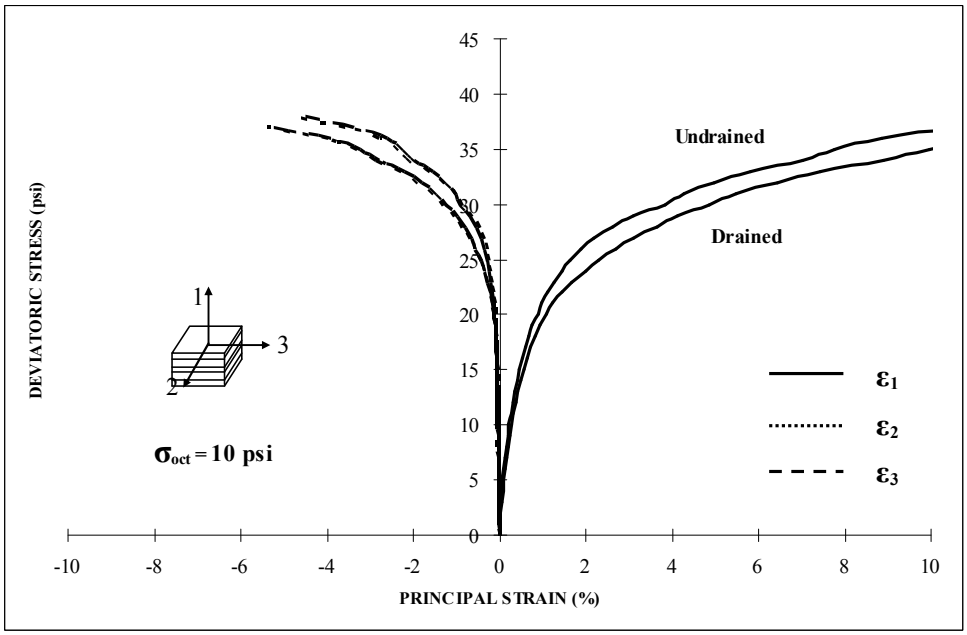

Figure 5.54 Comparison between Drained and Undrained CTC Test Results ($w = 6\%$, $\sigma_{oct} = 10$ psi)

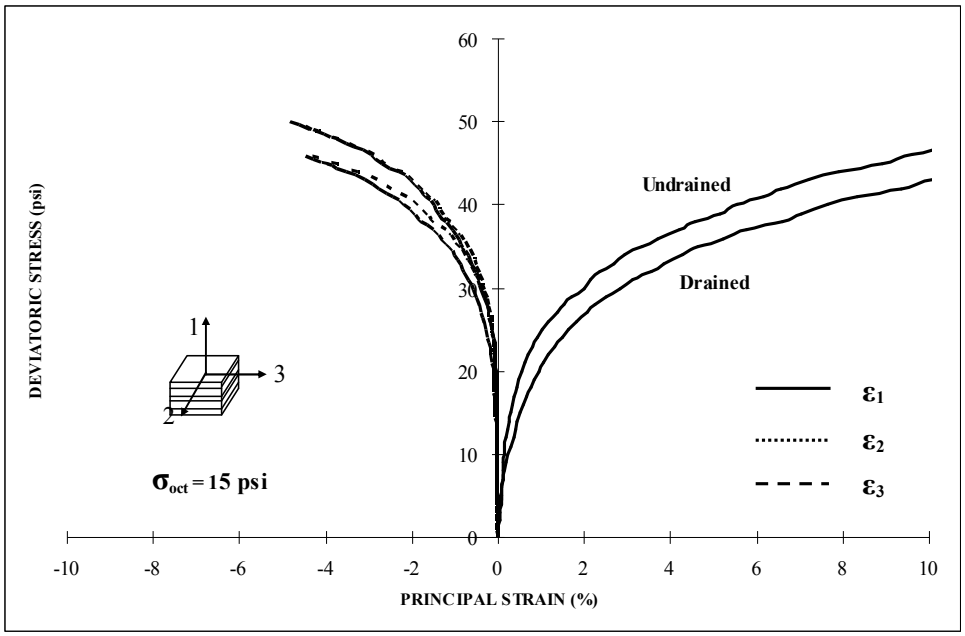

Figure 5.55 Comparison between Drained and Undrained CTC Test Results ($w = 6\%$, $\sigma_{oct} = 15$ psi)

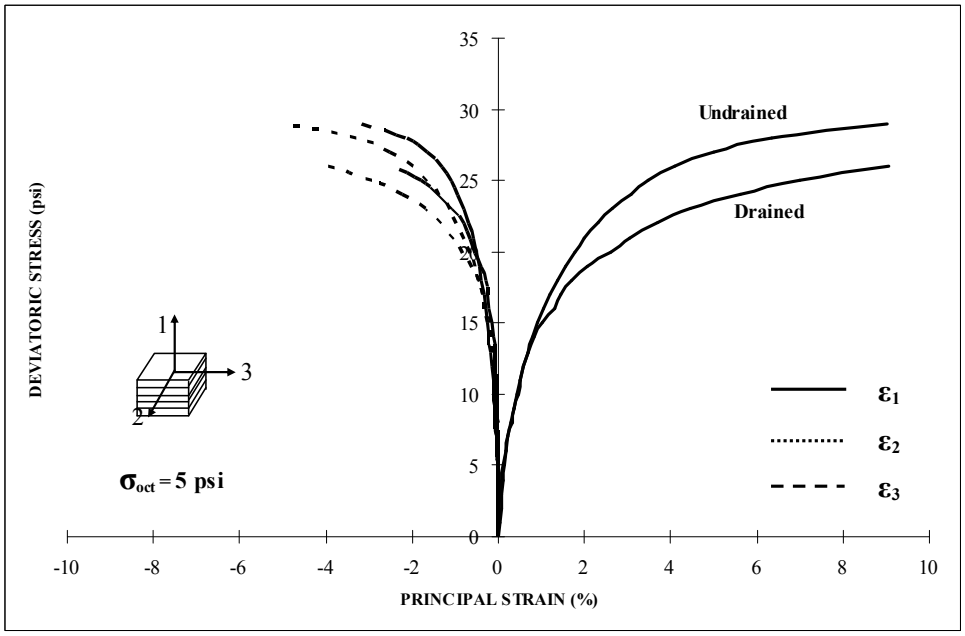

Figure 5.56 Comparison between Drained and Undrained CTC Test Results ($w = 8\%$, $\sigma_{oct} = 5$ psi)

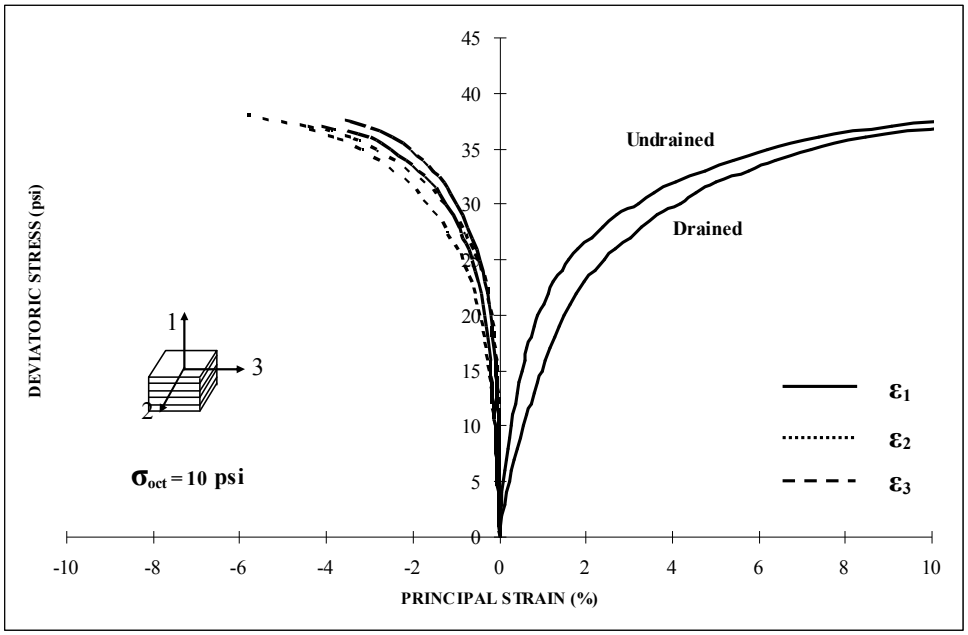

Figure 5.57 Comparison between Drained and Undrained CTC Test Results ($w = 8\%$, $\sigma_{oct} = 10$ psi)

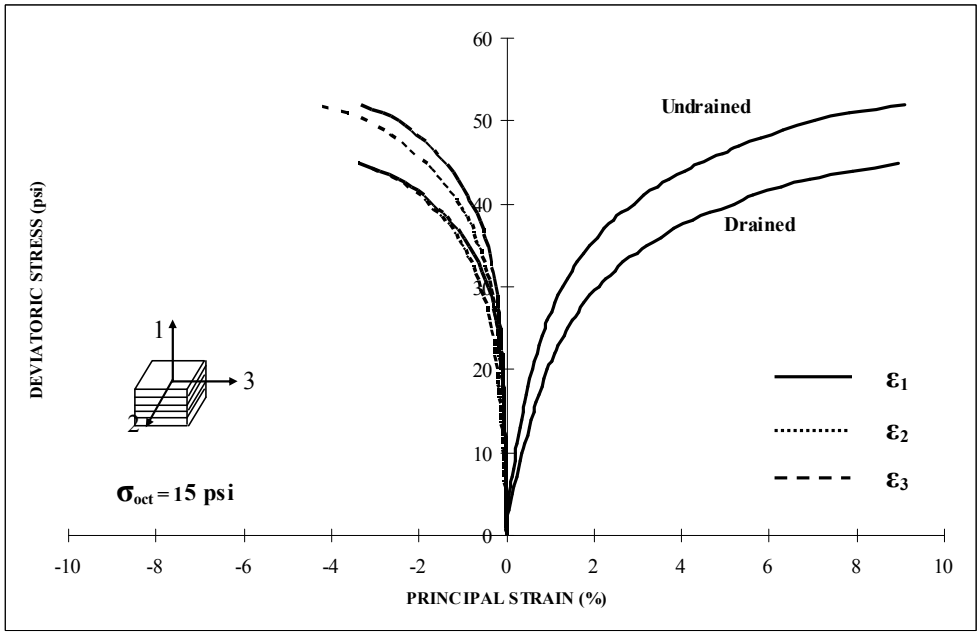

Figure 5.58 Comparison between Drained and Undrained CTC Test Results ($w = 8\%$, $\sigma_{oct} = 15$ psi)

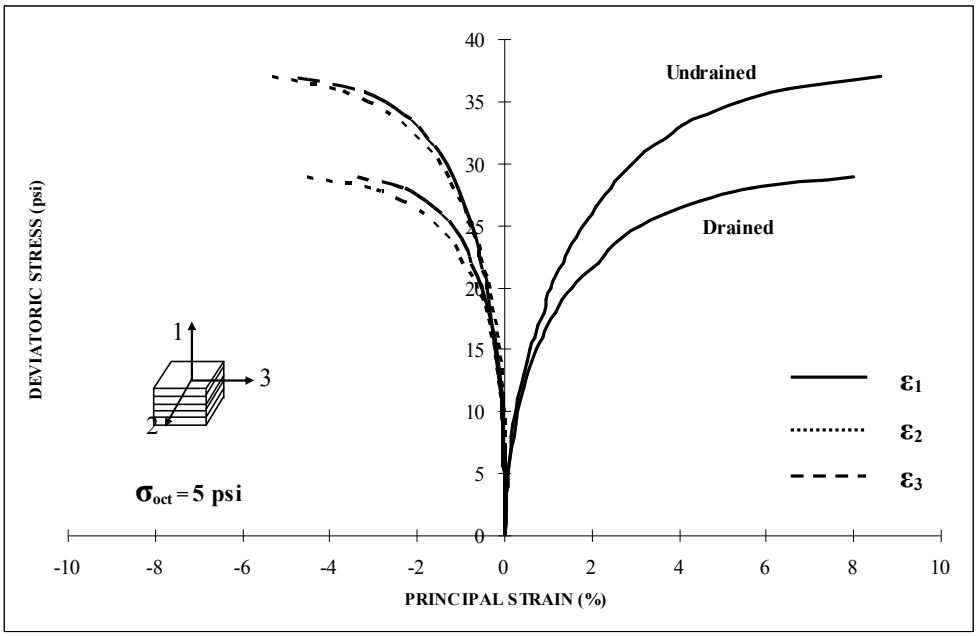

Figure 5.59 Comparison between Drained and Undrained CTC Test Results ($w = 10\%$, $\sigma_{oct} = 5$ psi)

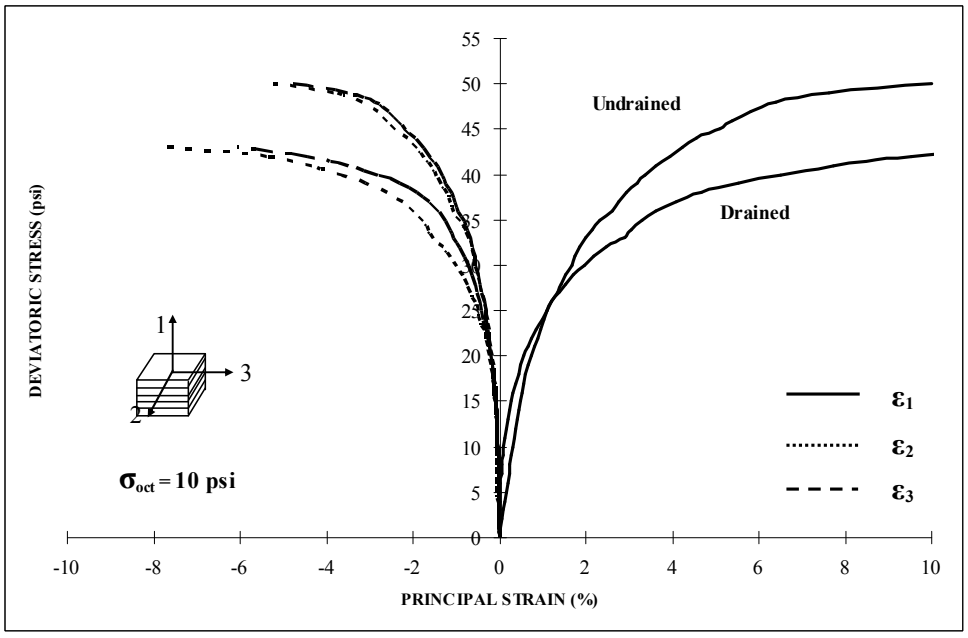

Figure 5.60 Comparison between Drained and Undrained CTC Test Results ($w = 10\%$, $\sigma_{oct} = 10$ psi)

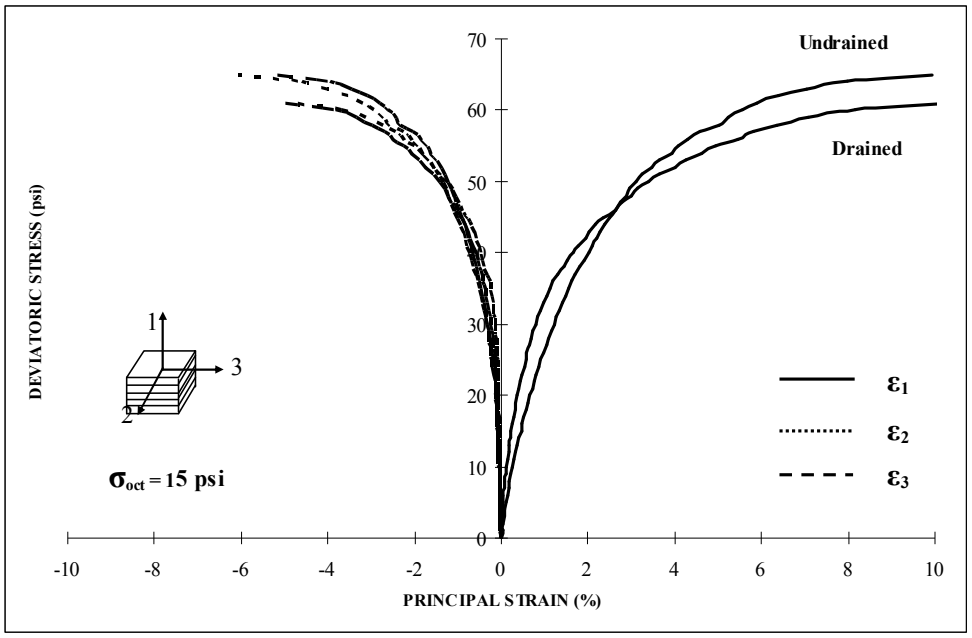

Figure 5.61 Comparison between Drained and Undrained CTC Test Results
(w = 10%, σ_{oct} = 15 psi)

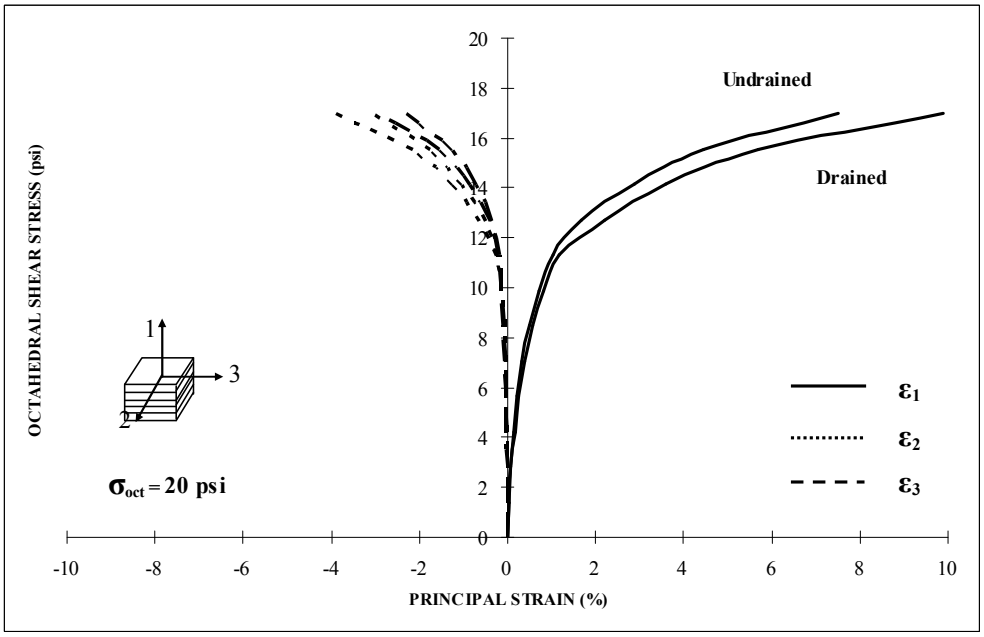

Figure 5.62 Comparison between Drained and Undrained TC Test Results
(w = 6%, σ_{oct} = 20 psi)

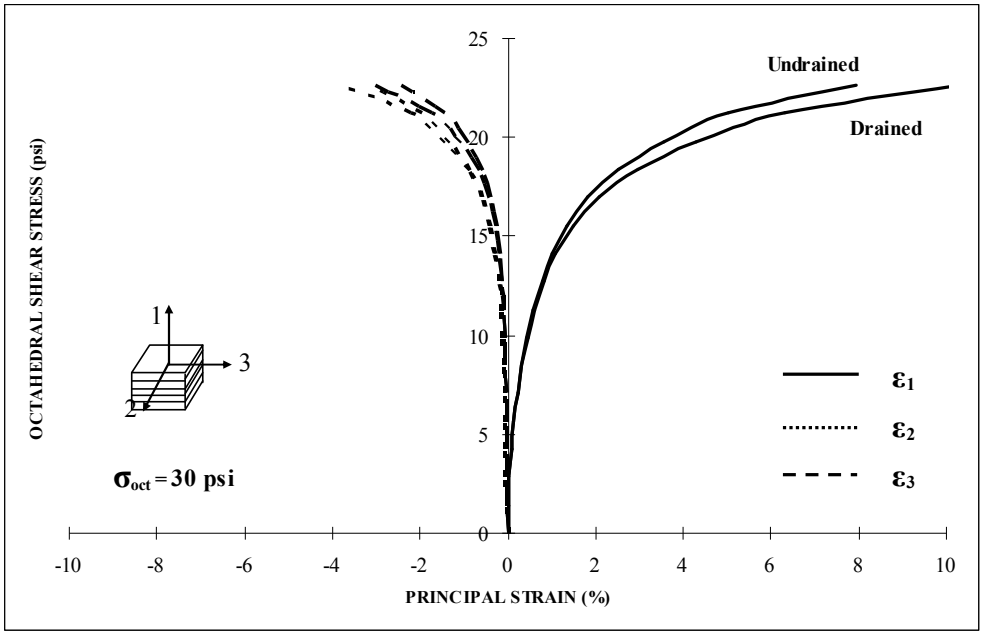

Figure 5.63 Comparison between Drained and Undrained TC Test Results ($w = 6\%$, $\sigma_{oct} = 30$ psi)

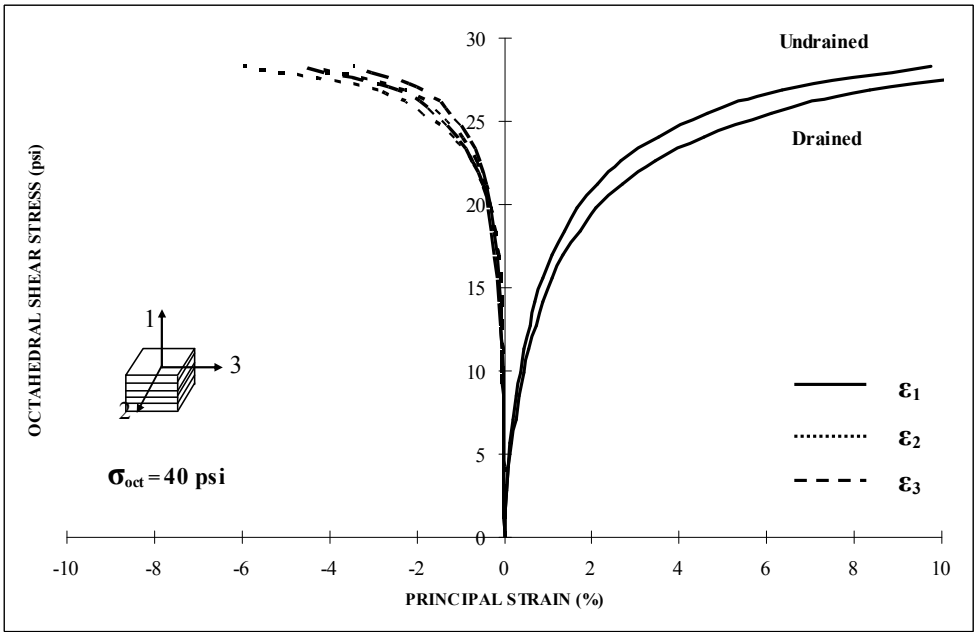

Figure 5.64 Comparison between Drained and Undrained TC Test Results ($w = 6\%$, $\sigma_{oct} = 40$ psi)

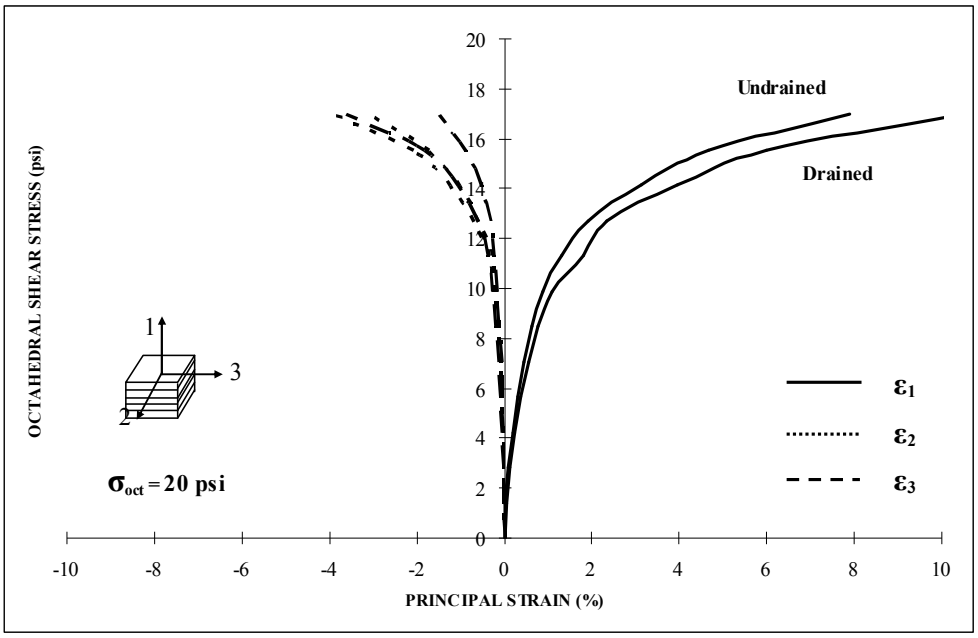

Figure 5.65 Comparison between Drained and Undrained TC Test Results ($w = 8\%$, $\sigma_{oct} = 20$ psi)

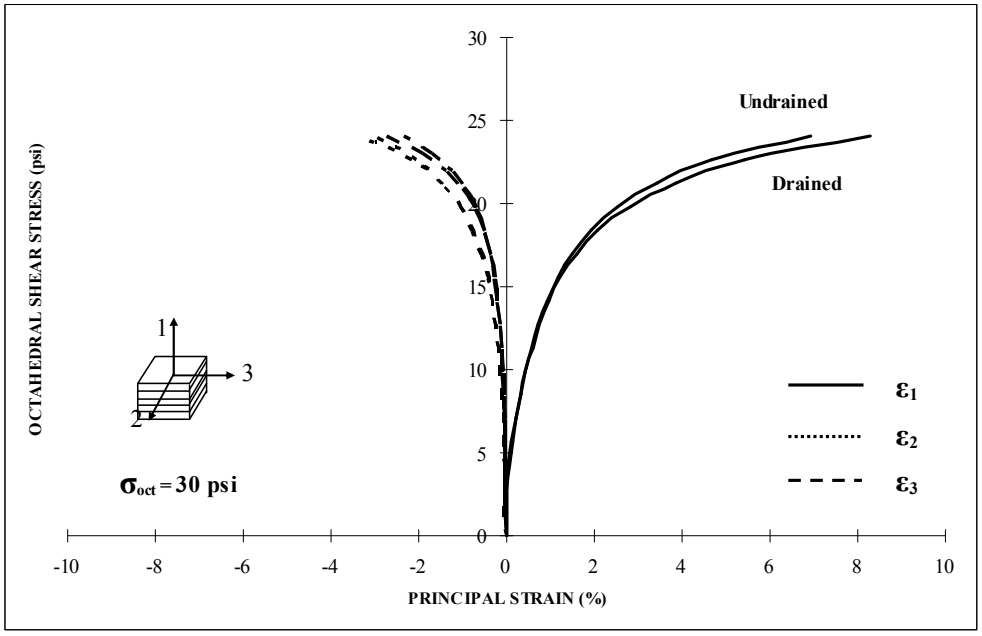

Figure 5.66 Comparison between Drained and Undrained TC Test Results ($w = 8\%$, $\sigma_{oct} = 30$ psi)

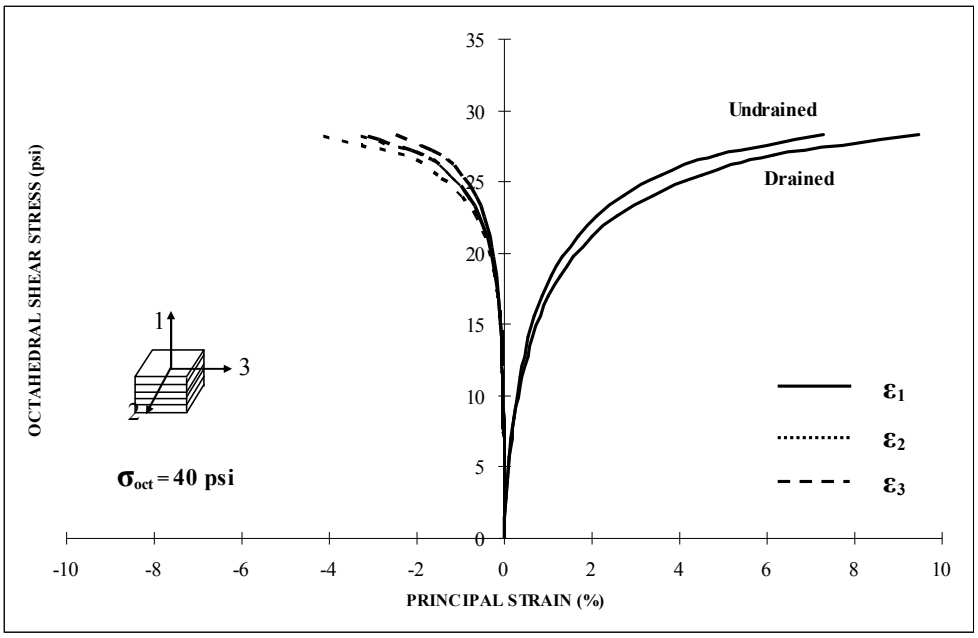

Figure 5.67 Comparison between Drained and Undrained TC Test Results ($w = 8\%$, $\sigma_{oct} = 40$ psi)

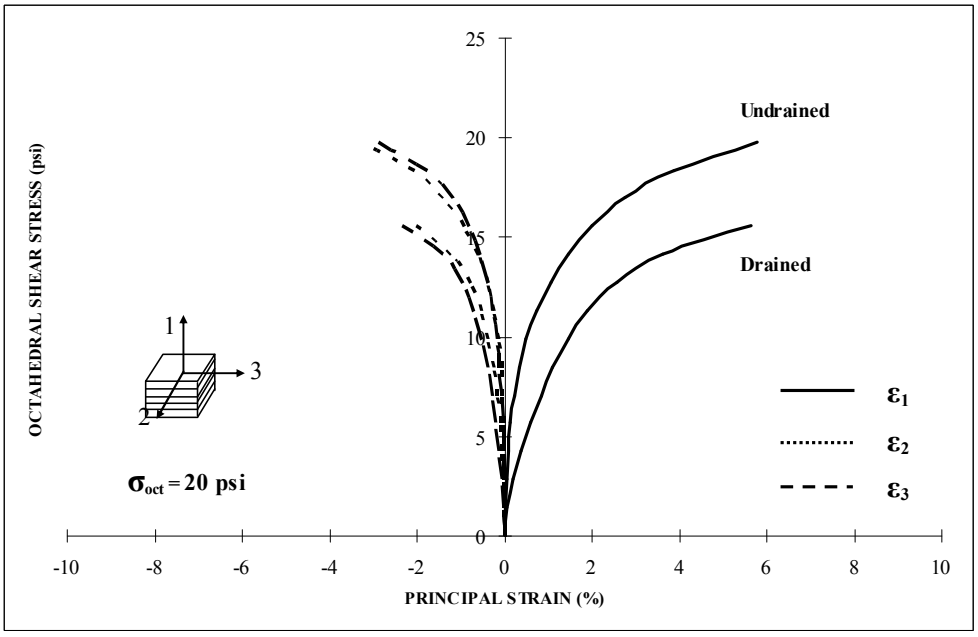

Figure 5.68 Comparison between Drained and Undrained TC Test Results ($w = 10\%$, $\sigma_{oct} = 20$ psi)

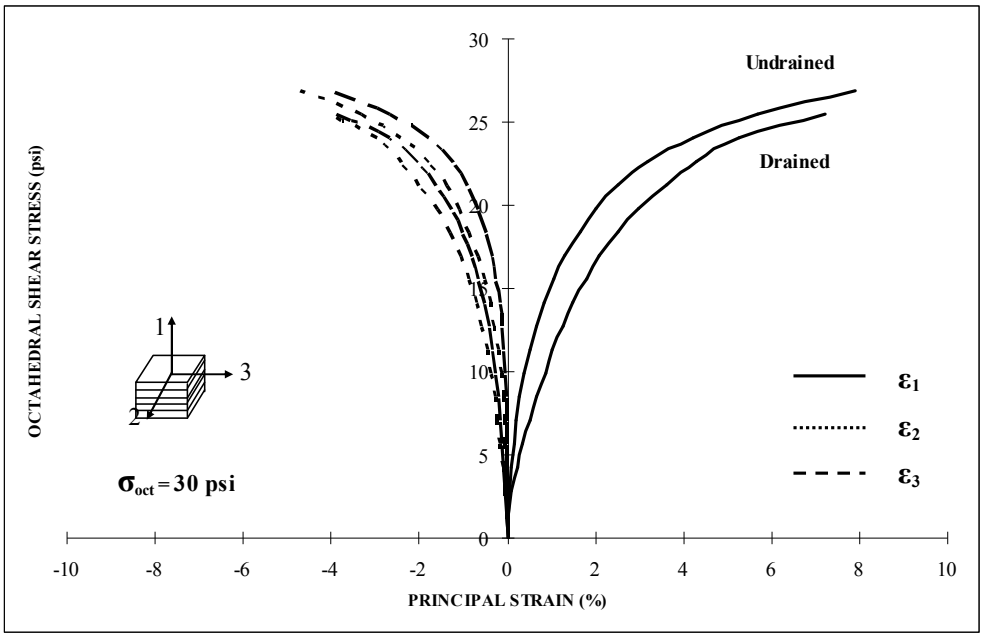

Figure 5.69 Comparison between Drained and Undrained TC Test Results ($w = 10\%$, $\sigma_{oct} = 30$ psi)

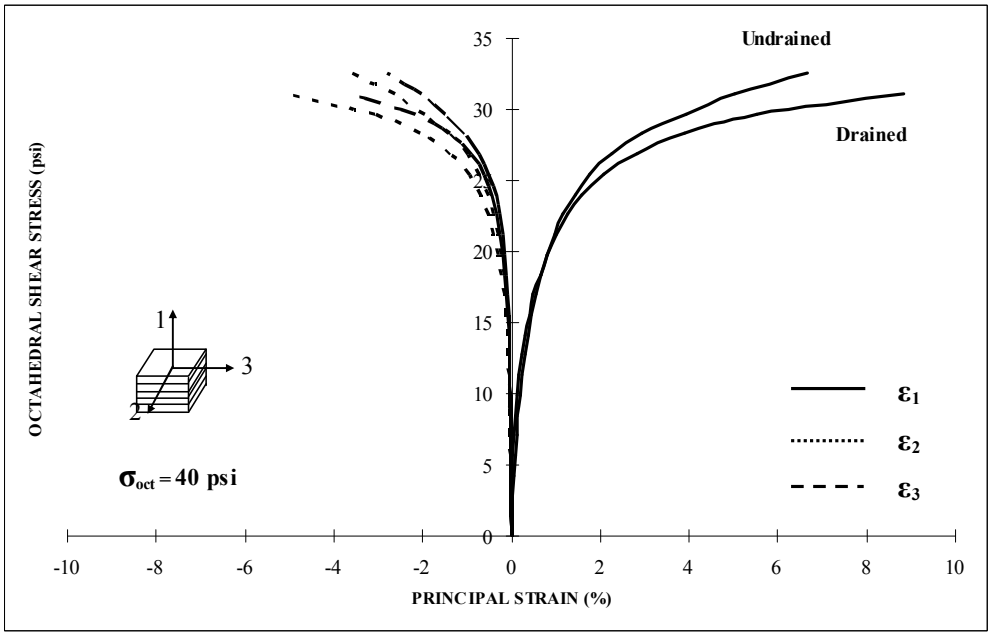

Figure 5.70 Comparison between Drained and Undrained TC Test Results ($w = 10\%$, $\sigma_{oct} = 40$ psi)

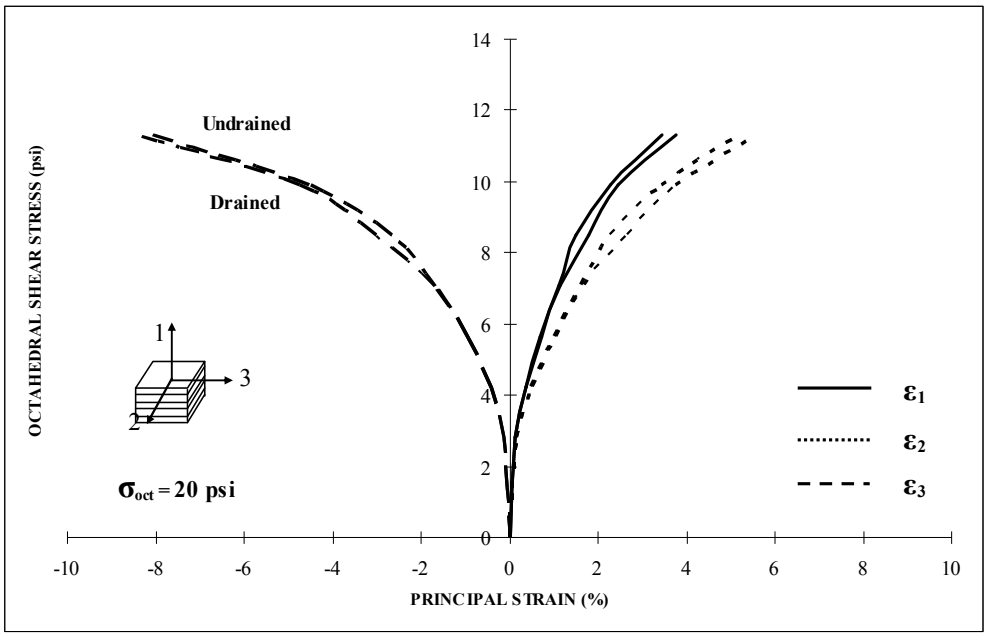

Figure 5.71 Comparison between Drained and Undrained TE Test Results ($w = 6\%$, $\sigma_{oct} = 20$ psi)

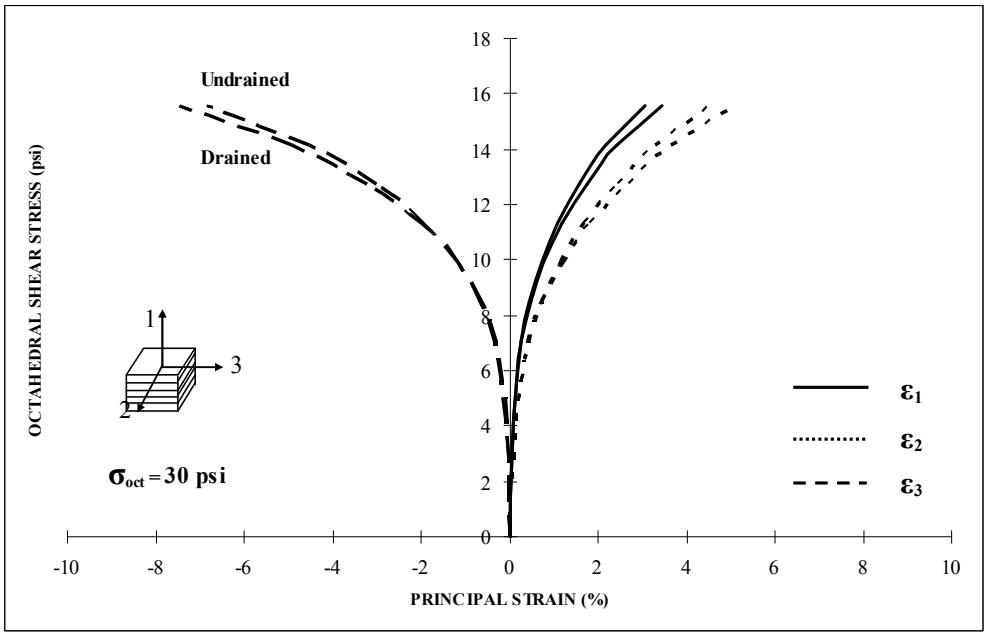

Figure 5.72 Comparison between Drained and Undrained TE Test Results ($w = 6\%$, $\sigma_{oct} = 30$ psi)

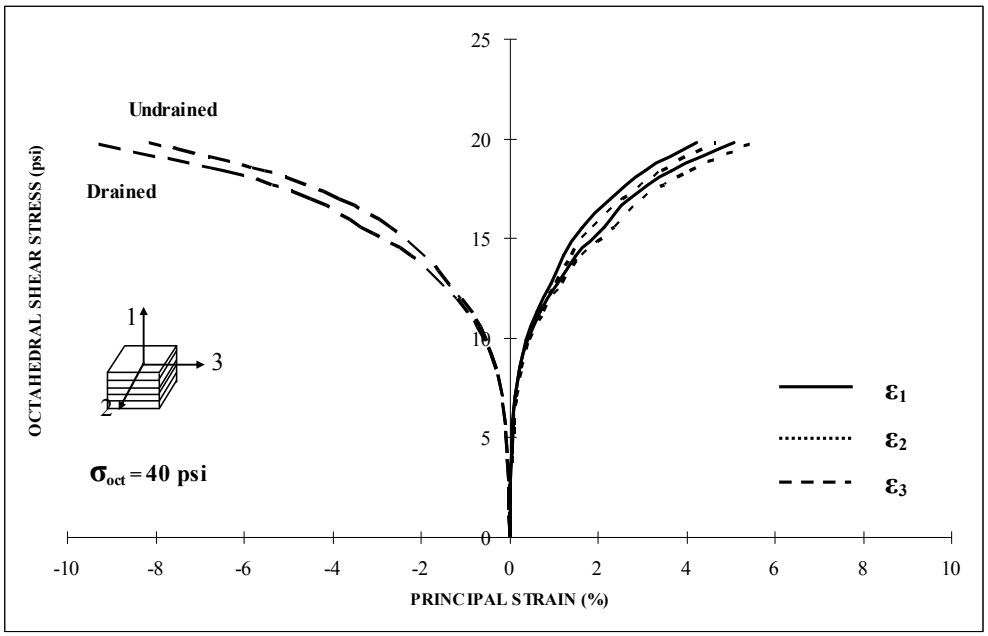

Figure 5.73 Comparison between Drained and Undrained TE Test Results ($w = 6\%$, $\sigma_{oct} = 40$ psi)

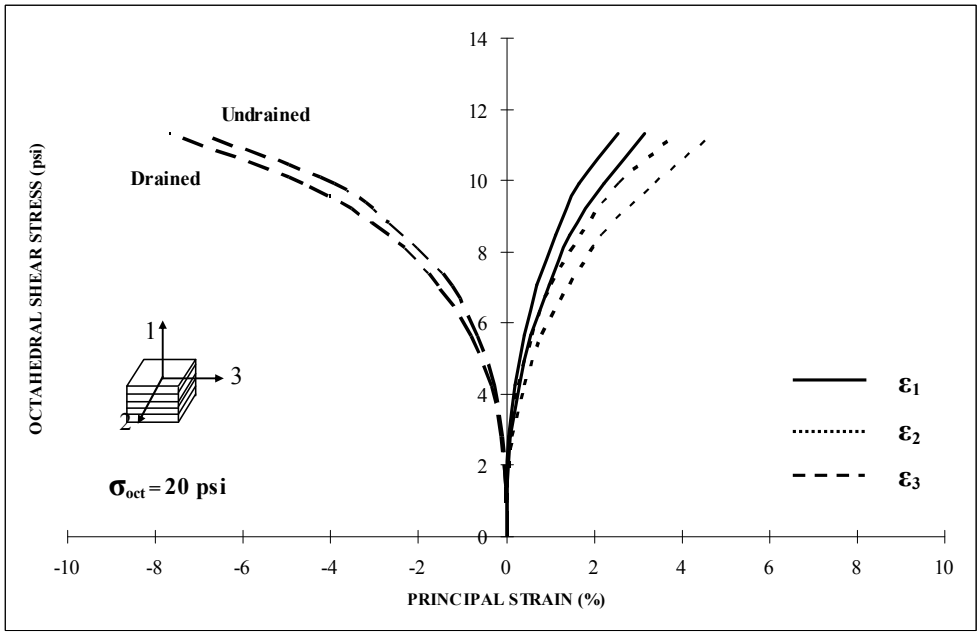

Figure 5.74 Comparison between Drained and Undrained TE Test Results ($w = 8\%$, $\sigma_{oct} = 20$ psi)

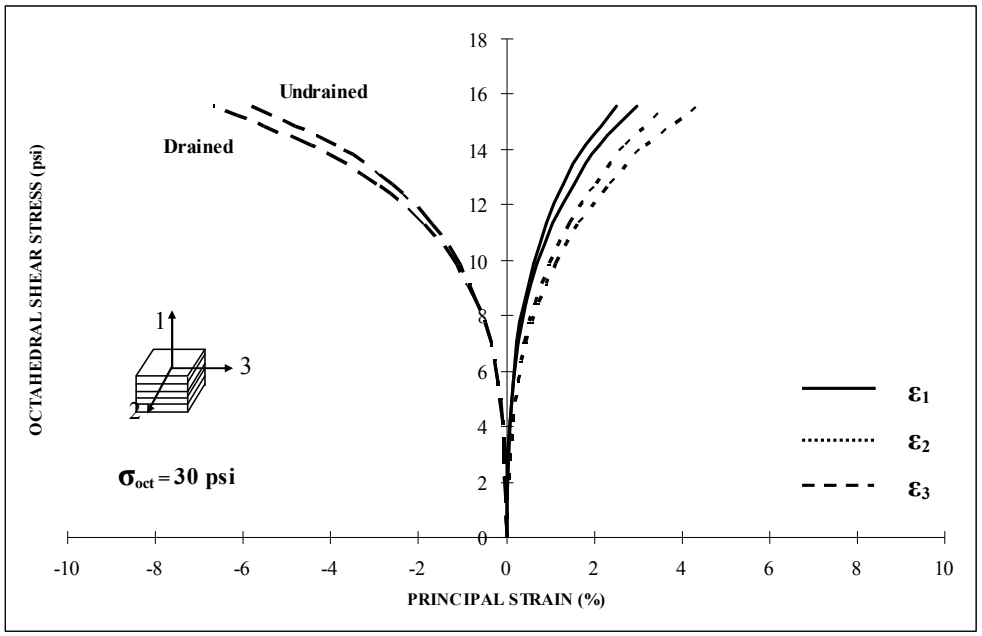

Figure 5.75 Comparison between Drained and Undrained TE Test Results
(w = 8%, σ_{oct} = 30 psi)

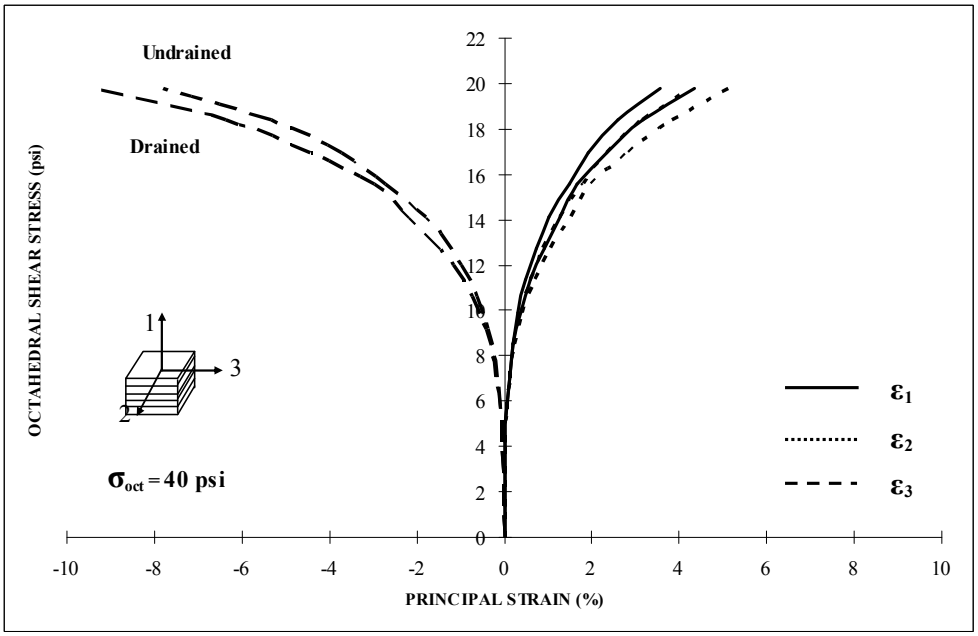

Figure 5.76 Comparison between Drained and Undrained TE Test Results
(w = 8%, σ_{oct} = 40 psi)

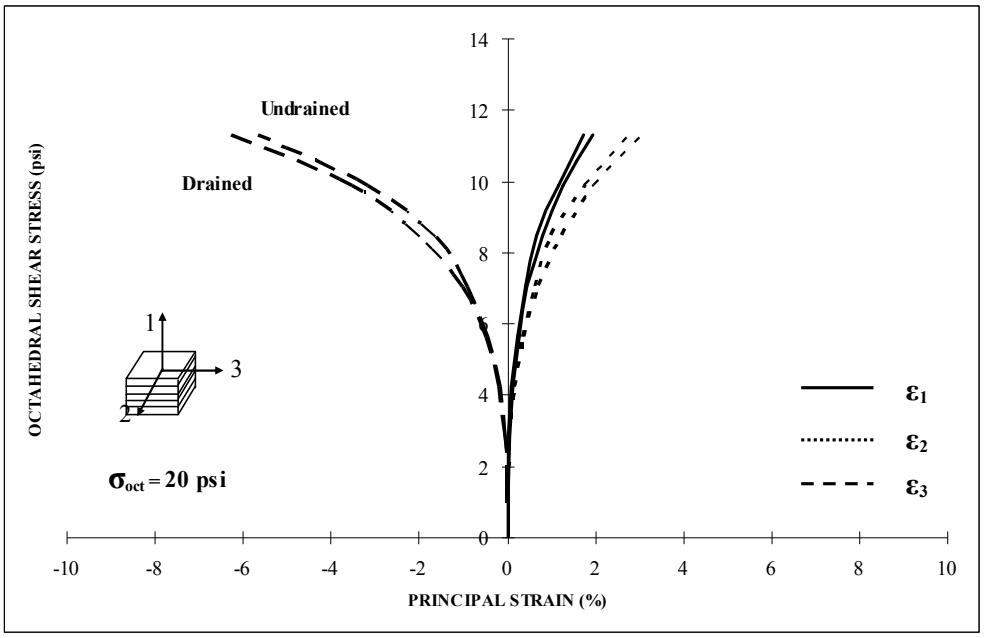

Figure 5.77 Comparison between Drained and Undrained TE Test Results
(w = 10%, σ_{oct} = 20 psi)

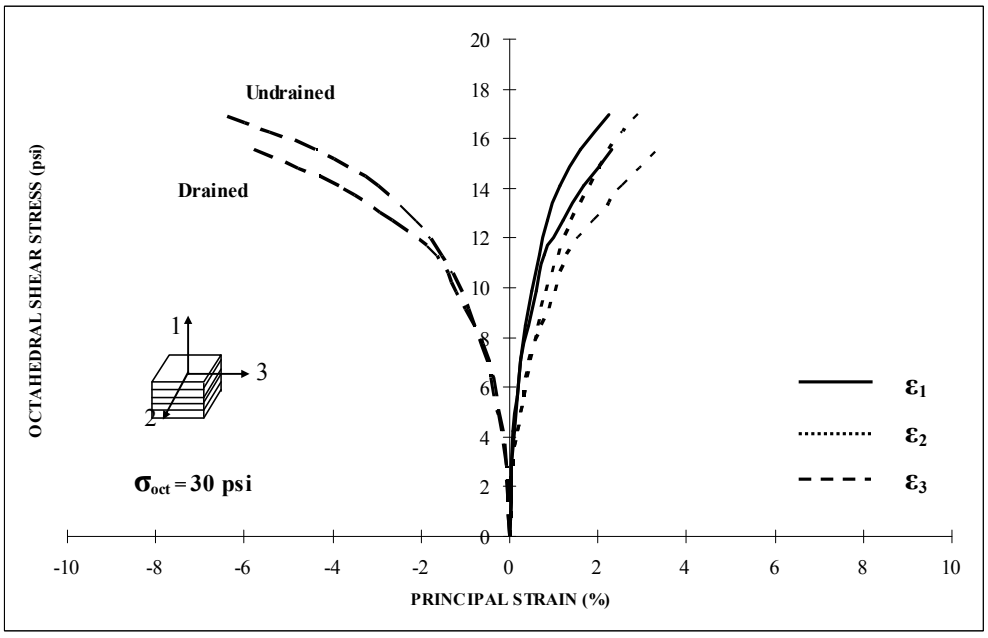

Figure 5.78 Comparison between Drained and Undrained TE Test Results
(w = 10%, σ_{oct} = 30 psi)

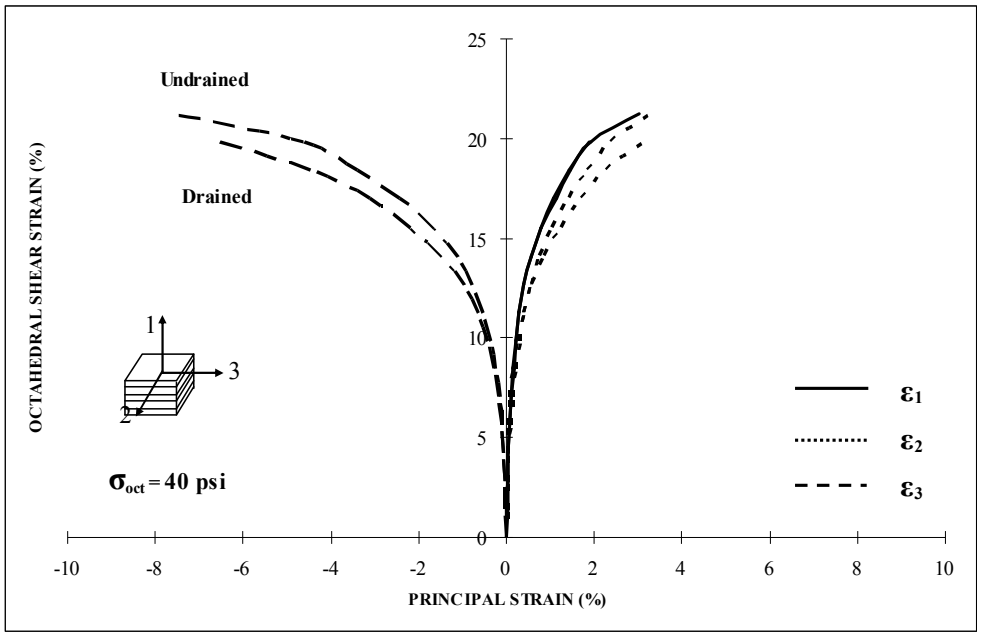

Figure 5.79 Comparison between Drained and Undrained TE Test Results
($w = 10\%$, $\sigma_{oct} = 40$ psi)

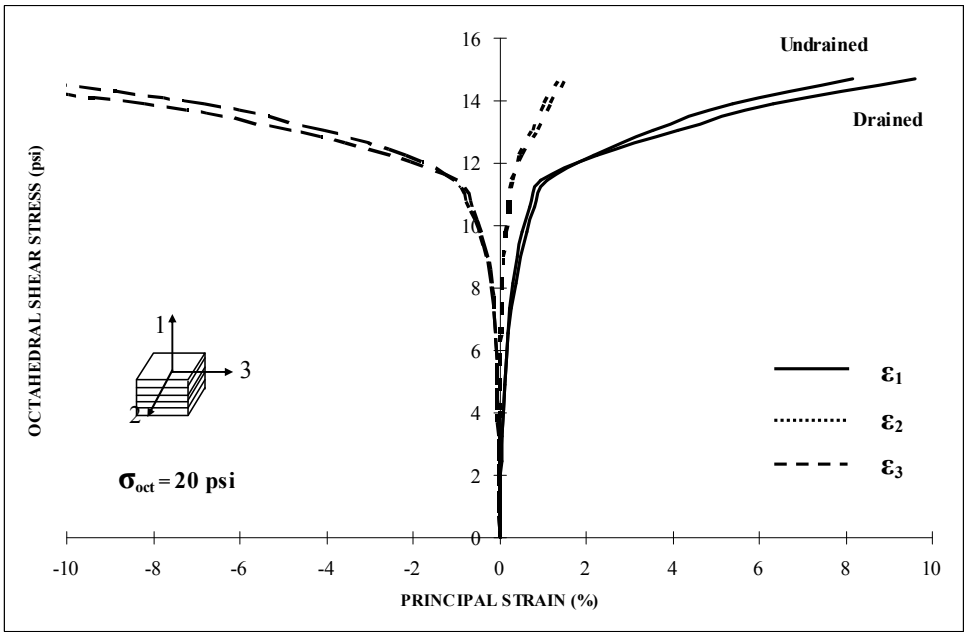

Figure 5.80 Comparison between Drained and Undrained SS Test Results
($w = 6\%$, $\sigma_{oct} = 20$ psi)

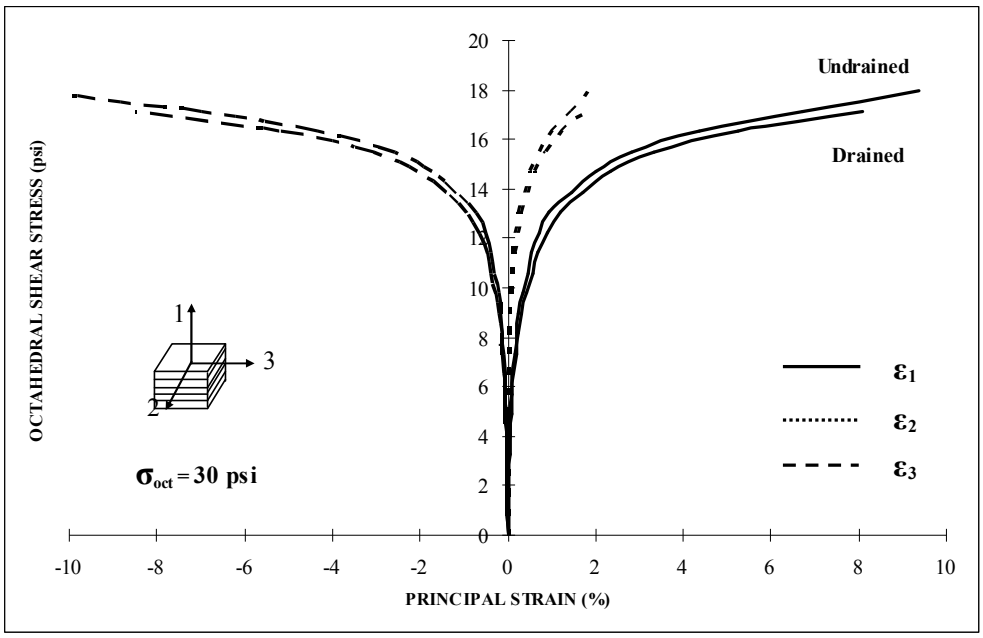

Figure 5.81 Comparison between Drained and Undrained SS Test Results
(w = 6%, σ_{oct} = 30 psi)

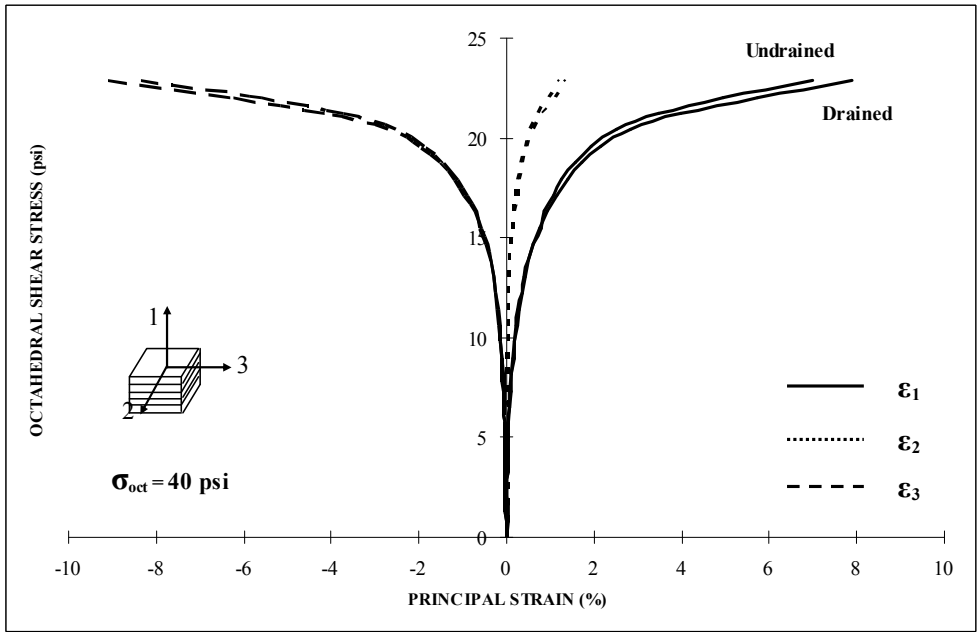

Figure 5.82 Comparison between Drained and Undrained SS Test Results
(w = 6%, σ_{oct} = 40 psi)

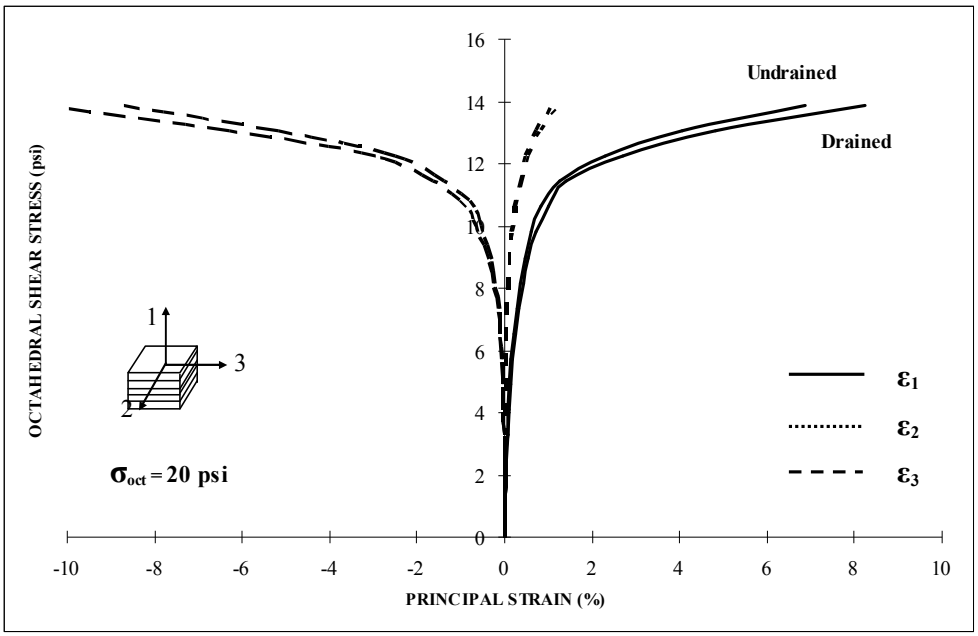

Figure 5.83 Comparison between Drained and Undrained SS Test Results ($w = 8\%$, $\sigma_{oct} = 20$ psi)

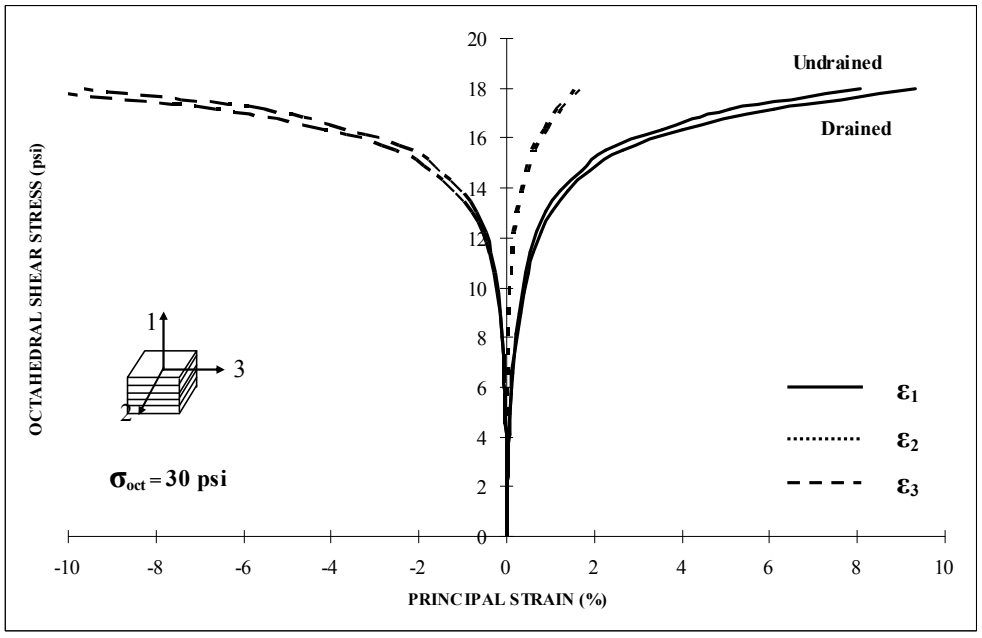

Figure 5.84 Comparison between Drained and Undrained SS Test Results ($w = 8\%$, $\sigma_{oct} = 30$ psi)

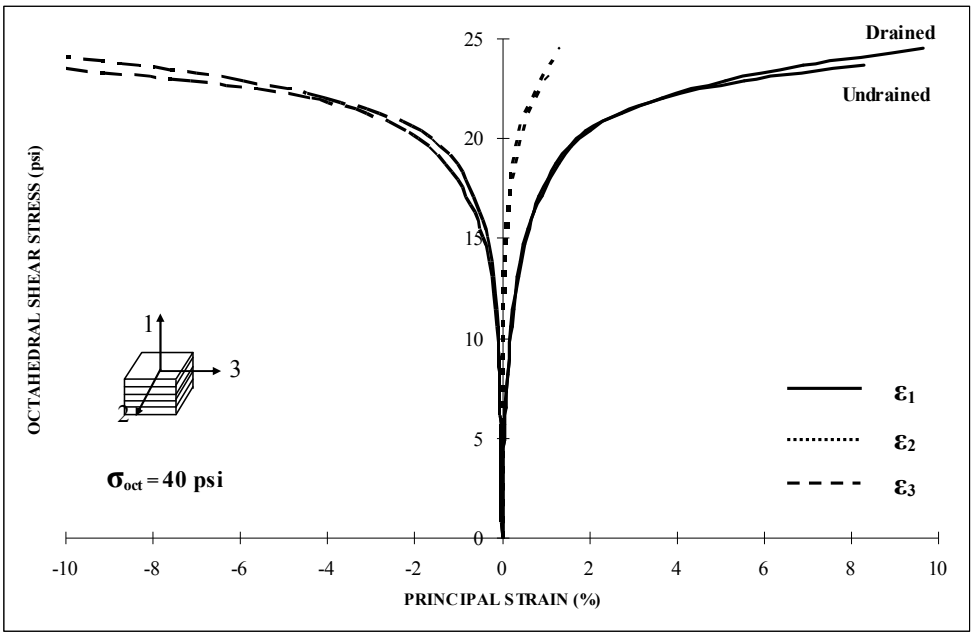

Figure 5.85 Comparison between Drained and Undrained SS Test Results
(w = 8%, σ_{oct} = 40 psi)

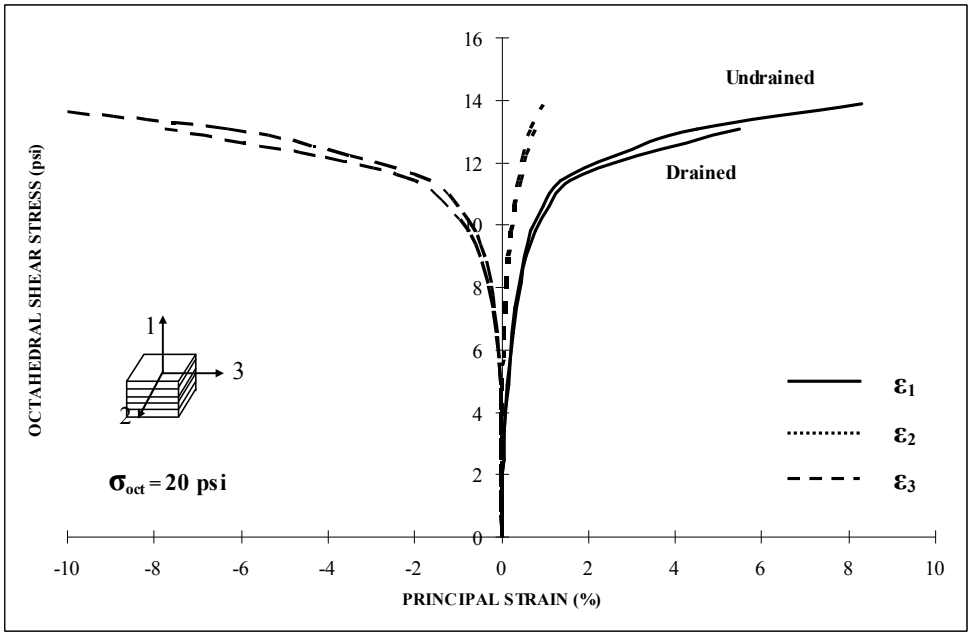

Figure 5.86 Comparison between Drained and Undrained SS Test Results
(w = 10%, σ_{oct} = 20 psi)

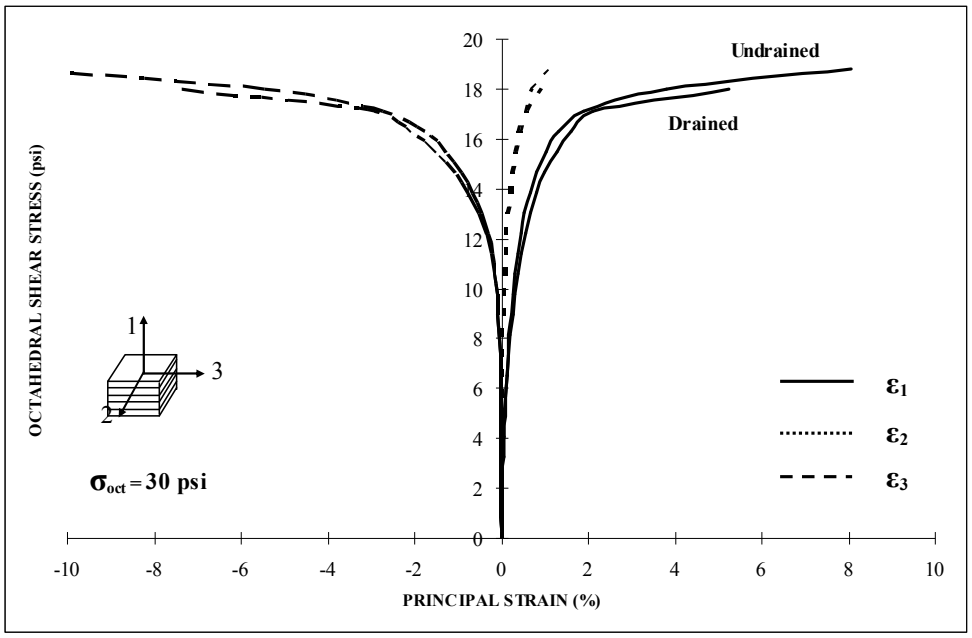

Figure 5.87 Comparison between Drained and Undrained SS Test Results
(w = 10%, σ_{oct} = 30 psi)

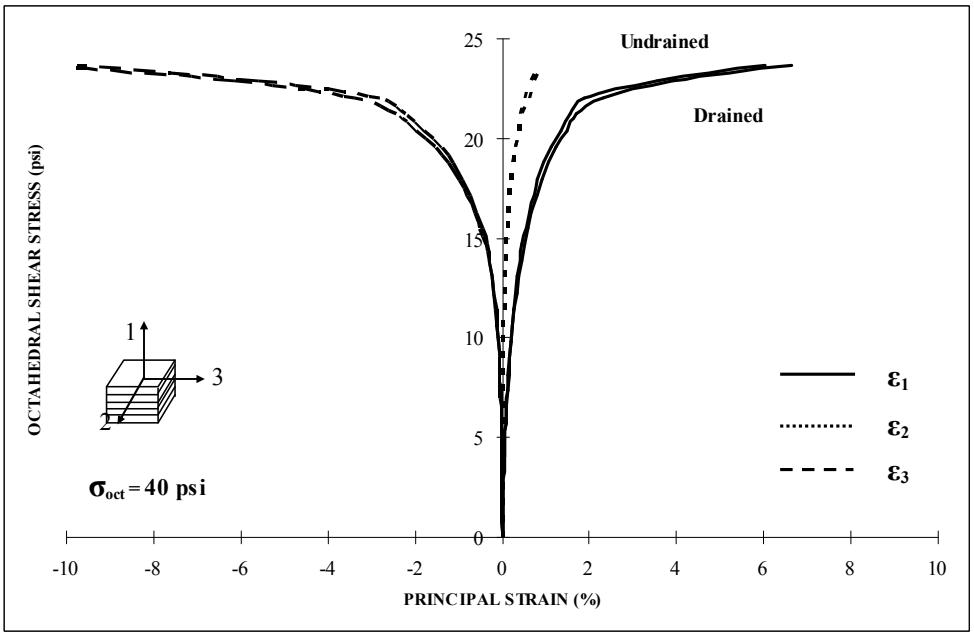

Figure 5.88 Comparison between Drained and Undrained SS Test Results
(w = 10%, σ_{oct} = 40 psi)

On the other hand, the results of drained and undrained loading were presented on the (q : p) plane as shown in Figure 5.89 to 91. The slopes of best-fit critical state line, M of undrained loading are parallel to those of drained loading.

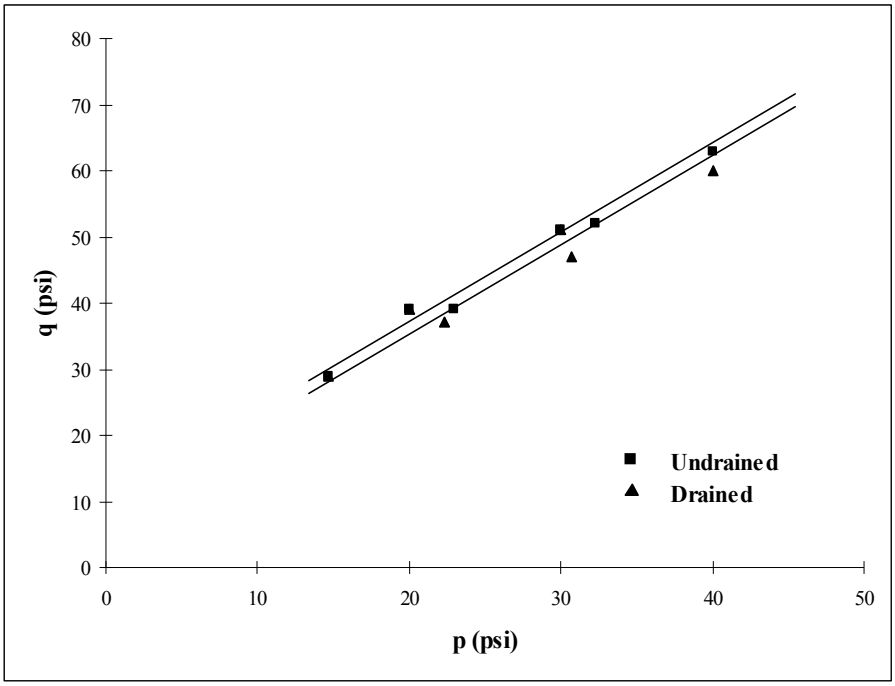

Figure 5.89 P-q Diagram for Kneading-Compacted Unsaturated Silty Sand (w = 6%)

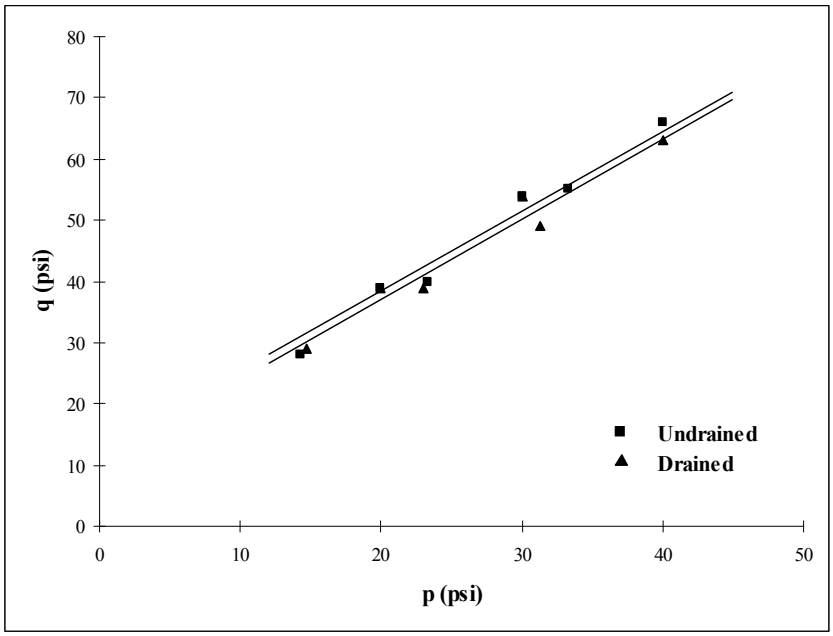

Figure 5.90 P-q Diagram for Kneading-Compacted Unsaturated Silty Sand (w = 8%)

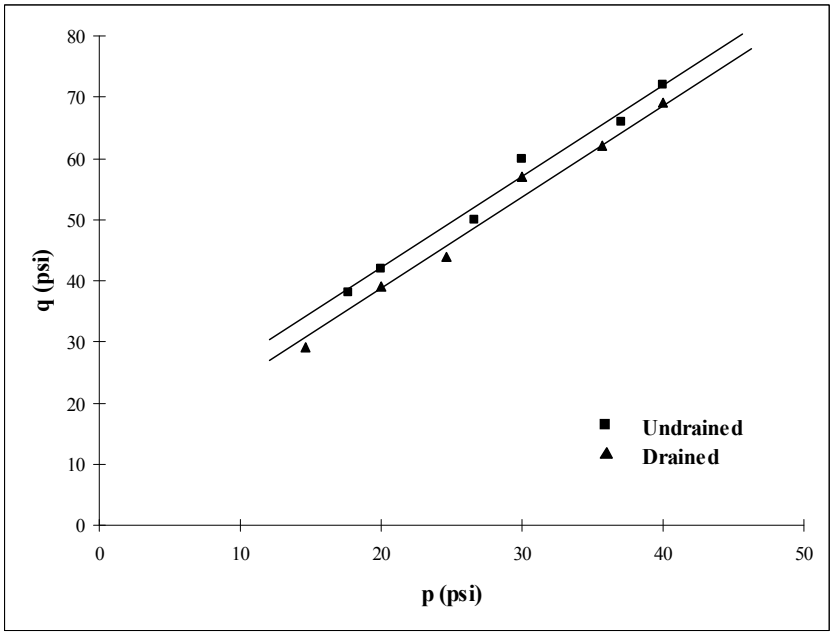

Figure 5.91 P-q Diagram for Kneading-Compacted Unsaturated Silty Sand (w = 10%)

Figure 5.92 to 95 shows the relationship between degree of saturation and peak octahedral shear stress. In general, soil strength increases as the initial degree of saturation increases from 27 to 61% under both drained and undrained loading. It also can be seen that soil strength under undrained loading at a given initial degree of saturation is slightly higher than that under drained loading. These trends are clear in CTC and TC tests. It is because soil possessing an anisotropic behaviour behaves differently according to the imposed stress path.

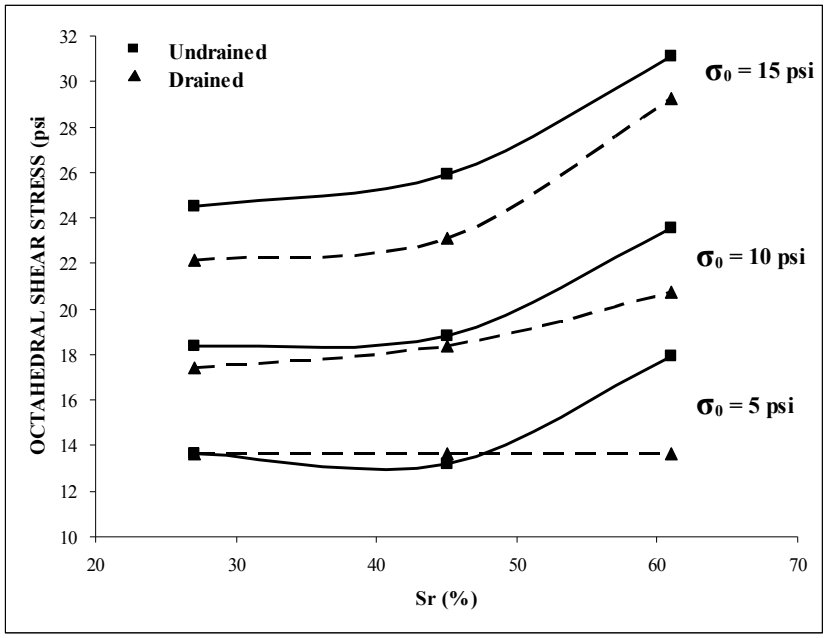

Figure 5.92 Relationship between Degree of Saturation and Peak Octahedral Shear Stress under CTC Tests

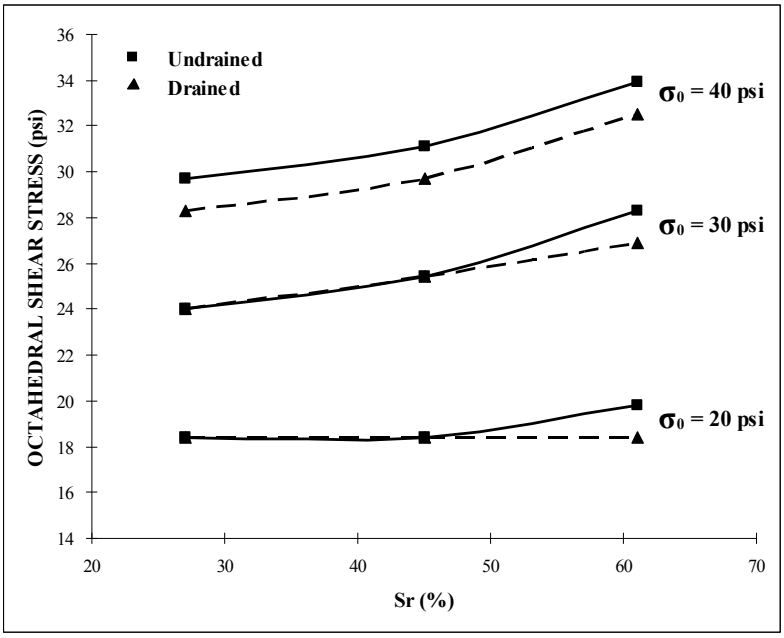

Figure 5.93 Relationship between Degree of Saturation and Peak Octahedral Shear Stress under TC Tests

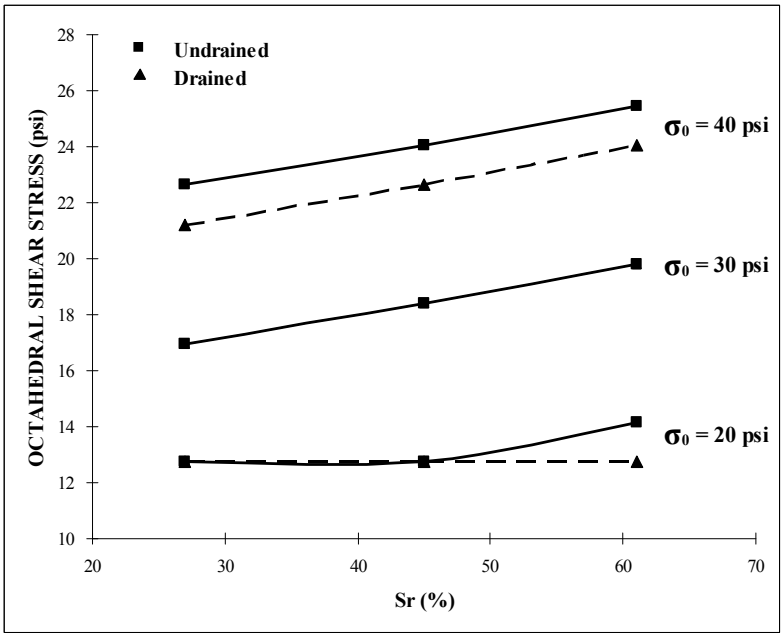

Figure 5.94 Relationship between Degree of Saturation and Peak Octahedral Shear Stress under TE Tests

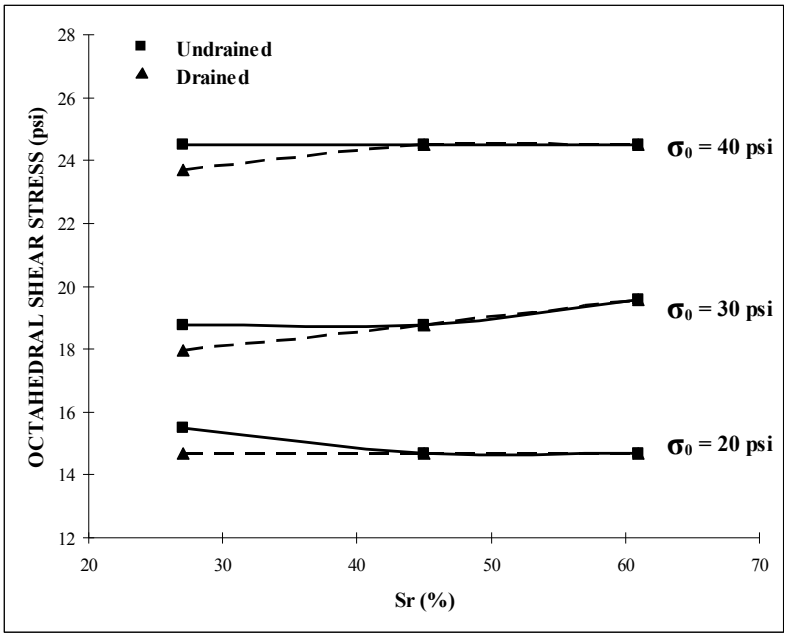

Figure 5.95 Relationship between Degree of Saturation and Peak Octahedral Shear Stress under SS Tests

CHAPTER 6

CONCLUSIONS AND RECOMMENDATIONS

6.1 Conclusions

Main conclusions drawn as a result of this thesis work are summarized as follows:

1. The shear strength of kneading-compacted unsaturated silty sand, for any stress path, increases as confining pressure increases under both drained and undrained loading.
2. It is clear that initial compaction-induced soil states such as degree of saturation, dry density, and void ratio play an important role in the strength of kneading-compacted unsaturated silty sand under both drained and undrained loading.
3. As degree of saturation increases from 27 to 61%, and initial dry density increases from 16.40 to 18.12 kN/m^3, the strength of kneading-compacted unsaturated silty sand increases. This means that soils with higher initial degree of saturation and dry density yield a lower pore size and therefore, a decrease in particle spacing contributes to the increase in effective negative pore water pressure. In addition, in soils with lower values of degree of saturation and dry density, the water phase can be assumed to be a lot more discontinuous while the air phase is more continuous. Therefore, this soil can be easily cracked (water menisci brake-up) and exhibit lower shear strength.

4. Soil with higher initial degree of saturation and dry density exhibits more expanded failure envelopes on the octahedral plane (π-plane).
5. The slope of the critical state line, M, was found to be nearly constant and non-dependent on the initial compaction-induced degree of saturation and dry density.
6. In general, the undrained strength of soil shows slightly higher peak values than that for drained conditions. There are two possible reasons to explain this behaviour. According to previous work, starting from a low degree of saturation, the soil strength increases with an increase in degree of saturation up to a certain optimum value, beyond which the strength drops due to further increase in degree of saturation. In general, the degree of saturation in unsaturated soil increases slightly during undrained loading and on the contrary, decreases slightly during drained loading. For the unsaturated specimens containing initially same degree of saturation before tests, the results generally show that the strength of soil under undrained condition is slightly greater than that under drained condition. Therefore, it can be concluded that the three values of degree of saturation (27, 45, and 61%) undertaken in this thesis work are below a certain optimum value. Another possible reason is that water menisci in soil under drained loading can be easily broken up and therefore the contribution of suction on soil strength is lost, whereas under undrained loading the compaction-induced menisci can be better kept due to the help of pore-air pressure buildup to hold them.

6.2 Future Research Recommendations

1. Suction measurements during true triaxial testing via tip tensiometers adapted to cubical cell working conditions.
2. Suction-controlled true triaxial testing on kneading-compacted unsaturated silty sand with change in initial degree of saturation and density.
3. True triaxial testing on kneading-compacted unsaturated clay soil under drained and undrained loading condition
4. True triaxial testing on kneading-compacted unsaturated silty sand with various loading rates under drained and undrained condition.

REFERENCES

1. Atkinson, R.H. (1972). “A Cubical Test Cell for Multiaxial Testing of Materials”, Ph.D. Dissertation. University of Colorado at Boulder, Boulder, CO.
2. Bishop, A.W. (1959). “The Principle of Effective Stress”, Teknisk Ukeblad 39, Oct., 859-863.
3. Chen, K.J., Miao, L.C., and Cui, Y. (2005). “Triaxial Tests on Unsaturated Expansive Soils with Different Initial Dry Densities”. Rock and Soil Mechanics. 26, 87-90
4. Coleman, J. D. (1962). "Stress-Strain Relations for Partially Saturated Soils." Geotechnique, 12(4), 348–350.
5. Edlefsen, N.E. and Anderson, A.B.C. (1943). “Thermodynamics of Soil Moisture.” Hilgardia. 15.
6. Fredlund, D.G. and Morgenstern, N.R. (1977). “Stress State Variables and Unsaturated Soils”. Journal of the Geotechnical Engineering Division, ASCE, 103(GT5), 447-466.
7. Fredlund, D.G., Morgenstern, N.R., and Widger, R.A. (1978) “The Shear Strengths of Unsaturated Soil,” Canadian Geotechnical Journal. 15, 313-321.
8. Fredlund, D.G. (1989). “Soil Suction Monitoring for Roads and Air Fields”. Proc, Simp. on the State-of-the-Art of Pavement Response Monitoring Systems

for Roads and Airfields, Sponsored by the U.S. Army Crops of Engineers, Hanover, NH.

9. Fredlund, D.G. (1991). “How Negative Can Pore-Water Pressure Get ?”. Geotechnical News, Canadian Geotech. Soc., 9(3), 44-46.
10. Fredlund, D.G. and Rahardjo, H. (1993). “Soil Mechanics for Unsaturated Soils,” New York: John Wiley and Sons Inc.
11. Hoyos, L.R. and Macari, E.J. (2001). “Development of a Stress/Suction-Controlled True Triaxial Testing Device for Unsaturated Soils”. Geotechnical Testing Journal, 24(1), 5-13.
12. Janoo, V.C. (1986). “Drained and Undrained Behaviour of Sand under High Pressures”. Ph.D. Dissertation, University of Colorado at Boulder, Boulder, CO.
13. Jennings, J.E. and Burland, J.B. (1962). Limitations of the Use of Effective Stresses in Partly Saturated Soils. Geotechnique, 12(2), 125-144.
14. Kaye, G.W.C. and Laby, T.H. (1973). “Tables of Physical and Chemical Constants”, 14th ed. Longman, 386.
15. Kjellman, W. (1936). "Report on an Apparatus for Consummate Investigation of the Mechanical Properties of Soils." Proc., 1st Int. Conf. on Soil Mechanics and Foundation Engineering, 2, 16–20.
16. Ko, H-Y. and Scott, R. F. (1967a). "A New Soil Testing Apparatus." Geotechnique, 17(1), 40–57.
17. Ko, H-Y. and Scott, R. F. (1967b). "Deformation of Sand in Shear." J. Soil Mech. Found. Div., 93(5), 283–310.

18. Maaitah, O.N. and Mahadin, S.A. (2004). “Variation on Shear Strength of Unsaturated Subgrade Causes Road Cracks.” Journal of Applied Sciences, 4(3), 335-339
19. Maaitah, O.N. (2005). “Experimental Verification of a Theoretical Model for the Shear Strength of Unsaturated Soil.” Electronic Journal of Geotechnical Engineering, 10(C), 1-9
20. Murthy, M.K., Sridharan, A., and Nagaraj, T.S. (1987). “Shear Behaviour of Partially Saturated Soils.” Indian Geotechnical Journal, 17(2), 142-158
21. Park, J.H. (2005). “Performance and Check-out Verification Testing of a New True Triaxial apparatus Using Partially Saturated Silty Sand,” M.Sc. thesis, University of Texas at Arlington, Arlington, TX.
22. Richards, B.G. (1974). “Behavior of Unsaturated Soils, “ in Soil Mechanics-New Horizons, I.K.Lee, Ed. New York: American Elsevier, 112-157.
23. Rahardjo, H. (1990). “The Study of Undrained and Drained Behaviour of Unsaturated Soil.” Ph.D. Dissertation, University of Saskatchewan, Saskatoon, Sask.
24. Reddy, K.R., Saxena, S.K., and Budiman, J. (1992). "Development of a True Triaxial Testing Apparatus," Geotechnical Testing Journal, GTJODJ, 15(2), 89-105.
25. Terzaghi, K. (1936) “The Shearing Resistance of Saturated Soils and the Angle between the Planes of Shear,” Proceedings 1st International Conference on Soil Mechanics and Foundation Engineering, 1, 54-56.

26. Wiebe, B., Graham., J., Tang, G.X.M., and Dixon, D. (1998). “Influence of Pressure, Saturation, and Temperature on the Behaviour of Unsaturated Sand-Bentonite,” Canadian Geotechnical Journal, 35(2), 194-205.
27. Yong, R.N. and Warkentin, B.P. (1975). “Soil Properties and Behaviour,” Elsevier Scientific Publishing Co., New York, 449.

BIOGRAPHICAL INFORMATION

Sang Chul Pyo was born on April 17, 1976, at the City of Seoul, Korea. He received his bachelor's degree in Civil Engineering from Dongguk University, Korea, in Feburary 2003. After graduation, he worked as a civil engineer in a highway design company for a few months. Afterwards, he decided to pursue graduate studies majoring in geotechnical engineering at The University of Texas at Arlington in 2004. During his studies, he had the opportunity to work as a graduate research assistant under supervision of Dr. Laureano R. Hoyos in the area of unsaturated soil mechanics. He received his Master of Science Degree in Civil Engineering from The University of Texas at Arlington in August 2006.